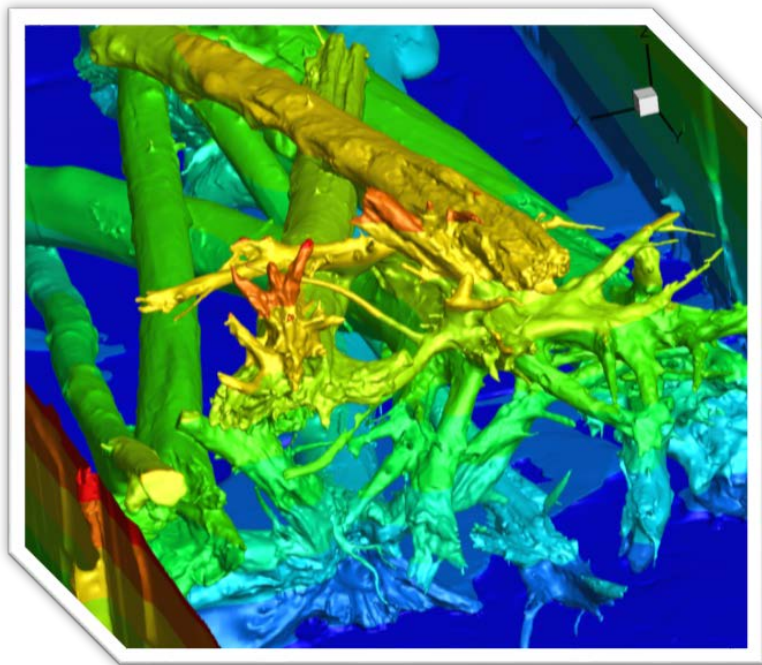


# RECLAMATION

*Managing Water in the West*

## Quantitative Modeling Tools for Large Wood Debris and Other In-Stream Structures

Research and Development Office  
Science and Technology Program  
Final Report ST-2016-4495-01



U.S. Department of the Interior  
Bureau of Reclamation  
Research and Development Office

September 2016



## **Mission Statements**

The U.S. Department of the Interior protects America's natural resources and heritage, honors our cultures and tribal communities, and supplies the energy to power our future.

The mission of the Bureau of Reclamation is to manage, develop, and protect water and related resources in an environmentally and economically sound manner in the interest of the American public.



| REPORT DOCUMENTATION PAGE  |                                    | Form Approved<br>OMB No. 0704-0188  |
|--|------------------------------------|---|
| <b>T1. REPORT DATE</b><br>09/2016  | <b>T2. REPORT TYPE</b><br>Research | <b>T3. DATES COVERED</b><br>10/2013 – 09/2016   |
| <b>T4. TITLE AND SUBTITLE</b><br>Quantitative Modeling Tools for Large Wood Debris and Other In-Stream Structures  |                                    | <b>5a. CONTRACT NUMBER</b><br>16XR0680A1  |
|  |                                    | <b>5b. GRANT NUMBER</b>   |
|  |                                    | <b>5c. PROGRAM ELEMENT NUMBER</b><br>1541 (S&T)   |
| <b>6. AUTHOR(S)</b><br><br>Yong G. Lai, Ph.D., Hydraulic Engineer<br>303-445-2560  |                                    | <b>5d. PROJECT NUMBER</b><br>4495   |
|  |                                    | <b>5e. TASK NUMBER</b>  |
|  |                                    | <b>5f. WORK UNIT NUMBER</b><br>86-68240   |
| <b>7. PERFORMING ORGANIZATION NAME(S) AND ADDRESS(ES)</b><br>Sedimentation and River Hydraulics Group<br>Technical Service Center, Bureau of Reclamation<br>Denver, CO 80225   |                                    | <b>8. PERFORMING ORGANIZATION REPORT NUMBER</b><br>SRH-2016-26  |
| <b>9. SPONSORING / MONITORING AGENCY NAME(S) AND ADDRESS(ES)</b><br>Research and Development Office<br>U.S. Department of the Interior, Bureau of Reclamation,<br>PO Box 25007, Denver CO 80225-0007   |                                    | <b>10. SPONSOR/MONITOR'S ACRONYM(S)</b><br>R&D: Research and Development Office<br>BOR/USBR: Bureau of Reclamation<br>DOI: Department of the Interior |
|  |                                    | <b>11. SPONSOR/MONITOR'S REPORT NUMBER(S)</b><br>ST-2016-4495-01  |
| <b>12. DISTRIBUTION / AVAILABILITY STATEMENT</b><br>Final report can be downloaded from Reclamation's website: <a href="https://www.usbr.gov/research/">https://www.usbr.gov/research/</a>   |                                    |   |
| <b>13. SUPPLEMENTARY NOTES</b>   |                                    |   |
| <b>14. ABSTRACT (Maximum 200 words)</b><br><br>This report documents the research and development carried out to address various priority issues facing the Large Wood (LW) installation at Reclamation river restoration projects. In particular, it focuses on determining the feasibility of using suitable computational modeling tools for LW installation as well as the development of relevant modeling tools at Reclamation.<br><br>After a screening study of evaluating a number of open-source modeling tools that may be suitable to this project and a literature survey, a three-dimensional (3D) semi-automated mesh generator is revised and updated based on OpenFOAM's snappyHexMesh. In addition, an independent stand-alone semi-automated mesh generator is also developed. Then, the project focused on the extension and update of a 3D Reynolds-Averaged Navier-Stokes model U2RANS. A combination of 3D mesh generator and U2RANS allow engineers to simulate complex flows around LW structures in a riverine environment.<br><br>A number of demonstration cases and project applications are used to test and verify the developed modeling tools. Results are compared with field measured data when available. It is shown that the developed 3D modeling tools can be used by engineers to predict flows around complex in-stream structures on desktop PCs. |                                    |   |

|   |                         |  |                            |   |
|---|-------------------------|--|----------------------------|---|
| <b>15. SUBJECT TERMS</b><br>Computational Fluid Dynamics; 3D Model; Large Wood; In-Stream Structure |                         |  |                            |   |
| <b>16. SECURITY CLASSIFICATION OF:</b><br>U   |                         | <b>17. LIMITATION OF ABSTRACT</b><br><br>U | <b>18. NUMBER OF PAGES</b> | <b>19a. NAME OF RESPONSIBLE PERSON</b><br>Yong G. Lai |
| <b>a. REPORT</b><br>U   | <b>b. ABSTRACT</b><br>U |  |                            | <b>c. THIS PAGE</b><br>U                              |

S Standard Form 298 (Rev. 8/98)  
P Prescribed by ANSI Std. Z39-18

# PEER REVIEW DOCUMENTATION

## Project and Document Information

Project Name Quantitative Modeling Tools WOID 4495

Document Quantitative Modeling Tools for Large Wood Debris and Other In-Stream Structures

Document Author(s) Yong G. Lai Document date 09/2016

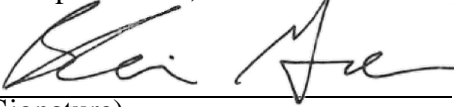
Peer Reviewer Blair P. Greimann

For Reclamation disseminated reports, a disclaimer is required for final reports and other research products, this language can be found in the peer review policy:

***“This information is distributed solely for the purpose of pre-dissemination peer review under applicable information quality guidelines. It has not been formally disseminated by the Bureau of Reclamation. It does not represent and should not be construed to represent Reclamation’s determination or policy.”***

## Review Certification

**Peer Reviewer:** I have reviewed the assigned items/sections(s) noted for the above document and believe them to be in accordance with the project requirements, standards of the profession, and Reclamation policy.

Reviewer  Date reviewed 9-22-2016  
(Signature)



# Acknowledgements

This project was carried out in collaboration with a number of internal and external engineers and scientists. Significant contribution and participation in the model development by Prof. Xiaofeng Liu, Pennsylvania State University, are acknowledged. His work is documented in a separate final report as Attachment D. Other collaborators in the project are listed below:

- David Smith, Ph.D., Ecologist; US Army Corps of Engineers, Engineer Research and Development Center (ERDC), Vicksburg, MS
- David (DJ) Bandrowski, P.E., Senior Project Engineer/Hydraulic Design Engineer with the Yurok Tribe, Weaverville, California.
- Josh Israel, Ph.D., Biologist; Bay-Delta Office, U.S. Bureau of Reclamation, Sacramento, CA
- R. A. Goodwin, Ph.D., US Army Corps of Engineers, Engineer Research and Development Center (ERDC), Vicksburg, MS
- R. L. Reeves, California Department of Water Resources, Sacramento, CA
- Prof. Jennifer Duan, Ph.D., [gduan@email.arizona.edu](mailto:gduan@email.arizona.edu), University of Arizona, Tucson, Arizona

Their participation and contribution are reflected in three full conference papers as Attachments A, B and C



# Executive Summary

This report documents the Science and Technology (S&T) project carried out during fiscal year 2014 through 2016 (a 3-year study). The research is an effort to address various priority issues facing the Large Wood (LW) installation at Reclamation river restoration projects. The priority issues of LW structures were proposed and discussed at a Reclamation and U.S. Army Corp of Engineers (USACE) Workshop held in 2012. This research study involves both internal and external engineers and scientists as a collaborative effort with the objective of determining the feasibility of using suitable computational modeling tools for LW installation as well as the development of relevant modeling tools at Reclamation. Collaborative partners include:

- Yong Lai, Ph.D., Hydraulic Engineer, Technical Service Center, Bureau of Reclamation, Denver, Colorado
- Prof. Xiaofeng Liu, Ph.D., P.E., Department of Civil and Environmental Engineering, Pennsylvania State University, University Park, PA
- David Smith, Ph.D., Ecologist; US Army Corps of Engineers, Engineer Research and Development Center (ERDC), Vicksburg, MS
- David (DJ) Bandrowski, P.E., Senior Project Engineer/Hydraulic Design Engineer with the Yurok Tribe, Weaverville, California.
- Josh Israel, Ph.D., Biologist; Bay-Delta Office, U.S. Bureau of Reclamation, Sacramento, CA
- R. A. Goodwin, Ph.D., US Army Corps of Engineers, Engineer Research and Development Center (ERDC), Vicksburg, MS
- R. L. Reeves, California Department of Water Resources, Sacramento, CA
- Prof. Jennifer Duan, Ph.D., [gduan@email.arizona.edu](mailto:gduan@email.arizona.edu), University of Arizona, Tucson, Arizona

Key accomplishments of the project are summarized below:

- Conducted a screening study, evaluating a number of open-source modeling tools that may be suitable to this project;
- Conducted a literature study in 3D flow and sediment transport modeling in hydraulic engineering;
- Identified major challenges in developing a practical 3D flow and sediment transport model;
- Formed a strategy on how to develop new models to overcome previous challenges and to achieve the objective of the study;
- Developed a 3D mesh generator which is easy-to-use and can be automated which included both revised version of OpenFOAM's snappyHexMesh and independent stand-alone mesh generator;
- Modified and extended 3D flow model U2RANS to solve the complex flows around LW structures using the new mesh generators;
- Carried out flow module test and validation using a number of practical cases.

In the main body of this report, the above efforts carried out at Reclamation are documented.

## Quantitative Modeling Tools for Large Wood

In addition, a separate final report is delivered to Reclamation by Prof. Xiaofeng Liu at the Penn State University. The report, titled “Quantitative Modeling Tools for Large Wood Flow Simulation,” is submitted as Attachment D. The 3-year work by Prof. Liu is accomplished through a grant from Reclamation to Penn State University. The two major tasks include: (1) develop a 3D automated mesh generator based on OpenFOAM’s snappyHexMesh and suitable for running on Window based PCs; and (2) develop a stand-alone independent 3D mesh generator.

Further, part of the Reclamation work has been published at international conferences and three full papers are included as Attachment A, B and C.

Below is a summary of the work carried out at Reclamation.

The screening study narrowed the model tools considered for further comprehensive testing and development to the following: U2RANS, snappyHexMesh, and our own independent 3D mesh generator.

Literature review shows that 3D flow and sediment transport modeling is rarely performed in hydraulic engineering. This is mainly due to (a) lack of such models in the public-domain, (b) complexity in usage and labor-intensiveness of such modeling, and (c) the need for supercomputing power. 3D flow and sediment transport modeling has been mostly limited to research; testing and verification studies are mostly done with simple geometry and/or under laboratory conditions. There exist a number of 3D hydrostatic-assumption (HA) models for flow and sediment transport modeling. But few non-hydrostatic, Reynolds-averaged Navier-Stokes (RANS) models are available to engineers; in particular, few are adequate for sediment transport modeling. Among the models reviewed, we found SSIIM, VSL3D and Wu models have the capabilities to predict the gradation of sediment mixtures. They, however, are research models developed at universities and have limited distribution.

The literature review also shows that a number of challenges need to be overcome before apply 3D models. We group these challenges into four categories: (a) mesh generation; (b) free surface modeling; (c) mobile bed representation; and (d) sediment transport modeling. Each is discussed in detail in the report.

The new U2RANS consists of three modules: the mesh generation module, the flow module, and the sediment transport module. This research focused primarily on the mesh generation and flow module development. 3D mesh generation is a prerequisite for any 3D modeling and is the first hurdle to overcome. We have worked on the development of an automated 3D mesh generation module since 2014; its development is continued in 2015 and will continue into future years. At present, a mesh generator has been developed, named SHM, based on the existing open-source model OpenFOAM’s snappyHexMesh. SHM has the following features:

- A simple background mesh is generated first by users;
- Complex geometry is processed using CAD software and the surface representation of any geometry is through the Stereolithography (STL) format; and
- A 3D mesh is generated automatically, with a few user inputs, through interception of the geometry with the background mesh.

## Executive Summary

Use of STL files facilitates the representation of complex geometry. Our proposed arbitrarily shaped cell method of the 3D flow module provides complete flexibility in mesh generation.

Work has also carried out to develop an independent 3D mesh generator that does not rely on SHM (it is named U2-Mesh). The results are documented in the final report by Prof. Liu. U2-Mesh does not have the same capability as SHM, but it is developed for modeling flexibility and ease-of-use for some river engineering flows.

The 3D flow module is based on the unstructured, arbitrarily shaped cell method of Lai et al. (2003). A number of extensions and improvements have been made and incorporated into U2RANS. They include: (a) unsteady flow modeling capability, (b) ability to handle polyhedrons and cells with hanging nodes due to the added local mesh refinement capability; (c) free surface treatment and stream bed representation, and (d) new result outputs processed with Paraview and TECPLOT 360. The enhanced flow module has been tested and validated with a number of cases and results are documented in this report. In particular, the model has been applied to a couple of practical projects on the Sacramento River; and demonstrated with flows over LW structures. The application of the model to the Walnut Grove section of the Sacramento River is documented in the report as well as a full conference paper (Attachment B); the application of the model to the Fremont Weir section of the Sacramento River is documented in another full conference paper (Attachment C).



# Contents

|  | <i>Page</i>     |
|--|-----------------|
| <i>“This information is distributed solely for the purpose of pre-dissemination peer review under applicable information quality guidelines. It has not been formally disseminated by the Bureau of Reclamation. It does not represent and should not be construed to represent Reclamation’s determination or policy.”.</i> |                 |
| <b>Review Certification.....</b>   | <b>7</b>        |
| <b>Executive Summary .....</b>   | <b>11</b>       |
| <b>Contents</b>  | <b><i>i</i></b> |
| <b>1. Background .....</b>   | <b>3</b>        |
| <b>2. Results of Screening Study .....</b>   | <b>4</b>        |
| <b>2.1 SRH-2D and U<sup>2</sup>RANS.....</b>   | <b>4</b>        |
| <b>2.2 CART3D.....</b>   | <b>9</b>        |
| <b>2.3 VSL3D .....</b>   | <b>10</b>       |
| <b>2.4 Deflt3D .....</b>   | <b>12</b>       |
| <b>2.5 OpenFOAM .....</b>  | <b>14</b>       |
| <b>2.6 Summary .....</b>   | <b>19</b>       |
| <b>3. Literature Review .....</b>  | <b>21</b>       |
| <b>4. Major Challenges.....</b>  | <b>26</b>       |
| <b>5. 3D Model Governing Equations.....</b>  | <b>29</b>       |
| <b>5.1 Mesh Representation.....</b>  | <b>29</b>       |
| <b>5.2 Flow Module Equations.....</b>  | <b>30</b>       |
| <b>5.3 Boundary Conditions.....</b>  | <b>32</b>       |
| <b>6. Numerical Methods .....</b>  | <b>35</b>       |
| <b>6.1 Discretization of the Flow Equations.....</b>   | <b>35</b>       |
| <b>6.2 Velocity-Pressure Coupling and Solution Procedure.....</b>  | <b>40</b>       |
| <b>7. 3D Mesh Generation.....</b>  | <b>43</b>       |
| <b>7.1 Background Mesh .....</b>   | <b>43</b>       |
| <b>7.2 Object Representation .....</b>   | <b>44</b>       |
| <b>7.3 Mesh Castellation .....</b>   | <b>46</b>       |
| <b>7.4 Mesh Snapping .....</b>   | <b>50</b>       |
| <b>7.5 Surface Mesh Layer Addition.....</b>  | <b>53</b>       |
| <b>7.6 Potential Problems .....</b>  | <b>55</b>       |
| <b>7.7 A Sample Use for River Flow.....</b>  | <b>56</b>       |
| <b>8. Flow Module Results.....</b>   | <b>62</b>       |

## Quantitative Modeling Tools for Large Wood

|  |            |
|--|------------|
| <b>8.1 Flow over a Picnic Table .....</b>  | <b>63</b>  |
| <b>8.2 Flow over a Tree with Rootwad.....</b>  | <b>65</b>  |
| <b>8.3 Flow at the Junction of Sacramento River and Georgiana Slough Channel .....</b> | <b>76</b>  |
| 8.3.1 Background.....  | 76         |
| 8.3.2 Site Description and Available Data .....  | 77         |
| 8.3.3 Model Domain and Mesh .....  | 82         |
| 8.3.4 Boundary Conditions and Other Model Inputs.....                                  | 84         |
| 8.3.5 Model Results and Discussion.....  | 87         |
| <b>8.4 Flow at the Fremont Weir Section of Sacramento River .....</b>                  | <b>107</b> |
| 8.4.1 Model Domain and Field Data .....  | 108        |
| 8.4.2 Model Development .....  | 110        |
| 8.4.3 Boundary Conditions .....  | 113        |
| 8.4.4 Low Discharge Results and Comparison with ADCP Data .....                        | 116        |
| 8.4.5 High Discharge Results and Comparison with ADCP Data .....                       | 128        |
| <b>9. References.....</b>  | <b>138</b> |
| <b>Attachment A. Full Conference #1 .....</b>  | <b>145</b> |
| <b>Attachment B. Full Conference #2 .....</b>  | <b>145</b> |
| <b>Attachment C. Full Conference #3 .....</b>  | <b>145</b> |
| <b>Attachment D. Final Report of Prof. Liu.....</b>                                    | <b>145</b> |

# 1. Background

Reclamation Science and Technology Office and USACE sponsored a workshop in 2012 on large wood (LW) structures in fluvial environments. A number of key research needs relevant to Reclamation were identified. The highest priority group included focusing on the risk, safety, and the resultant scour and morphological impacts to streams due to placement of LW structures in rivers. Despite the existence of scour estimation methods such as bridge piers, methods or guidelines do not exist for predicting responses from construction of LW structures. Even with traditional scour methods, they mostly rely on flume data that suffers from scale problems. Field data are scarce and expensive to get and not practical for many projects. In recent years, however, 3D model predictions are becoming feasible with the availability of the state-of-the-art numerical modeling tools. These tools have not been evaluated and tested at Reclamation for LW structures, but they were identified at the workshop to have potential to become the primary quantitative predictive tools. This 3-year research (2014-2016) represents an effort to address the priority issues facing the LW installation at Reclamation projects. The research involves both internal and external engineers and scientists with the objective of determining the feasibility of using suitable modeling tools for LW installation, and the actual development of the modeling capability.

The proposed research intends to answer the following questions:

1. Do modeling tools exist to predict flows around LW and other in-stream structures with the eventual purpose of estimating bed scour and morphological changes caused by LW and in-stream structures?
2. Are these modeling tools adequate, if they exist, for assisting LW design related to risks associated with scour and morphological changes?
3. Can a strategy be defined and a model be developed for such purposes?

There are a number of state-of-the-art numerical modeling tools available to predict flows around in-stream structures. However, these recently advanced models are rarely used for practical applications for LW and in-stream structure design as they were developed mostly for research purpose. In addition, most are difficult to use or are not developed in the desktop computing environment. So the research strategy is that the study is divided into three phases. Phase I is the screening study; Phase II is the mesh development; and Phase III is the 3D model development. The research results and findings of the three phases are documented in this report.

## 2. Results of Screening Study

At the early stage of the research, a number of collaborators have been invited to identify potential existing modeling tools that are free to the public. Collaborators included Professor Fotis Sotiropoulos at the University of Minnesota, Professor Peter Wilcock at the Johns Hopkins University, Professor Jennifer Duan at the University of Arizona, and Professor Xiaofeng Liu at the Penn State University. Potential modeling tools evaluated included the following:

- U<sup>2</sup>RANS and SRH-2D: U<sup>2</sup>RANS is a three dimensional (3D) numerical model developed at the University of Iowa and modified and improved for realistic river flows at Reclamation. SRH-2D is a two-dimensional (2D) depth-averaged model developed at Reclamation.
- CART3D: A NASA developed public domain model suitable for automated generation of 3D meshes to represent complex shapes of LWD and other in-stream structures.
- VSL3D: High-resolution 3D large eddy simulation (LES) models may be included through collaboration with Prof. Sotiropoulos.
- Deflt3D: A recently released 3D model for river flow and sediment transport. It may be evaluated through collaboration with Prof. Duan.
- OpenFOAM: A public-domain CFD model with both mesh generation and CFD modeling modules.

The results of the early screening study are summarized below.

### 2.1 SRH-2D and U<sup>2</sup>RANS

SRH-2D is a two-dimensional (2D) depth-averaged hydraulic and sediment transport model for river systems developed at the Bureau of Reclamation. It has been widely used for engineering projects at Reclamation and by outside institutions.

SRH-2D has a few salient features making it ideal for engineering applications. First, SRH-2D uses a flexible mesh that may contain arbitrarily shaped cells. In practice, a hybrid mesh of quadrilateral and triangular cells is normally adopted that uses quadrilaterals in the main stream and near structures and triangles in the floodplain and transition zones. The hybrid mesh achieves the best compromise between accuracy and computing efficiency, and it is relatively easy to generate with SMS software. Second, SRH-2D adopts very robust (stable) numerical schemes with a seamless wetting-drying algorithm. Reliable and stable solutions may be obtained with few tuning parameters. Third, SRH-2D has been developed with the objective of ease-of-use. Users do not have to memorize many commands; they are guided by a preprocessor in a question-and-answer session.

## 2. Results of Screening Study

The preprocessor provides guidelines on how to select input parameters. The SRH-2D model, along with its manual and selected publications, are freely downloadable. The model has been well documented and will not be repeated here. For the purposes of this research, the primary use of SRH-2D is to predict the water surface elevation for river engineering applications so that the results may be used by U<sup>2</sup>RANS.

U<sup>2</sup>RANS is a three-dimensional (3D) Unsteady and Unstructured Reynolds Averaged Navier-Stokes solver. The code was developed by Dr. Yong Lai while he was appointed as the senior research staff and adjunct associate professor at the Iowa Institute of Hydraulic Research, University of Iowa. The model is highly accurate, well verified and validated, and has been successfully applied to many research and engineering projects.

Briefly, U<sup>2</sup>RANS is a comprehensive general-purpose model. Three-dimensional hydraulic flow models such as U<sup>2</sup>RANS are accurate and mature tools, which have been routinely used to address many hydraulic engineering problems such as:

- Flow hydrodynamics in pools and river reaches;
- Detailed flow characteristics around hydraulic structures;
- Hydraulic impact of different project alternatives;
- Fish passage facility design and evaluation;
- Thermal mixing zone determination;
- Design optimization, reservoir/lake stratification, selective cold water withdrawal, etc.

The main limitation is that they are usually applied to a river reach less than five miles in length due to their large requirement for computer power.

U<sup>2</sup>RANS uses state-of-the-art, unstructured CFD technology, unifies multi-block structured mesh (quad or hex) and unstructured mesh (quad, triangle, tet, hex, wedge, pyramid, or hybrid) elements into a single platform, and combines 2D and 3D solvers in a common framework. A draft User's Manual is available, which provides a more detailed description about the general features and capabilities (Lai, 2003). Many difference physical processes may be modeled and sample processes include:

- Accurate solution of full three-dimensional water flows with complex geometry (the Navier-Stokes equations)
- 3D effects, such as secondary flows at the meandering bends and point bars, vortex/eddy generation due to hydraulic structures, vertical flow characteristics, are accurately captured; and
- Water temperature transport is simulated using the energy conservation equation

## Quantitative Modeling Tools for Large Wood

The current version lacks the mobile-bed sediment transport simulation. The sediment capability, however, is under development, and is funded by Taiwan Water Resources Agency (WRA).

The model inputs include detailed bathymetric data and hydraulic structure geometric data, river discharge, and water surface elevation at the downstream boundary. The model output include the 3D spatial distribution of velocity magnitude and flow direction, location and strength of flow eddies and vortices, secondary flows due to meandering, bed shear stresses, water surface elevation distribution and backwater effect. The potential use of output results include the evaluation of erosion/deposition potential at the point bar due to secondary flows, assessment of scouring potential due to hydraulic structures, hydraulic impact assessment of modified or new structures, etc.

Numerous applications have been made and some are documented in many publications. U<sup>2</sup>RANS related papers are listed below, with the first five papers discussing the basic theory and numerical procedures.

- Lai, Y.G. (2002). "User's Manual for U2RANS: An Unsteady and Unstructured Reynolds Averaged Navier-Stokes Solver – A Draft," IIHR draft document, University of Iowa.
- Lai, Y.G., Weber, L.J., Patel, V.C. (2003a). "A non-hydrostatic three-dimensional method for hydraulic flow simulation - part I: formulation and verification," ASCE Journal Hydraulic Engineering, 129(3), 196-205.
- Lai, Y.G., Weber, L.J., Patel, V.C. (2003b) "A non-hydrostatic three-dimensional method for hydraulic flow simulation - part II: application," ASCE Journal Hydraulic Engineering, 129(3), 206-214.
- Lai, Y.G. (2000). "Unstructured grid arbitrarily shaped element method for fluid flow simulation," AIAA Journal, 38 (12), 2246-2252.
- Lai, Y.G., Weber, L., Patel, V.C. (2000). U2RANS: a comprehensive hydraulic flow simulation code – its development and application, Proceedings 4th Int. Conference on HydroInformatics, Iowa City, IA.
- Lai, Y.G. (1997) "An unstructured grid method for a pressure-based flow and heat transfer solver," Numerical Heat Transfer, Part B, 32, 267-281.
- Li, S., Lai, Y.G., Weber, L.J., Silva, J.M., Patel, V.C. (2003) "Validation of a three-dimensional model for water-pump intakes", to appear in IAHR Journal Hydraulic Research.
- Lai, Y.G., Weber, L.J. (2001). Three-dimensional hydraulic simulation of wetting-drying process, 29th IAHR Congress, Beijing, China, Sept. 16-21, 2001.
- Weber, L.J., Huang, H., Lai, Y.G. (2001). Numerical modeling of total dissolved gas downstream of a spillway, 29th IAHR Congress, Beijing, China, Sept. 16-21, 2001.
- Goodwin, R.A., Nestler, J.M., Weber, L.J., Lai, Y.G., Loucks, D.P. (2001). Ecologically sensitive hydraulic design for rivers: lessons learned in coupled modeling for improved fish passage, Proc. ASCE Specialty

## 2. Results of Screening Study

Conference on Wetlands Engineering and River Restoration, Reno, NV, August 25-31, 2001.

- Ettema, R., Chen, Z., Lai, Y.G. (2001). Hydraulic performance of offshore water intakes: some CFD findings,” Proc. Ports and Ocean Engineering under Arctic Conditions Conference, Ottawa Canada, August, 2001.
- Lai, Y.G. and Patel, V.C. (2001). Effect of boundary conditions on simulation of flow in the T99 draft tube, Turbine99-2nd ERCOFTAC Workshop on Draft Tube Flow, Alvkarleby, Sweden, June 17-20 2001.
- Lai, Y.G. and Patel, V.C. (1999). CFD simulation and assessment of the draft tube flow,” Turbine-99, ERCOFTAC Workshop on Draft Tube Flow, Porjus, Sweden, June 1999.
- Weber, L.J., Lai, Y.G., Blank, J.C., Andrade, F.De. (2000). Rocky Reach Dam: a comprehensive look at the calibration of a numerical model applied to fish passage,” Proceedings 4th Int. Conference on HydroInformatics, Iowa City, IA.
- Lai, Y.G., Weber, L.J., Moedinger, J. (2001). A three-dimensional unsteady method for simulating river flows, Proceedings ASCE World Water and Environmental Resource Congress, Orlando, FL, May 20-24, 2001.
- Weber, L.J., Lai, Y.G., Andrade, F. (2001). Three-dimensional numerical model validation: issues and directions, Proceedings ASCE World Water and Environmental Resource Congress, Orlando, FL, May 20-24, 2001.
- Huang, W. and Lai, Y.G. (2000). A parallel implementation of a multi-block three-dimensional incompressible flow solver on a DSM machine, Proceedings 4th Int. Conference on HydroInformatics, Iowa City, IA.
- Li, S., Lai, Y.G., Patel, V.C., Silva, J. M. (2000). Water-intake pump bays: three-dimensional flow modeling, validation, and application, Proceedings 4th Int. Conference on HydroInformatics, Iowa City, IA.

A specific application of  $U^2$ RANS is to the river reach upstream of the Palo Verde Diversion Dam on the Colorado River. The model was used to simulate the flow near a point bar and to evaluate the impact of installing a training structure to protect the bank erosion. Model outputs, which are illustrated in Figure 1 include geometry with the training structure, simulated velocity and secondary flow, and the predicted bed shear stress.

# Quantitative Modeling Tools for Large Wood

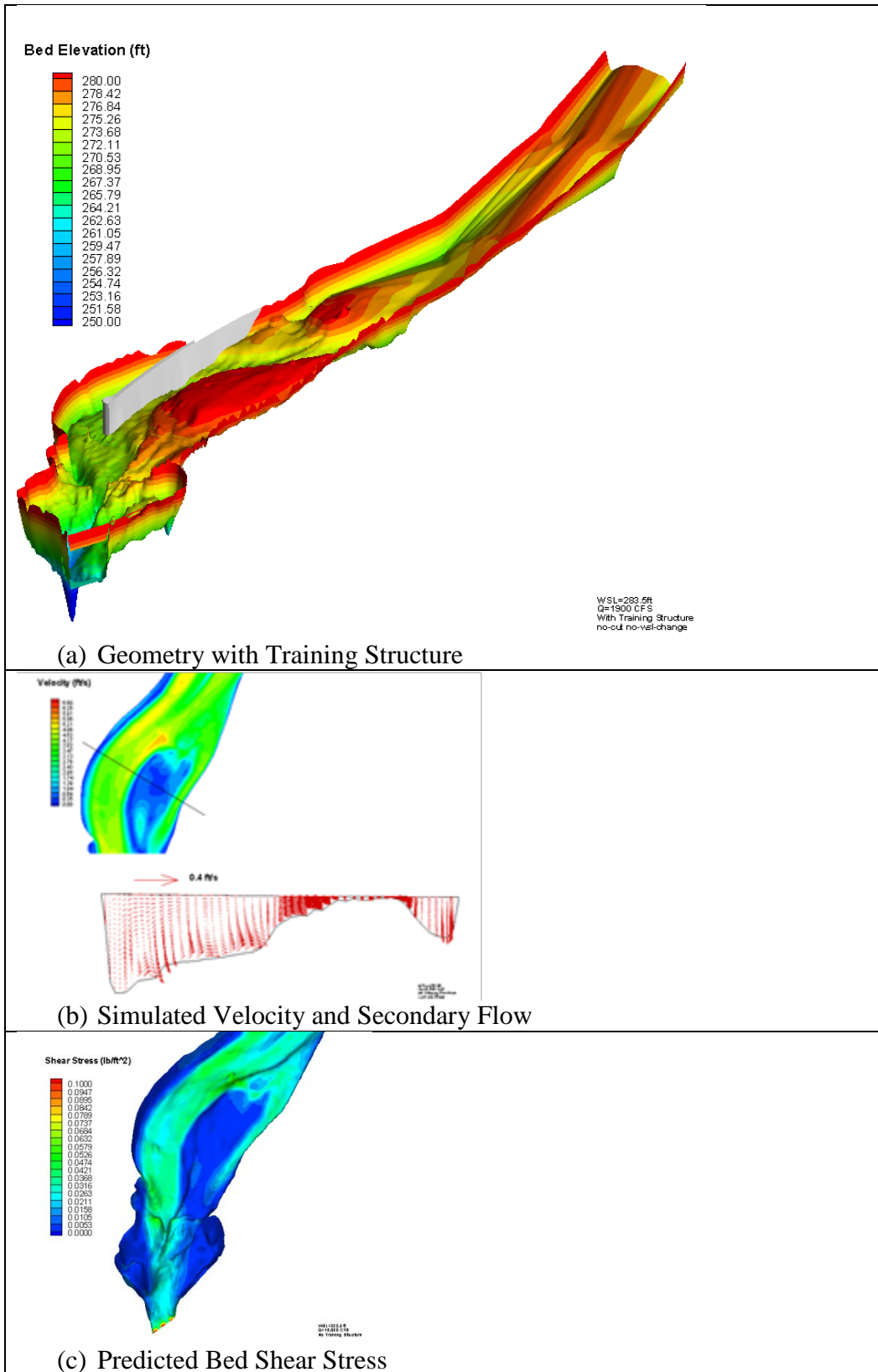


Figure 1. Example output from U2RANS Model Application on Colorado River

### 2.2 CART3D

Cart3D is a high-resolution inviscid analysis package for conceptual and preliminary aerodynamic design. It allows users to perform automated CFD analysis on complex geometry. The package includes utilities for geometry import, surface modeling and intersection, mesh generation, flow simulation and post-processing of results. The geometry and mesh generation portion of Cart3D is our interest as the package is highly automated so that geometry acquisition, and mesh generation can usually be performed within a few minutes on most current desktop computers.

Geometry enters into Cart3D in the form of surface triangulations. These may be generated from within a CAD packages, from legacy surface triangulations or from structured surface grids. Cart3D uses adaptively refined Cartesian grids to discretize the space surrounding a geometry and cuts the geometry out of the set of "cut-cells" which actually intersect the surface triangulation. The flow solver is parallel and can take full advantage of multi-core and multi-cpu hardware.

Collaboration has been established with Professor Jennifer Duan at the University of Arizona through a grant. CART3D has been obtained from NASA and the model was installed at both the University of Arizona by Prof. Duan and at Reclamation. Prof. Duan and her students have been able to

- Establish the procedure to run CART3D
- Develop the necessary tools (Matlab) to generate CAD objects as inputs to CART3D; and
- Demonstrate the mesh generation process with CART3D using a simple test case: the flow around a sphere.

However, her study showed that CART3D had a lot of issues and restrictions in applications to the LW structures. For example, it considers only external flows around a body and river bathymetry cannot be taken into consideration. It is not selected for further evaluation with the project.

### 2.3 VSL3D

A conference call with Professors Fotis Sotiropoulos at the University of Minnesota and Peter Wilcock at the Johns Hopkins University discussed the capabilities of VSL3D. Both agreed to provide in-kind service to the initial screening study, with the objective of determining VSL3D, a high-resolution 3D large eddy simulation (LES) model developed by Prof. Sotiropoulos, may be valuable to the LW modeling. Basic information about the model and selected study cases are discussed below.

VSL3D (<http://cfdlab.safl.umn.edu>) is developed by Professor Fotis Sotiropoulos and his students at the St. Anthony Falls Laboratory (SAFL) of University of Minnesota. VSL3D can: (1) resolve turbulence in arbitrarily complex waterways with embedded natural and/or man-made hydraulic structures using unsteady Reynolds-averaged Navier-Stokes (URANS) or Large-Eddy Simulation (LES) turbulence models (Kang et al. 2011; Kang and Sotiropoulos 2011, 2012a); (2) account for the presence of the water-surface with level-set method in a coupled, fully non-linear manner (Kang and Sotiropoulos 2012b); and (3) simulate sediment transport (suspended- and bed-load), conservative /non-conservative contaminants and nutrients transport, density current, and morphodynamics in real-life waterways and past hydraulic structures with complex geometries (Escauriaza and Sotiropoulos 2011a,b; Khosronejad et al. 2011; 2012a; 2012b). Two types of inputs data are required for VSL3D model to simulate a specific test case which includes geometrical data of the river and immersed subjects and model setup information. The geometrical information describes the geometry of waterway and/or any immersed subject in the simulation domain (e.g. river's bed bathymetry and mounted bridge piers or LW). Various types of scanned or surveyed geometrical data can be imported to VSL3D. The setup information is required to be introduced to the model through a text file which will be read at the beginning of simulations and includes information about the type of desired turbulence model to be used, time step, and duration of simulation. The output variables of VSL3D consist of 3D flow velocity components, pressure, and shear stress on the stream bed, banks, and any other immersed subjects such as LWD as a function of time. 3D distribution of bed- and suspended sediment load in the computational domain plus the bathymetry of the water way at equilibrium can be simulated by VSL3D. VSL3D is also capable of simulating the transport of any scalar term including pollutions, nutrients, and so on in the real-life stream environments.

The VSL3D employs a novel computational approach based on the Curvilinear Immersed Boundary Method (CURVIB) (Ge and Sotiropoulos 2007; Borazjani et al. 2008), which can account for arbitrarily complex domains with embedded arbitrarily complex rigid (e.g. hydraulic structures) or dynamically evolving boundaries that interact with the flow in a fully coupled manner (e.g. the sediment-water and/or the air-water interfaces in rivers). The method has been extended by Kang et al. (2011) to carry out URANS and LES of turbulent flows

## 2. Results of Screening Study

in natural waterways using wall models for bridging the gap between the first grid node in the fluid domain and the wall. The VSL3D model is fully parallelized using Message Passing Interface (MPI) and scales efficiently on thousands of CPUs. The predictive capabilities of the model in simulating flows in natural streams were demonstrated through extensive comparisons with laboratory and field scale measurements in Kang et al. (2011) and Kang and Sotiropoulos (2012a, b). Kang and Sotiropoulos (2012b) extended the VSL3D to incorporate a two-phase flow formulation with level-sets to enable coupled simulations of free-surface effects in turbulent flows over arbitrarily complex bathymetry. Khosronejad et al. (2011; 2012; 2013) developed the coupled hydro-morphodynamic version of the VSL3D and applied it to simulate streambed erosion and scour under clear water conditions in curved open channels (Khosronejad et al 2011) and past bridge piers (Khosronejad et al. 2012) and stream-restoration rock structures (Khosronejad et al. 2013). More recently the VSL3D has been further extended to simulate sediment transport under live-bed conditions and has been shown to be able to simulate realistic bedforms across a range of scales: from cm-scale ripples in a laboratory flume to tens of meters scale dunes in large meandering rivers.

Some of the references cited above are as follows:

- Borazjani, I., Ge, L., and Sotiropoulos, F. (2008). "Curvilinear immersed boundary method for simulating fluid structure interaction with complex 3D rigid bodies." *Journal of Computational Physics*, 227, 7587–7620.
- Ge, L. and Sotiropoulos, F. (2007). "A numerical method for solving the 3D unsteady incompressible Navier Stokes equations in curvilinear domains with complex immersed boundaries." *Journal of Computational Physics*, 225, 1782–1809.
- Gilmanov, A. and Sotiropoulos, F. (2005). "A hybrid Cartesian/immersed boundary method for simulating flows with three-dimensional, geometrically complex, moving bodies." *Journal of Computational Physics*, 207, 457.
- Kang, S., Lightbody, A., Hill, C. and Sotiropoulos, F. (2011), "High-resolution numerical simulation of turbulence in natural waterways," *Advances in Water Resources*, Volume 34, pages 98-113.
- Kang, S. and Sotiropoulos, F. (2011), "Flow phenomena and mechanisms in a field-scale experimental meandering channel with a pool-riffle sequence: Insights gained via numerical simulation," *J. of Geophysical Research*, Volume 116, F03011.
- Kang, S., Borazjani, I., Colby, J. A. and Sotiropoulos, F. (2012), "Numerical simulation of 3D flow past a real-life marine hydrokinetic turbine," *Advances in Water Resources*, Volume 39, pages 33-43.
- Kang, S. and Sotiropoulos, F. (2012a), "Assessing the predictive capabilities of isotropic, eddy-viscosity Reynolds-averaged turbulence models in a natural-like

## Quantitative Modeling Tools for Large Wood

- meandering channel,” *Water Resources Research*, Volume 48, W06505, doi:10.1029/2011WR011375.
- Kang, S. and Sotiropoulos, F. (2012b), “Numerical modeling of 3D turbulent free surface flow in natural Waterways,” *Advances in Water Resources*, Volume 40, pages 23-36.
  - Kang, S., Khosronejad, A., and Sotiropoulos, F., (2012) “Numerical simulation of turbulent flow and sediment transport processes in arbitrarily complex waterways,” *Environmental Fluid Mechanics*, Memorial Volume in Honor of Prof. Gerhard H. Jirka, Eds. W. Rodi & M Uhlmann, CRC Press (Taylor and Francis group), pp. 123-151.
  - Khosronejad, A., Kang, S., Borazjani, I. and Sotiropoulos, F. (2011), “Curvilinear immersed boundary method for simulating coupled flow and bed morphodynamic interactions due to sediment transport phenomena,” *Advances in Water Resources*, Volume 34, pages 829-843.
  - Khosronejad, A., Kang, S. and Sotiropoulos, F. (2012), “Experimental and computational investigation of local scour around bridge piers,” *Advances in Water Resources*, Volume 37, pages 73-85.
  - Khosronejad, A., Hill, C., Kang, S., and Sotiropoulos, F. (2013), “Computational and experimental investigation of scour past laboratory models of stream restoration rock structures,” *Advances in Water Resources*, Volume 54, pages 191-207.

## 2.4 Delft3D

Collaboration has been established with Professor Jennifer Duan at the University of Arizona through a grant. Dr. Duan has evaluated Delft3D, a recently released 3D model for river flow and sediment transport, using a number of application cases.

Delft3D is developed by Delft Hydraulics. Its application areas include the following:

- Tide and wind-driven flows (i.e.. storm surges)
- Stratified and density driven flows
- River flow simulations
- Simulations in deep lakes and reservoirs.
- Simulation of tsunamis, hydraulic jumps, bores and flood waves
- Fresh-water river discharge in bays
- Slat intrusion
- Thermal stratification in lakes, seas and reservoirs
- Cooling water intakes and waste water outlets
- Transport of dissolved material and pollutants
- Sediment transport and morphology
- Wave-driven currents

- Non-hydrostatic flows

Delft3D-FLOW is available from <http://oss.deltares.nl/web/opendelft3d/source-code>. Delft3D model suite (or software) consists of six modules: Delft3D-flow, Delft3D-Wave, Delft3D-Part, Delft3D-Eco, Delft3D-Sed. The Delft3D-flow is the hydrodynamic module that provides hydrodynamic conditions including velocities, water elevations, density, salinity, vertical eddy viscosity, and vertical eddy diffusivity to other modules. Delft3D-FLOW is capable of simulating three dimensional (3D) unsteady incompressible flow and transport phenomena resulting from tidal and/or meteorological forcing.

Delft3D-flow solves the Navier-Stokes equations for an incompressible fluid under the shallow water and the Boussinesq assumptions. In the vertical momentum equation the vertical accelerations are neglected that leads to the hydrostatic pressure equation. In the 3D models the vertical velocities are computed from the continuity equation. In the horizontal direction Delft3D-flow uses orthogonal curvilinear co-ordinates. Two coordinate systems are supported: 1) Cartesian co-ordinates ( $\xi, \eta$ ) and 2) spherical co-ordinates ( $\lambda, \phi$ ). The vertical coordinates can be 1)  $\sigma$ -grid (body-fitted grid); or 2) Z-grid (Cartesian uniform grid). The governing equations are written in curvilinear coordinate.

Delft3D-FLOW offers two different vertical grid systems  $\sigma$ -grid and Z-grid, and four turbulence closure models: constant eddy viscosity coefficient, algebraic eddy viscosity model,  $k$ - $L$  model, and  $k$ - $\epsilon$  model. Delft3D-FLOW also has a facility to define the bed and flow resistance on each sub-grid using a function called Trachytopes. Three classes are available in the Trachytopes function, area class, line class and point class. The area class has three types: the first type is a constant coefficient for bed roughness, such as White Colebrook, Chezy, and Manning's coefficients, the second type accounts for the form resistance resulting from sand dunes, and the third type is for the roughness coefficient in vegetated channels. The first type often remains a constant with time, while the second type is determined by dune height, and the third by vegetation properties. The line class of Trachytopes function can be used to approximate flow resistance for elements with hedge, bridge piers, and other structures. The point class can be used to represent a set of point flow resistance elements, such as groups of individual tree or smaller scale plant. Geometric data of simulation domain including bathymetry and boundaries, boundary friction coefficient (e.g., Manning's  $n$  values), bed sediment gradation, cohesive or non-cohesive sediment, upstream and downstream boundary conditions for flow (e.g. flow discharge, water surface elevation), upstream boundary conditions for sediment load. Delft3D-Flow solves the Reynolds Averaged Navier-Stokes equations on a structured staggered curvilinear grid using a finite difference scheme (Stelling and van Kester 1994). The governing equations are solved with an Alternating Direction Implicit (ADI) technique (Stelling 1984).

## Quantitative Modeling Tools for Large Wood

A number of cases have been simulated with Delft3D. The first case is to simulate the vegetation impacts on flow field. The case has been documented by a paper of Khalid and Duan, "Case Study: Three-dimensional Hydrodynamic Simulation of Tidal Flow through a Vegetated Marsh Area," which was submitted to J. Hydraulic Engineering for review. The second case is to model sediment plug occurring in Rio Grande. The case is documented in a manuscript by Posner and Duan, "3D numerical modeling of sediment plugs in Rio Grande River," which is submitted to Earth Surface Process and Land Forms for review. The third case is to simulate Lake Mills Drawdown Experiments. This study is funded by Reclamation and results have been documented in a project report by Khalid and Duan, "Simulation of Lake Mills Drawdown Experiments using Delft3D."

## 2.5 OpenFOAM

Collaboration has also been established with Prof. Xiaofeng Liu at the Penn State University. Prof. Liu is an expert in 3D computational fluid dynamics (CFD) model development and applications for river engineering. He builds his models around an open-source, publically available model, OpenFOAM. Prof. Liu developed a novel immersed boundary technique (IBT) that takes complex geometries into consideration automatically by the CFD model. The IBT has high potential to be suitable for modeling flows around LWD structures and it is the reason Prof. Liu was invited to participate in the present study.

Dr. Liu has been using OpenFOAM<sup>®</sup> for almost ten years. The history of Dr. Liu's involvement of the open source platform OpenFOAM<sup>®</sup> goes back to his Ph.D. thesis work at University of Illinois at Urbana-Champaign. His doctoral research studied the flow field and sediment scour around structures such as bridge piers and offshore foundations. He also used OpenFOAM<sup>®</sup> to study the erosion problem in the St. Clair River in Great Lakes region. Besides doing the research using OpenFOAM<sup>®</sup> by himself, he has also shared his experience with the research community through workshops and short courses on OpenFOAM<sup>®</sup>. Regarding OpenFOAM<sup>®</sup> itself, it is an open source computational physics platform (<http://www.openfoam.com/>). It has gained a lot of popularity in many disciplines across most areas in engineering and science. It was originally designed for computational fluids. Now it has been used as a general framework for solving differential equations. It uses finite volume method as its main discretization scheme. Key required inputs by a user include bathymetry of the river section, geometry of the LWD or any other in-stream structures, inflow and outflow (discharge, stage, etc.), sediment composition in the stream, selection of turbulence models, selection of numerical schemes, etc. Key outputs include 3D flow field, shear stresses on the river bed and banks for the evaluation of erosion potentials, forces on the LWD or other structures for the evaluation of their stability.

OpenFOAM uses finite volume method to discretize governing equations. For 3D river flows, the equation it solves is the Navier-Stokes equation which describes

## 2. Results of Screening Study

the conservation of mass and momentum of fluids. For turbulent flows, which are usually the case for rivers and streams, it provides a library of turbulence models. It also provides parallel computation capability using MPI.

Some of the applications performed by Prof. Liu are discussed below.

Local scour around object was carried out. Dr. Liu implemented a 3D local scour simulation solver in OpenFOAM, which has three components: the flow field solver, the sediment transport solver, and the mesh deformation solver. The flow field solver comes with the OpenFOAM package and the user can choose from a library of turbulence models (RANS or LES). It also has the capability for free surface flows. The fluid solver simulates the flow field and gives the bottom shear stresses. With the results from the flow solver, sediment transport (both bed load and suspended load) can be solved. Erosion and deposition will change the bathymetry around the object, which changes the computational domain. Since unstructured mesh is used in OpenFOAM, a special solver is designed to automatically deform the mesh. The details can be found in Liu and García (2008).

## Quantitative Modeling Tools for Large Wood

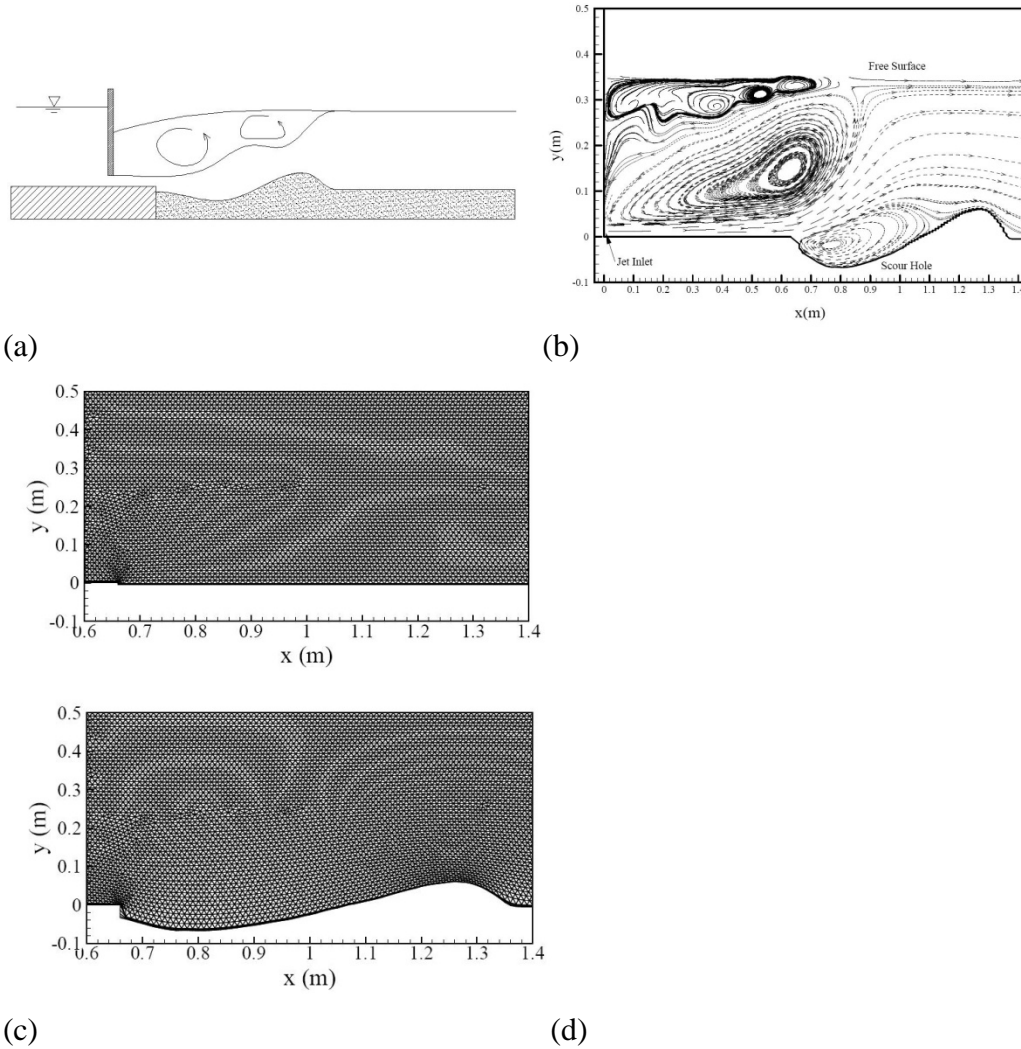


Figure 2. Turbulence wall jet scour simulation using OpenFOAM (Liu and García, 2008): (a) Scheme of the case, (b) Flow field, (c) Initial mesh, and (d) Final mesh.

Hydrodynamics in large rivers is simulated using OpenFOAM for bend flows in the St. Clair River for the evaluation of scour and erosion potentials. In this study, the morphological change was not activated. Instead, only the hydrodynamics were simulated with RANS turbulent model. The bed shear stress was evaluated at different flow discharges (low, medium, and high) to check the potential of erosions. The details can be found in Liu et al. (2011).

## 2. Results of Screening Study

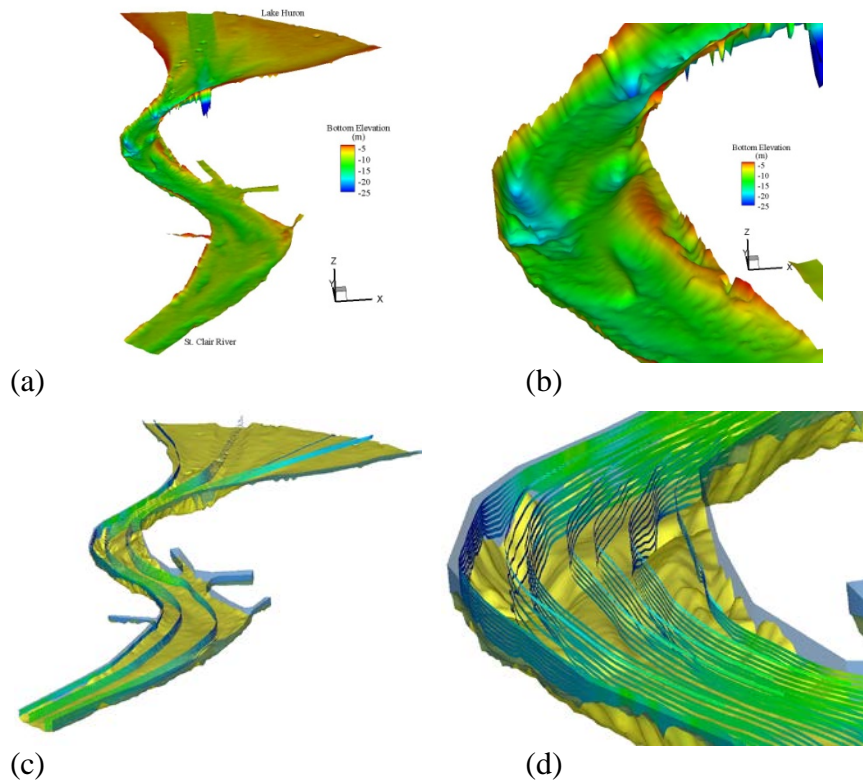


Figure 3. OpenFOAM simulation of 3D hydrodynamics in a large river (Liu et al., 2011): (a) Overall bathymetry of the St. Clair River entrance, (b) Local bathymetry in the bend, (c) Overall flow streamlines, and (d) Flow streamlines over the dunes in the bend.

Scour protection assessment is modeled using OpenFOAM. A new immersed boundary method is developed to do pore-scale modeling of riprap and other porous scour protections. The details can be found in Liu et al. (2012) and similar idea has also been documented in Nielsen et al. (2013).

The major incentive, similar to the idea of this proposal, is to relieve the burden of the user to generate meshes for complicated geometry and objects. In a typical design of using LWD for river restoration, the geometries of wood stems and other auxiliary components are so complicated that a body-fit mesh is almost impossible. The same situation happens in riprap where large amount of armor units are loosely packed together.

Dr. Liu has developed an innovative way to handle problems like these. In his model, he used the collision detection and rigid body dynamics algorithms to generate the physical and realistic spatial arrangement of different objects (LWD or rocks) in the domain. This part of the model mimics the physical process of placing these objects in the rivers during construction.

## Quantitative Modeling Tools for Large Wood

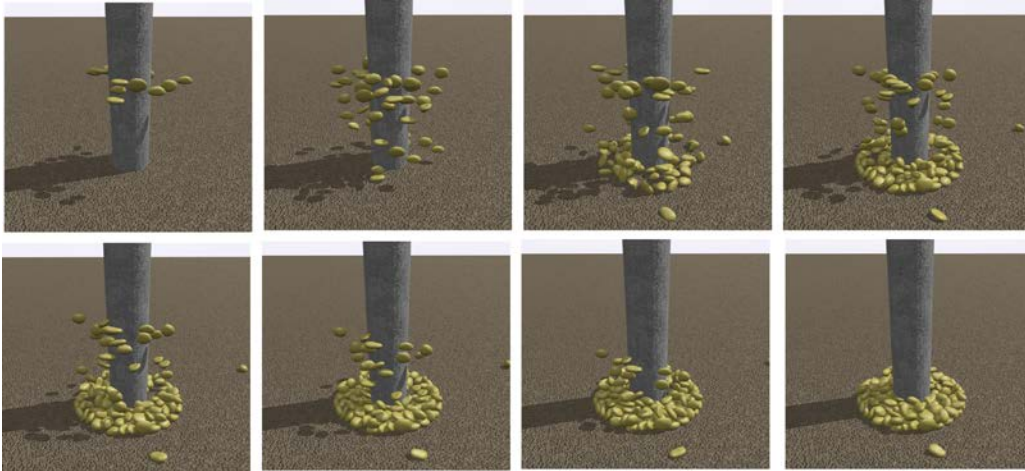


Figure 4. Computer simulation of the placing (dumping) process of riprap rocks into the domain around a pile. This part of the model uses the collision detection and rigid body dynamics algorithms.

When the spatial arrangement of the objects is available, they are represented in the fluid solver model by the immersed boundary method. Again, there is no need to generate a body-fit mesh for them.

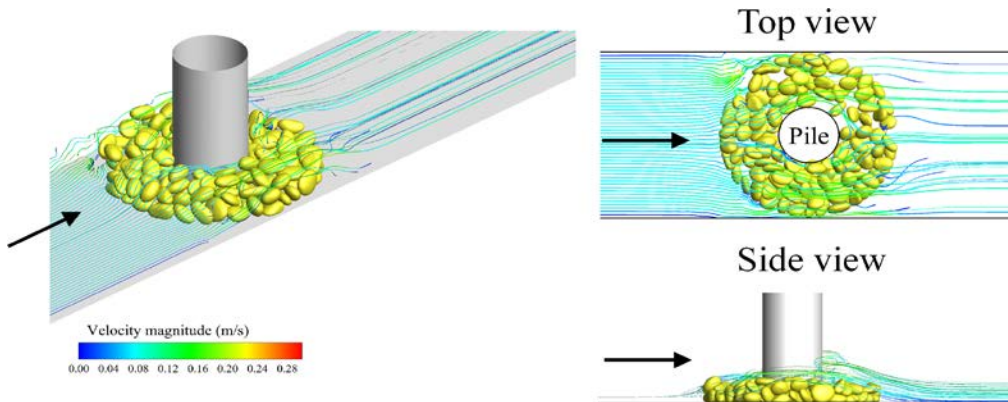


Figure 5. Simulated flow structure around the riprap (scour protection) and the pile. Immersed boundary method was used and no body-fit mesh for the rocks is needed.

Some of the references of the study are included below:

- X. Liu and M.H. García (2008). A 3D Numerical Model with Free Water Surface and Mesh Deformation for Local Sediment Scour. *Journal of Waterway, Port, Coastal, and Ocean Engineering*. 134(4): 203-217.
- X. Liu, G. Parker, J. Czuba, K. Oberg, J.M. Mier, J.L. Best, D.R. Parsons, P. Ashmore, and M.H. Garcia (2011). Sediment Mobility and Bed Armoring in the St. Clair River: Insights from Hydrodynamic Modeling. *Earth Surface Processes and Landform*, 37(9):957-970.
- X. Liu, Y. Jiang, and R. Sinir, Simulation of flow field around and inside porous scour protection with physical and realistic particle configurations

from computer graphics, Computational Methods in Water Resources XIX International Conference, Champaign, IL, 2012

- A.W. Nielsen, X. Liu, B.M. Sumer, J. Fredsoe (2013). Flow and Bed Shear Stresses in Scour Protections around a Pile in a Current, *Coastal Engineering*, 72:20-38

### 2.6 Summary

The screening study has evaluated five modeling tools as discussed above. The following are our recommendations.

U<sup>2</sup>RANS and SRH-2D are developed by Dr. Yong Lai, the PI of this study. Both models have been updated and demonstrated. This scoping study finds that U<sup>2</sup>RANS is potentially applicable to the LWD modeling since it adopts the arbitrarily shaped mesh elements and has the capability to import the complex cut cells and perform the CFD modeling. U<sup>2</sup>RANS is found to be practical and suitable for modeling flows around LWD structures. The morphological components of the SRH-2D model are found to be easily incorporated into U<sup>2</sup>RANS so that the sediment transport and morphological modeling can also be carried out with U<sup>2</sup>RANS. U<sup>2</sup>RANS and SRH-2D will continued to be developed in this research.

CART3D is an open source mesh generation software developed by NASA. CART3D has been installed at Reclamation. Dr. Lai has hired a student intern, Monica Sullivan, to work with CART3D. After much effort of evaluating the software, it is decided to be discontinued as a better product (snappyHexMesh provided by OpenFOAM) is found.

OpenFOAM and the immersed boundary technique (IBT) implemented in OpenFOAM has been developed by Prof. Liu. It is found to have great potential in modeling flows and sediment transport around the LWD structures. Major advantages of OpenFOAM include: easy mesh generation as no boundary meshes are needed; easy accessibility due to its open-source public-domain policy; and wide range of technical developments and supports in the future. IBT and OpenFOAM will be included in the full-proposal study and Prof. Liu will be the collaborator of the study effort.

VSL3D, developed by Prof. Fotis Sotiropoulos at the Univ. of Minnesota, has been demonstrated with several cases. Evaluation of the model shows that VSL3D is a very good and accurate modeling tool for flows around LWD structures; it is probably one of the best modeling tools available today. However, VSL3D requires the use of supercomputers, along with tremendous modeling expertise required of a user. The screening study concludes that VSL3D is not yet practical for engineers, who have availability of only desktop computers, to use for project design purposes. The model, however, can be a candidate in the future when computing power has been drastically increased. VSL3D is not to pursued further.

## **Quantitative Modeling Tools for Large Wood**

Delft3D model has been evaluated by Prof. Duan using selected cases for its capabilities for morphological modeling. Our evaluation determines that Delft3D is very limited in its ability to simulate flows and sediment transport around LWD structures due to the use of restrictive meshes the model can handle. Delft3D is not to be pursued further in this project.

### 3. Literature Review

Early three-dimensional (3D) flow and sediment models are mostly based on the hydrostatic assumption, i.e., shallow water is assumed in which the characteristic flow length scale in the vertical direction is much smaller than the characteristic length scale in the horizontal direction. These are called HA (Hydrostatic Assumption) models in this report. These models are widely used in the coastal and oceanic simulation; they are also widely used for lake, reservoir and river modeling. 3D HA modeling represents an improvement over the 2D depth-averaged modeling by providing a viable way to obtain vertical distribution of important variables such as velocity components and suspended sediment concentration. In the following, only non-hydrostatic 3D flow and sediment models are reviewed.

3D CFD models for hydraulic engineering applications have attracted much attention in the last two decades owing to their greater versatility and accuracy. Applications of 3D non-hydrostatic models become possible owing to advances in computer technology and numerical algorithms. These models are based on the steady or unsteady Reynolds averaged Navier-Stokes (RANS) equations (they are called RANS models in this report), coupled with appropriate turbulence models. RANS models are distinguished from other 3D modeling methods such as the large eddy simulation (LES) and direct numerical simulation (DNS).

Most of the reported 3D RANS models are limited to flow modeling without mobile-bed capability. Early studies include the following: Sotiropoulos and Patel (1992) developed a finite-difference model using the structured mesh. This was later modified and applied to simulate flows downstream (Sinha 1996) and upstream (Meselhe and Weber 1997) of Wanapum Dam on the Columbia River and upstream of Lower Granite Dam on the Snake River (Huang and Weber 1998). Lai et al. (2003) developed a finite-volume unstructured mesh model that has been applied to many river engineering projects (e.g., Li et al., 2004; Weber et al. 2004). The primary contribution of the model by Lai et al. (2003) is that the mesh can be very flexible as polyhedrons may be used for mesh shape. Other finite-difference, finite-volume, or finite-element RANS models have been reported such as Demuren (1993), Olsen and Melaaen (1993), Behr and Tezduyar (1994), Cokljat and Younis (1995), Yost (1995), Casulli (1997), Berger and Stockstill (1999), Ye and McCorquodale (1998), Huang (2000), etc. Most finite-difference and finite-volume 3D models used structured grids with hexahedral cells, while finite element models used unstructured grids with fixed mesh shapes (hexahedrons or tetrahedrons).

Mahadevan et al. (1996a, b) reported a non-hydrostatic ocean model, along with conservative substance transport, in order to resolve flow phenomena with horizontal length scales of 100 km. The model, however, can only be classified as a weakly non-hydrostatic model. In the vertical direction a sigma grid is used and

## Quantitative Modeling Tools for Large Wood

in the horizontal plane a boundary-fitted curvilinear mesh is adopted. The model solution procedure consists of two steps: In the first step a hydrostatic computation is carried out while in the second step the effect of non-hydrostatic pressure is taken into consideration. A similar model was proposed by Casulli and Stelling (1998) who used Z-grid in the vertical direction and an orthogonal grid in the horizontal plane. In these models, there is only a one way coupling between the hydrostatic and the non-hydrostatic pressure components, because the surface elevation is determined in the first step without taking into account the effect of the non-hydrostatic pressure. This one-way coupling works fine for weakly non-hydrostatic cases. For strong non-hydrostatic cases, however, the two pressure components should be coupled in a tight manner. Such a two-way coupling method was proposed by Casulli (1999) where a correction of the surface elevation was incorporated in the second step. The approach of Casulli (1999) was implemented in the software TRIM-3D.

The above models are based on the fractional step method. The second step of computations always features an unknown related to pressure variable. Deviating from the fraction step method is the model of Fringer et al. (2006). They developed a scheme which uses pressure correction as an unknown, with the dimension of pressure multiplied by the time step. This pressure-correction method is not new, however, and has been used in earlier 3D RANS models (e.g., Lai and Przekwas, 1994 and Lai, 2000). It was shown by Armfield and Street (2002) that pressure-correction method had a higher order of convergence with respect to the time step than the fractional step method. The Fringer method was implemented in the SUNTANS code for coastal ocean simulations. With a similar pressure-correction method for strongly non-hydrostatic flow applications, Ullmann (2008) developed a non-hydrostatic free-surface flow model in the Z-grid formulation.

Many non-hydrostatic models placed the unknowns on a staggered grid. That is, velocities are located at the faces of the discretized cells and pressure is located at cell centers. In the ocean models, Stelling and Zijlema (2003) and Zijlema and Stelling (2005; 2008) proposed a pressure-correction method where pressure is located at the top faces of each cell. This approach is realized in the code TRIWAQ. The collocated approach, in which all main variables are located at cell centers, was shown to be more flexible for general model applications (e.g., Lai and Przekas 1994; Lai 2000; 2003).

Most 3D CFD models in the literature are of the research nature. General-use 3D CFD models which are available are often limited to commercial software. We will not review commercial models since their documentation are often limited. Herein we specifically recommend an open-source 3D CFD model: OpenFOAM - Open source Field Operation And Manipulation. OpenFOAM is a C++ toolbox for the development of customized numerical solvers for the solution of continuum mechanics problems, including computational fluid dynamics (CFD). The code is released as free and open source software under the GNU General Public License. OpenFOAM was developed by OpenCFD Ltd, maintained by the

OpenFOAM Foundation (<http://www.openfoam.org>), and sponsored by the ESI Group, the owner of the trademark to the name OpenFOAM. The original development of OpenFOAM started at Imperial College, London. The model has been released to public use since 2004.

Advantages of OpenFOAM include the following:

- Friendly syntax for partial differential equations;
- Unstructured polyhedral grid capabilities;
- Automatic parallelization of applications written using OpenFOAM high-level syntax;
- Wide range of applications and models ready for use;
- Commercial support and training provided by the developers; and
- No license costs.

We have spent significant time in understanding and using OpenFOAM. The disadvantages of the model, as found by us as well as other users, include the following:

- Absence of an integrated graphical user interface;
- The Programmer's guide does not provide sufficient details, making the learning curve very steep; and
- Lack of maintained documentation, making it difficult for the new users.

Despite its open-source nature, OpenFOAM has been mostly limited to CFD experts. Model customization is very challenging with increasing depth into the OpenFOAM library, owing to a lack of documentation and heavy use of template metaprogramming. We could not find any theoretical papers or reports related to the CFD technologies and algorithms used by the model.

The mobile-bed modeling capability has rarely been developed with 3D CFD model except for some commercial models. A few mobile-bed 3D models are briefly reviewed below.

Olsen (1994) is probably one of the few early developers of 3D RANS with mobile-bed modeling capabilities. His model, SSIIM, is based on the unstructured finite volume method. The model solves hydrodynamic and sediment transport equations and has the capability of simulating sediment transport in a movable riverbed with complex geometries. The model has been used for the modeling of meandering and bed forms in rivers and bed load and suspended load transport of non-uniform sediment and associated sorting and armoring processes. The model has also been extended to such hydraulic engineering applications as spillway modeling, head loss in tunnels, meandering in rivers, turbidity currents, etc. The model has also been used for water quality and habitat studies in river engineering project. Our review suggests SSIIM is probably one of only few models in its category that has been available to public use and is widely tested and validated.

## Quantitative Modeling Tools for Large Wood

Landsberg et al. (1998) developed a fully non-hydrostatic 3D finite-volume model named FAST3D. It used the flux-corrected transport (FCT) and a high-order–high-resolution algorithm. The model can handle complex geometric domains because of the added capabilities that are provided by an efficient parallel implementation of the virtual cell embedding (VCE) algorithms. The sediment component of the model accounts for non-equilibrium bed-load transport rate and advection-diffusion-based suspended load rate.

Wu et al. (2000) reported a 3D RANS and mobile-bed model with the k- $\epsilon$  turbulence model. Special attentions were paid to handle free surface and roughness treatments. In their free surface treatment, the water surface elevation is determined from a 2D Poisson equation derived from 2D depth-averaged momentum equations. The governing equations are solved numerically with the finite-volume method on an adaptive collocated mesh. The suspended sediment module is tested for open channel flows with net entrainment from a loose bed and net deposition. The total-load model is validated by calculating the flow and sediment transport in a 180 degree channel bend with movable bed. In the cases simulated and reported, good agreements were obtained with the measurements. The model was developed as a research code and its applicability to practical applications is yet to be demonstrated.

Zeng et al. (2005) developed a non-hydrostatic 3D model using generalized curvilinear coordinates that and the finite-difference scheme. The model solves the governing equations by integrating them up to the near-wall boundary to avoid any near-wall approximations. The solver uses movable grids in the vertical direction to account for changes in the free-surface elevation. The proper kinematic and dynamic conditions are imposed to account for changes in the bathymetry because of erosion or deposition at the bed. The suspended sediment is modeled by using an advection-diffusion equation with a settling velocity term. The model is a research code and does not seem available for public use.

Other reported research models include Salaheldin et al. (2004), Roulund et al. (2005), Khosronejad et al. (2007), Liu and Garca (2008), and Apsley and Stansby (2008). They are not reviewed in details herein as no significant algorithmic advancements have been developed.

Among above reviewed models, only SSIIM and the Wu models have the capabilities to predict the gradation of sediment mixtures whereas other models are applicable only to uniform sediments. Most models are limited in their sediment modeling capability. A recent review by Khosronejad et al. (2014) concluded that “existing models do not have the sophistication required for handling the real-life waterways with multiple realistic rock-structures embedded in them.”

Probably the most comprehensive 3D RANS model with mobile-bed module is VSL3D (Virtual StreamLab) developed by Professor Sotiropoulos and his colleagues at the Saint Anthony Falls Laboratory, University of Minnesota

### 3. Literature Review

(Khosronejad et al. 2014). VSL3D is a 3D flow and mobile-bed computational model capable of simulating turbulent flow and sediment transport in natural waterways with embedded and arbitrarily complex hydraulic structures. Geometric complexity is handled using the curvilinear immersed boundary (CURVIB) approach of Ge and Sotiropoulos (2007) coupled with wall modeling approach of Kang et al. (2011). VSL3D solves the unsteady Reynolds-averaged Navier-Stokes equations closed with the  $k-\omega$  turbulence model. Bed material transport is simulated by solving the non-equilibrium Exner equation for the bed surface elevation coupled with a transport equation for suspended load. In their latest application (Khosronejad et al. 2014), only a single material size is used and demonstrated.

## 4. Major Challenges

The above review of 3D RANS models in general and mobile-bed models in particular, along with years of our model development and application experience, show that a number of challenges need to be overcome before a 3D RANS-based mobile-bed model may become useful for river engineering applications. We group the major challenges into four categories:

- 3D mesh generation;
- free surface treatment;
- mobile bed representation; and
- sediment transport modeling.

3D modeling starts with the generation of a 3D mesh in order to represent the spatial domain of interest and geometry of the objects in the domain using a discretized set of points (mesh nodes). The generation of an appropriate and usable 3D mesh, however, has long been the grand challenge of 3D modeling. The mesh needs to take into account a number of factors that may constrain the meshing process. First, the shapes of mesh cells and the associated mesh connectivity may be limited by a specific 3D RANS model to be used. Many 3D models restrict the mesh topology to the structured mesh that assumes hexahedral mesh cells (some may even require an orthogonal mesh). Some models adopt the less restrictive unstructured tetrahedral mesh. Only a few adopt the most flexible polygonal mesh. The more flexible the mesh topology is, the less effort the mesh generation requires. Second, mesh generation may be severely constrained by the presence of complex geometry objects in the model domain as the mesh has to conform to the geometry. The ability to obtain object shapes and generate appropriate mesh around them is non-trivial. Third, refined meshes may be needed in regions such as at wall boundaries and free surfaces. Such needs are the result of required modeling accuracy which can be sensitive to the mesh resolution. Inadequate mesh density in boundary layers and/or free surfaces may result in high uncertainties in results. In particular, an accurate computation of bed shear stress is critical for mobile-bed modeling. Past experience showed that shear stress prediction is very difficult and requires a much refined mesh than other variables (e.g. pressure and velocity). Finally and more importantly, 3D RANS models have accuracy and stability constraints that may demand a good-quality mesh. Mesh cell orthogonality and aspect ratio are two of the most important mesh quality measures. 3D Mesh generation has long been a discipline of its own and requires expertise to carry out the task. Often, 3D mesh generation is accomplished using sophisticated mesh generation packages (e.g., the commercial packages GRIDGEN and ICEM-CFD). Even with commercial software, 3D mesh generation is time consuming for applications with complex geometry objects. It is probably the laborious mesh generation process that has prevented 3D models from more widespread use in river engineering.

Free surface treatment is necessary for river engineering applications. Its modeling is challenging as presence of free surface adds an additional variable, water surface elevation, to the governing equations. Physical processes near a free surface are complex, potentially involving wave action and modified turbulence. A number of numerical approaches have been especially proposed to treat the free surface such as (1) solid-lid method; (2) decoupled method (water elevation is computed using a separate set of equations decoupled from the RANS equations); (3) VOF (Volume of Fluid) method; (4) level-set method; and (5) kinematic wave method. Pros and cons of the different free surface approaches are debatable; but a stable and accurate approach is needed for practical applications.

Proper representation of a mobile bed in streams, reservoirs and coastal areas is another challenge to 3D modeling. The bed may be located at deep or shallow areas and is subject to wetting and drying. The bed may also be very steep, non-smooth. Further, bed elevation may change in time with mobile-bed modeling and 3D models need to have the dynamic capability to conform to bed changes. The dynamic mesh applies also to free surface with an unsteady modeling. At present, two meshing methods are widely used to handle dynamic free surface and stream bed: sigma-mesh and Z-mesh. Sigma-mesh employs an equal number of vertical mesh points everywhere and places mesh points on the bed and that moves with the bed. Through coordinate transformation, the computational mesh is fixed and does not change in time. An advantage of the sigma-mesh is that the mobile bed is accurately represented by the mesh points without stair-case approximation. In particular, bed shear stress may be reasonably computed in a straight forward manner. A drawback of the sigma-mesh is that it is difficult to represent shallow and steep areas simultaneously. Highly stretched and distorted mesh cells may be present in shallow areas or on steep slope terrain, which may degrade model accuracy and stability. Z-mesh was developed to overcome the drawback of the sigma-mesh method. Z-mesh uses a fixed vertical mesh size, not the same number of vertical mesh points, and parallel horizontal mesh lines. Z-mesh has the advantages that it does not require dense-packing of mesh points in shallow areas and it preserves the mesh quality throughout the mobile-bed modeling. However, the stream bed is now represented with the zig-zag staircase cells and additional bookkeeping and interpolation are required when the bed moves. Staircase bed representation has made bed shear stress computation difficult and even erroneous results have been reported. Corrective procedures have been proposed but complex interpolation is involved near bed and their generality is questionable. Other mesh alternatives have been proposed to overcome the shortcomings of both sigma-mesh and Z-mesh. For example, the Cartesian grid method (Udaykumar et al., 1996) and the immersed boundary method (Mittal and Iaccarino, 2005) were developed. These newer methods have their own challenges, in particular in resolving near wall turbulence properly.

Finally, mobile-bed modeling presents a major challenge to 3D modeling. First, mobile-bed modeling introduces many more partial differential equations to an already computing-intensive set of governing equations. Second, sediment modeling adds different temporal and spatial scales to the flow system, which

## Quantitative Modeling Tools for Large Wood

leads to increased stiffness of the equation set and potential numerical instability. Third, the governing equations of sediment transport were developed mostly for reach averaged models. Appropriate 3D forms of the sediment equations are still lagging behind. In their review, Papanicolaou et al. (2008) pointed out that sediment modeling is challenging because sediment transport is not only controlled by randomness in flow but also by irregularities in landform and bed surface geometry. They concluded that sediment transport models developed thus far are not as universal as a hydraulic engineer would like them to be. They summarized some of the limitations that the existing sediment transport models exhibit. A couple of the limitations are listed below:

- The assumption that sediment entrainment is not triggered by the near-bed flow turbulent characteristics but by the excess shear stress can be problematic. In most entrainment formulas, shear stress is determined by assuming uniform, cross-section averaged flow conditions. Studies have shown that turbulent sweeps, outward interactions, and ejections are the primary triggering mechanisms of sediment entrainment (Papanicolaou et al. 2001).
- The traditional approach calculates the sediment transport rate by using a single characteristic grain size, such as the median. This approach does not account for differential transport of sediment particles with different size or density; it is likely to produce large uncertainty in the predicted transport rate of individual fractions when bimodal or multimodal distributions are present on the surface bed. Expressions have been developed for the traveling velocity of particles (e.g., Parker et al. 2003; Francalanci and Solari 2007) that provides the resting and moving periods of particles of different sizes and the lag coefficient for the movement of different sediment fractions. These formulations allow different sizes to move at different rates, and their inclusion into future sediment transport modeling can perhaps improve the predictive ability of these models.

## 5. 3D Model Governing Equations

The proposed 3D modeling tools consist of three modules: the mesh generation module, the flow module, and the mobile-bed module. The model will be named U2RANS. The new model attempts to address the above four challenges as discussed in this chapter. In this effort, however, major efforts are on mesh generation and flow modules. The sediment module is being developed in the future.

### 5.1 Mesh Representation

A mesh generation module, SHM, is developed first, as it is the most challenging task and a prerequisite for 3D modeling. The objective is to develop a mesh generator that meets the following two features:

- Complex geometry of objects are obtained or created in a CAD system such as AutoCAD. Surface representation is stored to a file in the stereolithography (STL) format.
- 3D meshes are generated semi-automatically or automatically suitable for river engineering applications.

The use of STL files facilitates the representation of complex geometry and the automation is to reduce mesh generation complexity and associated user time. We have a much wider selection of mesh generation methods since our 3D model U2RANS adopts the unstructured mesh with polyhedral cells.

We have followed two routes in developing a mesh generator. In the first, we reviewed the existing public-domain 3D mesh generators and see whether we may develop a suitable mesh generator based on what has already been available. In the second, we want to develop our own independent mesh generation tools.

Two open-source mesh generation programs have been reviewed and studies: Cart3D and OpenFOAM. The Cart3D task was carried out by Prof. Jennifer Duan at the University of Arizona (UA) through a cooperative agreement between Reclamation and UA. The OpenFOAM task was carried out by both Prof. Xiaofeng Liu at the Penn State University through a cooperative agreement and Reclamation engineers. Specifically, the 3D mesh generation tool snappyHexMesh is evaluated which is available from the OpenFOAM suite of tools. Our study concludes that snappyHexMesh is more appropriate than Cart3D. Therefore, our mesh generator module SHM is built around the snappyHexMesh.

Since 2015, we have also embarked on the development of a stand-alone mesh module, named U2-MESH. The need for such a module is twofold: (a) SHM is not available in source form despite its open-source nature so it cannot be incorporated into U2RANS for dynamic meshing; (b) addition of new capabilities

## Quantitative Modeling Tools for Large Wood

specific to river engineering is hard to carry out. U2-MESH will achieve the following:

- Given a background mesh, either a multi-block structured mesh or an unstructured 3D mesh, SRH-MESH can insert STL objects into the background mesh through a six degree of freedom positioning;
- First, U2-MESH can perform local mesh refinement as instructed by the user through refinement parameters around and near the surface of the inserted object; and
- Next, U2-MESH will generate a new 3D mesh that removes mesh cells inside the inserted “objects” while retain mesh cells outside. This step generates a new 3D mesh with staircase (zigzag) representation of the object faces.

U2-MESH may be used to generate a 3D mesh with “staircase” effect. However, when the mesh is sufficiently refined, the staircase effect can be much reduced. Both SHM and U2-MESH are described in details later and they are also described in details by Prof. Liu in his final report as Attachment A.

## 5.2 Flow Module Equations

The flow module adopts the unstructured, arbitrarily shaped cell method of Lai (2000) and Lai et al. (2003). It is an extension of the U2RANS model developed by Lai et al. (2003). In the past, U2RANS was mostly limited to steady state modeling; unsteady modeling was not tested and validated extensively. Also, only mesh cells of pyre hexahedrons or tetrahedrons were used despite that the model could accept polyhedrons. In this study, we extend U2RANS into unsteady flows and using polyhedral meshes, then perform test, demonstration and validation cases. The polyhedron meshes are generated with SHM that allows local mesh refinements with hanging nodes.

The 3D flow module solves the following unsteady Reynolds averaged Navier-Stokes (RANS) equations:

$$\frac{\partial \rho}{\partial t} + \frac{\partial \rho U_j}{\partial x_j} = 0$$

$$\frac{\partial \rho U_i}{\partial t} + \frac{\partial \rho U_i U_j}{\partial x_j} = \frac{\partial}{\partial x_j} \left( \mu \frac{\partial U_i}{\partial x_j} + \tau_{ij} \right) - \frac{\partial P}{\partial x_i} + \rho g_i$$

In the above,  $t$  is time;  $x_j$  is the  $j$ -th Cartesian coordinate;  $\rho$  is the water-sediment mixture density;  $U_j$  is the mean velocity components along the Cartesian coordinate  $x_j$ ;  $\tau_{ij} = -\overline{\rho u_i u_j}$  is the turbulence stress with  $u_j$  the  $j$ -th

## 5. 3D Model Governing Equations

turbulent fluctuating velocity component;  $P$  is the mean pressure;  $\mu$  is the mixture viscosity; and  $g_i$  is the  $i$ -th component of the acceleration due to gravity.

The above equation can also be written in tensor form as:

$$\frac{\partial \rho}{\partial t} + \nabla \cdot (\rho \vec{V}) = 0$$

$$\frac{\partial \rho \vec{V}}{\partial t} + \nabla \cdot (\rho \vec{V} \vec{V}) = -\nabla P + \nabla \cdot (\mu \nabla \vec{V} - \vec{\tau}) + \rho \vec{g}$$

A turbulence model is used to relate the Reynolds stress tensor  $\tau_{ij}$  in the above equations to other variables. At present, two equation models such as the standard k- $\epsilon$  model of Launder and Spalding (1974) are implemented in U2RANS. That is, the Reynolds stresses is related to the mean strain rate through the turbulent eddy viscosity as:

$$\tau_{ij} = \mu_t \left( \frac{\partial U_i}{\partial x_j} + \frac{\partial U_j}{\partial x_i} \right) - \frac{2}{3} \rho k \delta_{ij} \quad \text{or}$$

$$\vec{\tau} = \mu_t \left[ \nabla \vec{V} + (\nabla \vec{V})^T \right] - \frac{2}{3} \rho k \vec{I}$$

where  $\delta_{ij}$  (or  $\vec{I}$ ) is the Kronecker delta ( a unit tensor) and the eddy viscosity is obtained from:

$$\mu_t = C_\mu \rho \frac{k^2}{\epsilon}$$

In the above,  $k$  is the turbulence kinetic energy and  $\epsilon$  is the turbulence dissipation rate. The transport equations for  $k$  and  $\epsilon$  for non-buoyant flows may be expressed as:

$$\frac{\partial \rho k}{\partial t} + \frac{\partial \rho U_j k}{\partial x_j} = \frac{\partial}{\partial x_j} \left( \left( \mu + \frac{\mu_t}{\sigma_k} \right) \frac{\partial k}{\partial x_j} \right) + G - \rho \epsilon$$

$$\frac{\partial \rho \epsilon}{\partial t} + \frac{\partial \rho U_j \epsilon}{\partial x_j} = \frac{\partial}{\partial x_j} \left( \left( \mu + \frac{\mu_t}{\sigma_\epsilon} \right) \frac{\partial \epsilon}{\partial x_j} \right) + C_{\epsilon 1} \frac{\epsilon}{k} G - C_{\epsilon 2} \rho \frac{\epsilon^2}{k}$$

## Quantitative Modeling Tools for Large Wood

where  $G = \tau_{ij} \frac{\partial U_i}{\partial x_j}$  is the turbulence generation rate due to velocity strain. The standard model constants take the following values:

$$C_\mu = 0.09; C_{\varepsilon 1} = 1.44, C_{\varepsilon 2} = 1.92, \sigma_k = 1.0, \sigma_\varepsilon = 1.3$$

U2RANS model of Lai et al. (2003) lacks the treatment of free surface and bed representation – two of the four challenges discussed previously. In our new flow module, free surface is to be handled with one of two approaches: the solid-lid method and the decoupled method. The solid-lid method treats the free surface by the slip boundary condition and the free surface is represented by the 3D mesh which has to be defined before the computation. The solid-lid method has been widely used in the past in 3D modeling of open channel flows. It is adequate for open channel flows with low Froude number and small variation of free surface elevation in space (e.g., Lai et al. 2003). The decoupled method does not require user definition of the free surface; instead the free surface elevation is computed using a set of equations apart from the 3D RANS equations. In this study, the decoupled method has been implemented as follows. The free surface elevation is first computed with SRH-2D solving the 2D depth-averaged equations. U2RANS will then obtain the free surface elevation and form a new 3D mesh based on the elevation. The decoupled method is adequate for most open channel flows and lake/reservoir modeling. The primary limitation is that the free surface does not experience sudden vertical changes such as occurring at weirs and gates. More sophisticated free surface treatment awaits future developments.

### 5.3 Boundary Conditions

Common boundary conditions encountered in the hydraulic flow problems include flow inlet, flow outlet, no-slip wall, plane of symmetry, and free surface boundary conditions. Boundary conditions for the flow and turbulence variables are discussed first.

At a flow inlet, Cartesian velocity components or flow discharge are specified at the cell face centers. Pressure is determined by means of an extrapolation from the value at the interior of the cell. These values of flow properties are needed in solving the flow equations (mass and momentum equations). The solution of the pressure correction equation, however, requires no pressure boundary condition because mass fluxes on these boundaries are specified and remain unchanged during the solution process. Turbulence quantities,  $k$  and  $\varepsilon$ , are specified at an inlet as user inputs.

At a flow outlet, pressure is specified at the cell face center while Cartesian velocity components and turbulence quantities are determined by means of an extrapolation from the values at the interior of the cell. For the pressure-correction equation, the pressure increment is set to be zero at the outlet because

## 5. 3D Model Governing Equations

pressure should not change during the solution. For unsteady flows, U2RANS dynamically determines if a boundary is an inlet or outlet in accordance with the flow-rate direction through the boundary.

At solid walls, the standard wall-function approach of Launder and Spalding (1974) is used to set the boundary condition. The functions include the log-law wall function that incorporated wall roughness effect. In the study of Stumpp (2001), several roughness-treatment methods were incorporated for river flow simulations. Results were compared to a large number of experimental data with varying surface roughness. Based on the findings of Stumpp (2001), we adopt a specific wall-function approach described below. The wall-function is used to solve for the velocity distribution within the inertial sublayer; it can be expressed in log-law form as

$$\frac{u}{u_\tau} = \frac{1}{\kappa} \ln\left(E \frac{u_\tau y}{\nu}\right) \quad u_\tau = \sqrt{\frac{\tau_w}{\rho}}$$

Open channel water surface is treated as a free surface condition. As discussed before, either the solid-lid or decoupled approach may be used to obtain the free surface elevation. At the free surface, the velocity component normal to the surface is set to be zero while the normal derivative of the tangential velocity is zero. At present, zero wind speed is assumed.

The boundary conditions are also needed for the turbulence kinetic energy and dissipation rate equations at walls and free surfaces. We use the Dirichlet boundary condition for  $k$  and  $\epsilon$ . This approach simplifies the model implementation as turbulence generation terms are not needed for the first cells touching the free surface and wall.

At a wall,  $k$  and  $\epsilon$  values are computed through the equilibrium assumption as:

$$k_B = \frac{u_{\tau B}^2}{\sqrt{C_\mu}} \quad \epsilon_B = \frac{u_{\tau B}^3}{\kappa \delta_B} = \frac{C_\mu^{3/4} k_B^{3/2}}{\kappa \delta_B}$$

where  $u_{\tau B}$  is the bed friction velocity, and  $\delta_B$  is the normal distance from the centroid of first cell near a wall to the wall face.

At a free surface, the following Dirichlet conditions are applied:

$$k_S = \frac{u_{\tau S}^2}{\sqrt{C_\mu}} \quad \epsilon_S = \frac{u_{\tau S}^3}{\kappa \delta_S}$$

## Quantitative Modeling Tools for Large Wood

where  $u_{\delta_s}$  is the free surface friction velocity due to wind forcing and is zero at present and  $\delta_s$  is the normal distance from the cell centroid near the free surface to the free surface face. At present both  $k$  and  $\epsilon$  are zero at free surface as there is no wind assumed.

## 6. Numerical Methods

This section describes the numerical methods to solve the 3D RANS equations described in Chapter 5.

### 6.1 Discretization of the Flow Equations

The 3D flow module, without the hydrostatic assumption, has been developed to solve flow problems in hydraulic engineering. The module is based on the previous work of Lai et al. (2003) which adopted the unstructured arbitrarily shaped element method. Use of the polyhedron mesh provides the most flexible mesh topology and has the advantage of uniting various mesh topologies into a single formulation.

Numerical solution of flow equations involves the use of a mesh to cover a model domain and the discretization of the governing equations. U2RANS adopts polyhedral cells that may have any number of polygonal faces. We select the cell-centered scheme with which all dependent variables are located at the centroid of mesh cells. The other alternatives include the cell-vertex scheme with which all variables are at cell's vertices or staggered scheme with which velocity and pressure are stored at difference locations.

The governing equations are discretized using the finite-volume approach using the Gauss theorem. The procedure has been discussed by Lai et al. (2003) but it is documented for completeness of the report. An advantage of the finite-volume method is that the conservation of any flow property can be achieved locally and globally. As an illustration, consider the general convection-diffusion equation representative of all of governing equations:

$$\frac{\partial \rho \Phi}{\partial t} + \nabla \cdot (\rho \vec{V} \Phi) = \nabla \cdot (\Gamma \nabla \Phi) + S_{\Phi}^*$$

Here,  $\rho$  = fluid density;  $\vec{V}$  = velocity vector;  $\Phi$  = any dependent variable, a scalar, or a component of a vector;  $\Gamma$  = diffusivity; and  $S_{\Phi}^*$  = one or more source and/or sink terms.

Integration over a polygonal cell leads to the following expression:

$$\iiint \frac{\partial \rho \Phi}{\partial t} + \sum_{all-faces} (\rho_f V_f A) \Phi_f = \sum_{all-faces} (\Gamma A \nabla \Phi \cdot \vec{n}) + S_{\Phi}^* \forall$$

in which  $V_f = \vec{V} \cdot \vec{n}$  is the velocity component normal to the cell face which is used to satisfy mass conservation,  $A$  is the cell face area;  $\Phi_f$  is the face value of the dependent variable  $\Phi$ ;  $\vec{n}$  is the cell face unit normal vector; and  $\forall$  is the cell

## Quantitative Modeling Tools for Large Wood

volume. The main task of the discretization is to obtain appropriate expressions for the time term and the convective and diffusive fluxes on each cell face.

The discretization of the unsteady term is as follows:

$$\iiint \frac{\partial \rho \Phi}{\partial t} d\mathcal{V} = \frac{m_0 \mathcal{V}^n \rho^n \Phi^n + m_M \mathcal{V}^{n-1} \rho^{n-1} \Phi^{n-1} + m_{MM} \mathcal{V}^{n-2} \rho^{n-2} \Phi^{n-2}}{\Delta t}$$

where  $\mathcal{V}$  is the volume of the cell; superscript “ $n$ ” refers to the time level;  $\Delta t$  is time step; and three parameters  $(m_0, m_M, m_{MM})$  determine the time discretization scheme used. For example,  $(m_0, m_M, m_{MM}) = (1, -1, 0)$  corresponds to the first-order Euler scheme, and  $(m_0, m_M, m_{MM}) = (1.5, -2, 0.5)$  is the second-order backward scheme.

The shapes of cells and cell faces must be uniquely defined before discretization can be carried out for convection and diffusion terms; such a procedure is described next. A polyhedron may consist of a number of enclosing faces, and the shape of a polyhedron is uniquely defined if each face is defined. Consider one cell face of a polyhedron with  $N$  vertices; such a sample polygonal face with  $N=5$  is illustrated in Figure 6(a). The face geometry is not completely defined because all vertex points may not be on the same plane. To define the face geometry, a center point  $F$  is calculated by taking the arithmetic average of all vertex position vectors.  $N$ -triangles are then formed by connecting point  $F$  with the  $N$  vertices. Taking the face in Figure 6(a) as an example, five triangles,  $F_1F_2F$ ,  $F_2F_3F$ ,  $F_3F_4F$ ,  $F_4F_5F$ , and  $F_5F_1F$ , are defined. A collection of these triangles uniquely defines the shape of the face, and all faces uniquely define the cell shape. Geometric quantities (e.g., cell volume, face area, and face unit normal vector) are calculated from this definition. These definitions of cell and face shapes are consistent with the finite-volume method.

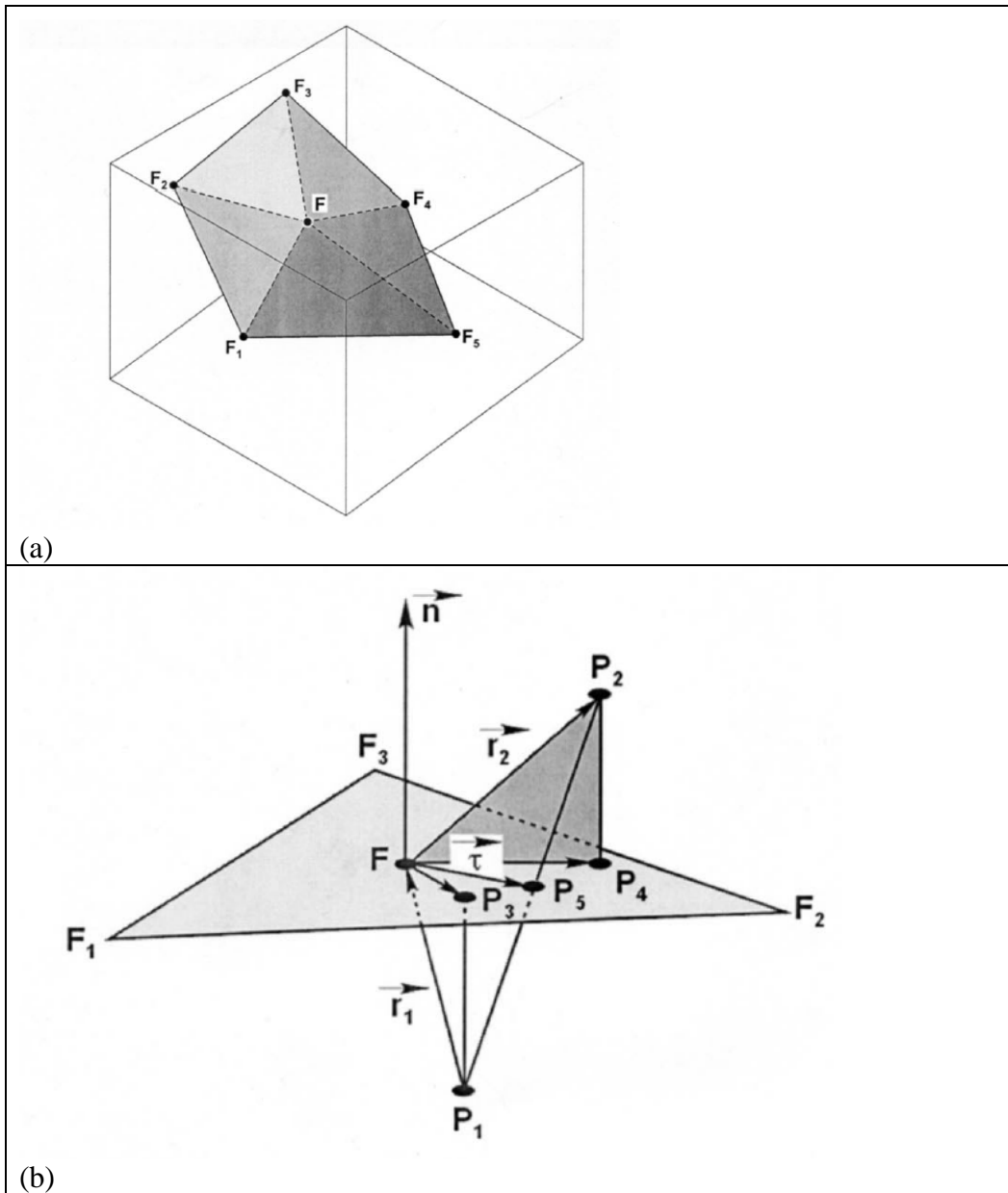


Figure 6. Illustration of an arbitrary cell face: A diagram for (a) a general cell face and (b) a triangular face

Discretization of the diffusive flux,  $\nabla\Phi \cdot \vec{n}$ , at a face is presented first. Without loss of generality, consider only a triangular face, as shown in Figure 6(b), as a general polygonal cell face consists of such triangles. The triangle has vertex points  $F_1, F_2$ , and  $F_3$ , unit normal vector  $\vec{n}$  and center point  $F$ . It is assumed that  $\Phi$  is known at the two cell center points  $P_1$  and  $P_2$  and at the vertices of the face. The diffusion term is calculated by locally establishing a general non-orthogonal coordinate system on the face with three covariant coordinate bases (

## Quantitative Modeling Tools for Large Wood

$(\vec{\varepsilon}_1, \vec{\varepsilon}_2, \vec{\varepsilon}_3)$  defined. Here,  $\vec{\varepsilon}_1$  is chosen as the vector from point P1 to P2, and  $\vec{\varepsilon}_2$  and  $\vec{\varepsilon}_3$  are on the cell face. Then a gradient can be expressed in this local coordinate system as

$$\nabla\Phi = \frac{\partial\Phi}{\partial\xi_1}\vec{\varepsilon}^1 + \frac{\partial\Phi}{\partial\xi_2}\vec{\varepsilon}^2 + \frac{\partial\Phi}{\partial\xi_3}\vec{\varepsilon}^3$$

in which  $\xi_1, \xi_2,$  and  $\xi_3 =$  coordinates along  $\vec{\varepsilon}_1, \vec{\varepsilon}_2,$  and  $\vec{\varepsilon}_3,$  respectively, and  $\vec{\varepsilon}^1, \vec{\varepsilon}^2,$  and  $\vec{\varepsilon}^3 =$  three contravariant coordinate bases (see Thompson et al. 1985). In these coordinates,  $\nabla\Phi \cdot \vec{n}$  can be split into a normal term plus a cross term. The normal term is represented by  $\Phi$  values at cell center points P1 and P2, while the cross term is evaluated on the cell face and can be expressed through  $\Phi$  values at the face vertices. Green's integral is used to transform the area integration of the cross diffusion term into the line integration on the edges of the face. Once obtained for the triangular face, the diffusion term for an arbitrary face is calculated by summing the contributions from each triangle. After mathematical manipulation, the diffusion term for an arbitrary cell face is

$$\nabla\Phi \cdot \vec{n}A = D_n(\Phi_2 - \Phi_1) + \sum_{all-edges} D_c^{edge} \Phi_{edge}$$

$$D_n = \frac{A}{(\vec{r}_1 + \vec{r}_2) \cdot \vec{n}} \quad D_c^{edge} = -\frac{(\vec{r}_1 + \vec{r}_2) \cdot (\delta\vec{r}_{edge} \times \vec{n})}{(\vec{r}_1 + \vec{r}_2) \cdot \vec{n}}$$

In the above equations,  $\Phi_1$  and  $\Phi_2$  are the  $\Phi$  values at cell center points P1 and P2,  $\sum_{all-edges}$  stands for summation over all edges of the face,  $\Phi_{edge}$  is the  $\Phi$  value at an edge center and it is calculated using vertex values,  $\delta\vec{r}_{edge}$  is the distance vector along the edge; and,  $\vec{r}_1$  and  $\vec{r}_2$  are the vectors from P1 to F and F to P2, respectively, as shown in Figure 6(b). The normal and cross term coefficients at each face involve only geometric quantities and need be calculated only once and used for all subsequent calculations so long as the mesh is not changed during the solution.

By way of a Taylor series expansion, the cross term in the above expression can be shown to have second-order accuracy, while the normal term is of second-order accuracy if the vectors  $\vec{r}_1$  and  $\vec{r}_2$  are equal. Otherwise, the discretization error in the normal term is proportional to the difference of the two distances. That distance is non-zero, due to non-uniform and non-regular meshes.

Calculation of the cell face value is discussed next, given the cell-center values. This is a center-to-face operation used often in the solution process for which a

second-order accurate expression is derived. Consider a triangular face F1F2F3 with two cell center points P1 and P2[Figure 6(b)]; a point P5 is defined as the intercept point between line P1P2 and the face; points P3 and P4 are defined on the face such that P1P3 and P2P4 are normal to the face. A second-order-accurate interpolation for point P5 gives

$$\Phi_{P5} = \frac{\delta_1 \Phi_2 + \delta_2 \Phi_1}{\delta_1 + \delta_2}$$

in which  $\delta_1 = \vec{r}_1 \cdot \vec{n}$  and  $\delta_2 = \vec{r}_2 \cdot \vec{n}$ .  $\Phi_{P5}$  can be used to approximate the value at face center F. This treatment, however, will not guarantee second-order accuracy unless  $\vec{r}_1$  and  $\vec{r}_2$  are parallel. A truly second-order expression can be derived as

$$\Phi_f = \Phi_{P5} - \nabla_\gamma \Phi \cdot \vec{\gamma}$$

where  $\vec{\gamma}$  is distance vector from F to P5, and  $\nabla_\gamma$  is the gradient operator defined on the face. It can then be shown

$$\Phi_f = \Phi_{P5} - \frac{\delta_1 \vec{r}_2 - \delta_2 \vec{r}_1}{(\delta_1 + \delta_2)A} \cdot \sum_{all-edge} (\delta \vec{r}_{edge} \times \vec{n}) \Phi_{edge}$$

The second term on the right hand side of the above equation is quite similar in form to the cross diffusion term.

The term  $\Phi_f$  in the evaluation of the convective term needs further discussion. If the second-order scheme is applied directly, spurious oscillations may occur for flows with high cell Peclet number (Patankar 1980). Therefore, a damping term is added to the second-order scheme similar to the concept of artificial viscosity. The damped scheme is derived by blending the first-order upwind scheme with the second-order central difference scheme and can be expressed as

$$\Phi_f = \Phi_f^{CD} + d(\Phi_f^{UP} - \Phi_f^{CD})$$

where

$$\Phi_f^{UP} = \frac{1}{2}(\Phi_1 + \Phi_2) - \frac{1}{2} \text{Sign}(V_f)(\Phi_2 - \Phi_1)$$

Here  $\Phi_f^{CD}$  is the second-order interpolation scheme and  $d$  defines the amount of damping used. In most applications,  $d = 0.2-0.3$  is used.

With all terms in the governing equation discretized, the final discretized governing equation for cell  $P$  can be expressed concisely as the following linear equation:

$$A_P \Phi_P = \sum_{nb} A_{nb} \Phi_{nb} + S_\Phi$$

where “ $nb$ ” refers to all neighbor cells that share the same vertices with element  $P$ .

## 6.2 Velocity-Pressure Coupling and Solution Procedure

For the co-located (non-staggered) mesh method, a special procedure is required to obtain the cell face normal velocity that is used to enforce mass conservation. Otherwise the well-known checkerboard instability, related to the velocity and pressure decoupling, may appear (Rhie and Chow 1983). Here, the velocity-pressure coupling procedure adopted follows the one proposed by Rhie and Chow (1983) and Peric et al. (1988) and implemented by Lai et al. (1995), Lai (2000) and Lai et al. (2003). That is, the face mass-conserving velocity is obtained by averaging the momentum equation from cell centers to cell faces, and the final equation is as follows:

$$V_f = \langle \vec{V} \rangle \cdot \vec{n} - \left\langle \frac{\nabla}{A_P} \right\rangle (\nabla P)_f \cdot \vec{n} + \left\langle \frac{\nabla}{A_P} \nabla P \right\rangle \cdot \vec{n}$$

where “ $\langle \rangle$ ” is the averaging operator from cell center to cell face discussed previously and  $\nabla$  is the mesh cell volume. When the averaging operator is applied to a vector, it implies application to each Cartesian component of the vector. This equation may be interpreted as: the mass-conserving face velocity is obtained with regular averaging, plus a 4<sup>th</sup>-order pressure damping. The damping was necessary to remove the spurious checkerboard instability (see Lai et al. 1995) and provides the needed velocity-pressure coupling.

The SIMPLE and SIMPLEC algorithms (Patankar 1980) are widely used and are adopted to derive the pressure correction equation from the mass conservation equations. The other alternative is the PISO algorithm (Issa 1986).

With a known pressure field  $P^o$  at time 0, a new velocity field is predicted by solving the following momentum equation (starred superscript denotes provisional predicted values at the new time  $t_n$ ):

$$A_P \vec{V}_P^* = H(\vec{V}_{nb}^*) - \nabla^o \nabla P^o + \vec{S}_V^o$$

where  $H$  stands for the linear operator  $H = \sum_{nb} A_{nb}$ . The new predicted face flow velocity is then computed as:

$$V_f^* = \langle \vec{V}^* \rangle \cdot \vec{n} - \left\langle \frac{\nabla^o}{A_p} \right\rangle (\nabla P^o)_f \cdot \vec{n} + \left\langle \frac{\nabla^o}{A_p} \nabla P^o \right\rangle \cdot \vec{n}$$

Next, a corrector step is performed to compute new pressure and velocity fields  $P^*$  and  $\vec{V}^{**}$  such that the following continuity and momentum equations are satisfied:

$$\nabla \cdot \vec{V}^{**} = 0$$

$$A_p \vec{V}_p^{**} = H(\vec{V}_{nb}^*) - \nabla^o \nabla P^* + \vec{S}_V^o$$

Expressed in increment form, the momentum equation becomes

$$A_p \vec{V}_p' = -\nabla^o \nabla P'$$

with  $\vec{V}' = \vec{V}^{**} - \vec{V}^*$  and  $P' = P^* - P^o$ . Substitution of the incremental equation into the continuity equation leads to the following pressure correction equation:

$$\nabla \cdot \left[ \left( \frac{\nabla^o}{A_p} \right) \nabla P' \right] = \nabla \cdot \vec{V}^*$$

After solution of  $P^*$ , new updated velocity  $\vec{V}^{**}$  is also computed with the above momentum equation and the mass-conserving face velocity computed by:

$$V_f^{**} = \langle \vec{V}^{**} \rangle \cdot \vec{n} - \left\langle \frac{\nabla^o}{A_p} \right\rangle (\nabla P^*)_f \cdot \vec{n} + \left\langle \frac{\nabla^o}{A_p} \nabla P^o \right\rangle \cdot \vec{n}$$

The above is the standard SIMPLE algorithm. SIMPLEC can be easily realized by replacing  $A_p$  in the pressure equation by  $\left( A_p - \sum_{nb} A_{nb} \right)$ .

For an unstructured mesh, the design of a data structure is important, and it is discussed herein. In this study, three across-the-field operations are encountered. The most frequently used operation is a loop over all cells. Therefore, cell-based data storage is used as it is natural to the cell-centered storage scheme. Operations such as property update and linear equation solvers are all cell based, and they represent a major portion of the CPU time. With cell-based data, connectivity

## Quantitative Modeling Tools for Large Wood

integer arrays are created that address mesh relations from cell to neighboring cells and from cells to cell faces. The second type of data structure is face based and is created to compute the convective and diffusive fluxes and the associated coefficients on cell faces. A face-based data structure requires the creation of connectivity arrays that provide information from the face to the neighboring cells. Finally, node-based data structure, which provides information from a mesh node to all neighboring cells is also used. The node-based data structure is used to compute node values from known cell centroid values of a variable and is used by the cross diffusion term and the pressure correction equation. The face- and node-based data structures are less frequently used and consume much less computing time. Therefore, the cell-based data structure dominates the efficiency of the numerical method.

All governing equations are solved in an equation-by-equation manner. In a typical solution process, momentum equations are solved first assuming known pressure and turbulence viscosity. The predicted velocity fields is used to compute the mass-conserving face velocity and used by the continuity equation. The predicted velocity will usually not satisfy the mass conservation. Therefore, the corrector step is applied by solving the pressure correction equation. Due to SIMPLE or SIMPLEC approximation, a number of inner iterations may be performed. After the momentum and continuity equations are solved, other scalar equations are solved such as the turbulence equations and sediment concentration equations, etc. This completes one outer iteration of the solution cycle. The above procedure is repeated until a preset residual criterion for each equation is met. Then, the computation may move on to the next new time. The residual of a governing equation is defined as the sum of absolute errors at all mesh cells.

## 7. 3D Mesh Generation

As discussed before, the mesh generator SHM is an automated 3D mesh generator based on the open-source software snappyHexMesh contained within the OpenFOAM software package. Key development and usage have been documented by Prof. X. Liu in his final report as Attachment A. So it is not repeated herein. Prof. Liu has been a collaborator of the work through a cooperative agreement grant between Penn State University and Reclamation. Major effort of the SHM work is to make it usable with Window-based PCs along with clear instructions of how to use it for typical river engineering applications. The original snappyHexMesh can only be executed with Linux-based PCs and has limited documentation.

Reclamation engineers have also worked with snappyHexMesh initially and SHM later in order to gain the experience of using the tool. Concise user guides are developed in the process for future use of the tool by others. This Chapter documents the use of SHM at Reclamation. The content serves as a future tutorial case in learning the procedure of running SHM.

The independent mesh generation tool, U2-Mesh, is described also in the final report by Prof. Liu. Reclamation is yet to use this product and so no separate documentation will be provided.

### 7.1 Background Mesh

SHM needs an initial background hexahedral mesh as an input. The purpose and the features of the background mesh include:

- The background mesh specifies the main domain and an initial set of boundaries to apply the boundary conditions.
- It consists of hexahedral mesh cells only.
- It provides the coarsest mesh the 3D solver will use for simulation.
- The background mesh may be locally refined by SHM in user specified zones.
- The background mesh is recommended to have mesh cell aspect ratio close to 1 although deviation is allowed. SHM may experience convergence difficulty if the aspect ratio is too far away from unity.
- Objects, whose surface is represented with STL files, may be inserted into the background mesh to generate a new 3D mesh by SHM. However, there must be interception of background mesh edges with the inserted objects.

The background mesh may be generated using the blockMesh that comes with the OpenFOAM package. Or, it may be generated with U2-MESH that is still under development at Reclamation.

## Quantitative Modeling Tools for Large Wood

A non-trivial demonstration case, flow over a picnic table, has been created in this project to show the mesh generation process with SHM. A simple rectangular background mesh is used for the picnic table case as shown in Figure 7. The dimension of the model domain is as follows: 20 meters long along x, 3 meters high along y, and 6 meters wide along z. The background mesh has 9,720 hexahedrons and 11,590 nodes and the cell aspect ratio is 1.0 for all cells.

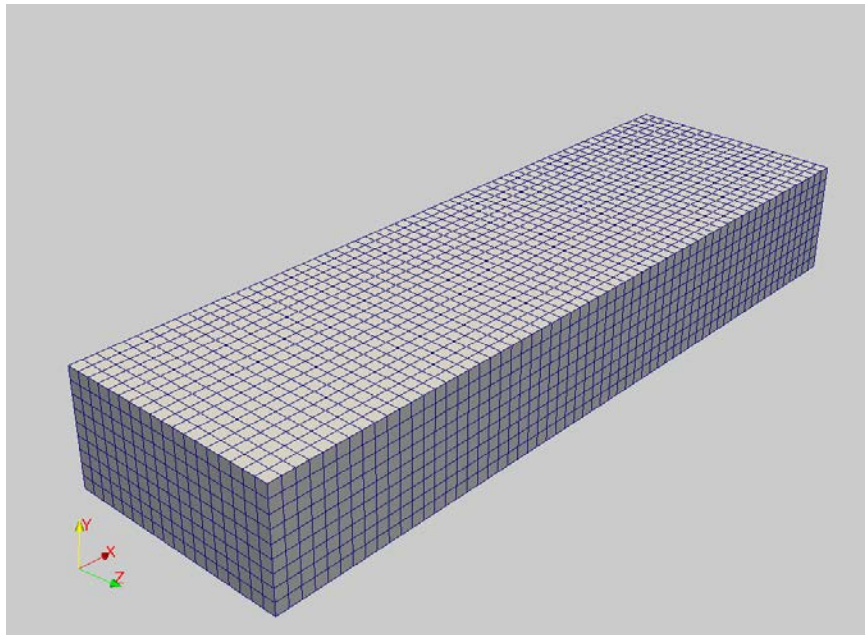


Figure 7. The background mesh generated for the picnic table flow case

## 7.2 Object Representation

Objects with complex geometry in a model domain should be represented by STL files (or Nastran .nas files). The STL files provide the triangulated mesh of the object surfaces and may be generated using CAD software. The STL file usually consists of closed surfaces; but it can also be open on special occasions such as bed terrain of a stream. It is required that the STL surface representing the stream bed is larger than the background mesh domain.

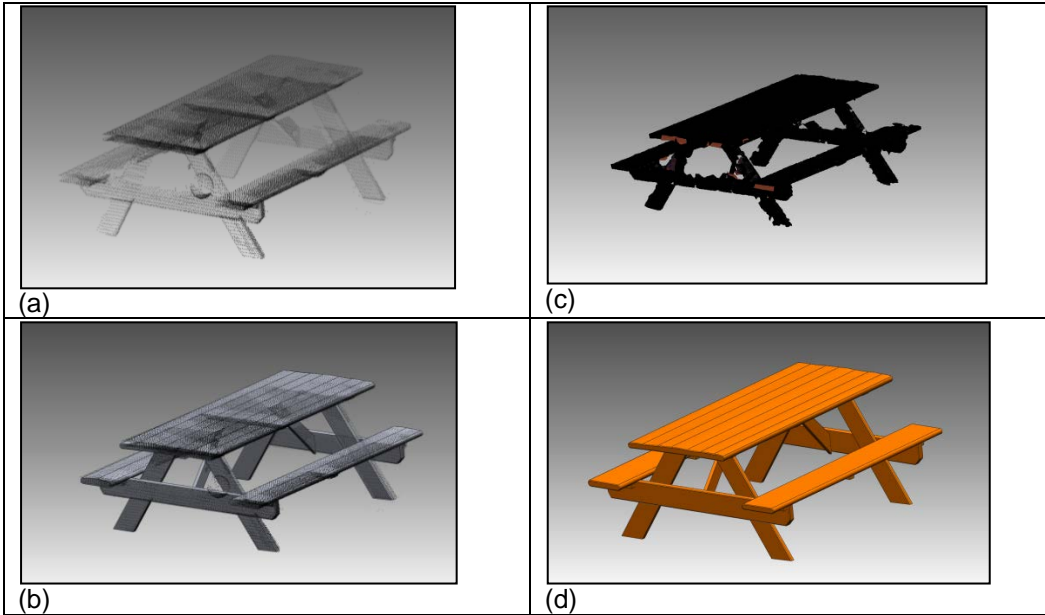
River flows often involve complex geometric features which are extremely difficult to represent in computer modeling or laboratory. With the recent advancement in laser scanner technology, however, the ability to capture complex objects in a three dimensional space is becoming feasible. Utilizing stationary terrestrial Lidar scanners deployed in the field, high resolution point cloud data may be captured with millions of 3D points representing in-stream structures or other features. An example of using the scanner to capture the in-stream large woody bar is shown in Figure 8 for a restoration project on the Trinity River, California.



Figure 8. Constructed wood jam on the Trinity River, California – ground photo (left) compared to LiDAR scan point cloud (right)

The raw 3D point cloud data is downloaded into computer environment and used as the foundational dataset for solid modelling. The point cloud may be edited and refined to develop a suitable 3D solid model for the in-stream feature. For example, the survey software of Trimble Realworks was used for scan registration and initial editing, and Geomatic software was used for point cloud manipulation into a water tight solid that produces the STL file. The power of the Geomatic software is that it can use the point cloud data and wrap a best fit surface mesh around it. At present, most effective solid modeling software are of commercial nature and can be expensive to purchase.

For the picnic table case, we have gone through the above 3D scanning and solid modeling process. A 3D Lidar scanner was used to scan a picnic table placed in the field. The point cloud such obtained is shown in Figure 9(a) and it was then processed within Geomatic software to obtain the final solid model. The workflow from a raw point cloud to a 3D solid is shown in Figure 9 for the picnic table case.



### 7.3 Mesh Castellation

Mesh castellation refers to the creation of a staircase 3D mesh based on the background mesh, the inserted 3D objects, and the local mesh refinement requested by the user. The mesh castellation procedure involves the following steps:

- The object, with surfaces represented by STL files, is inserted into the background mesh;
- SHM performs local mesh refinement first near the STL surface as specified by the user. A number of levels may be used for mesh refinement and terminology is illustrated in Figure 10 for a 2D example.

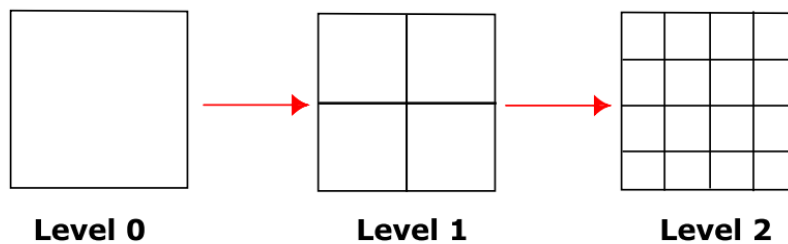


Figure 10. Illustration of 2D mesh refinement from level 0 to level 2

- SHM automatically detects all mesh cells completely inside and outside the inserted objects. User may determine which part of the mesh should be removed.

For the picnic table case, we placed the scanned picnic table in the STL file format into the background mesh shown in Figure 7. The spatial orientation of the table is displayed in Figure 11 in which a slice of the background mesh is also shown. With a few user inputs, SHM is used to automatically generate a 3D mesh through the mesh castellation step. The castellated 3D mesh for the flow around the picnic table is shown in Figure 12 while the zoom-in view of the mesh is shown in Figure 13. In the sample SHM mesh generation, 3 to 4 mesh refinement levels are used near the table. The number of buffer cells between each level is set to be 3. Besides the zones near the table, an extra region of mesh refinement is carried out using a box surrounding the table. The refinement box has a bounding range of  $(-1, 4)$  in  $x$ ,  $(0, 2)$  in  $y$  and  $(-2, 2)$  in  $z$ . The castellation step generates a staircase 3D mesh. Such stair-case meshes have been widely used for 3D environmental simulations (e.g., Blumberg and Mellor 1987; Hamrick 1992; Gessler et al. 1999).

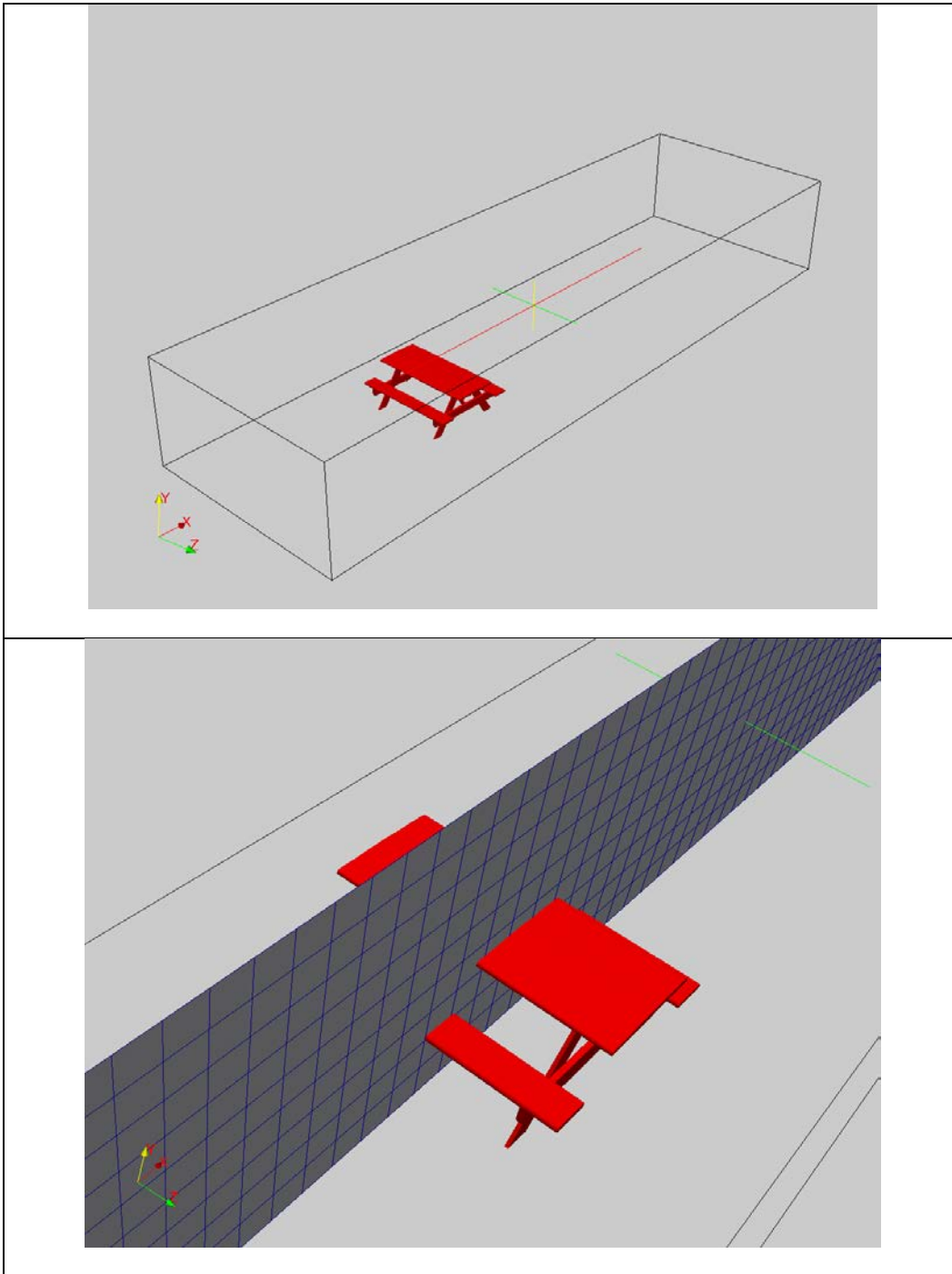


Figure 11. Insertion of the picnic table into the background mesh; only a slice of the background mesh is shown here

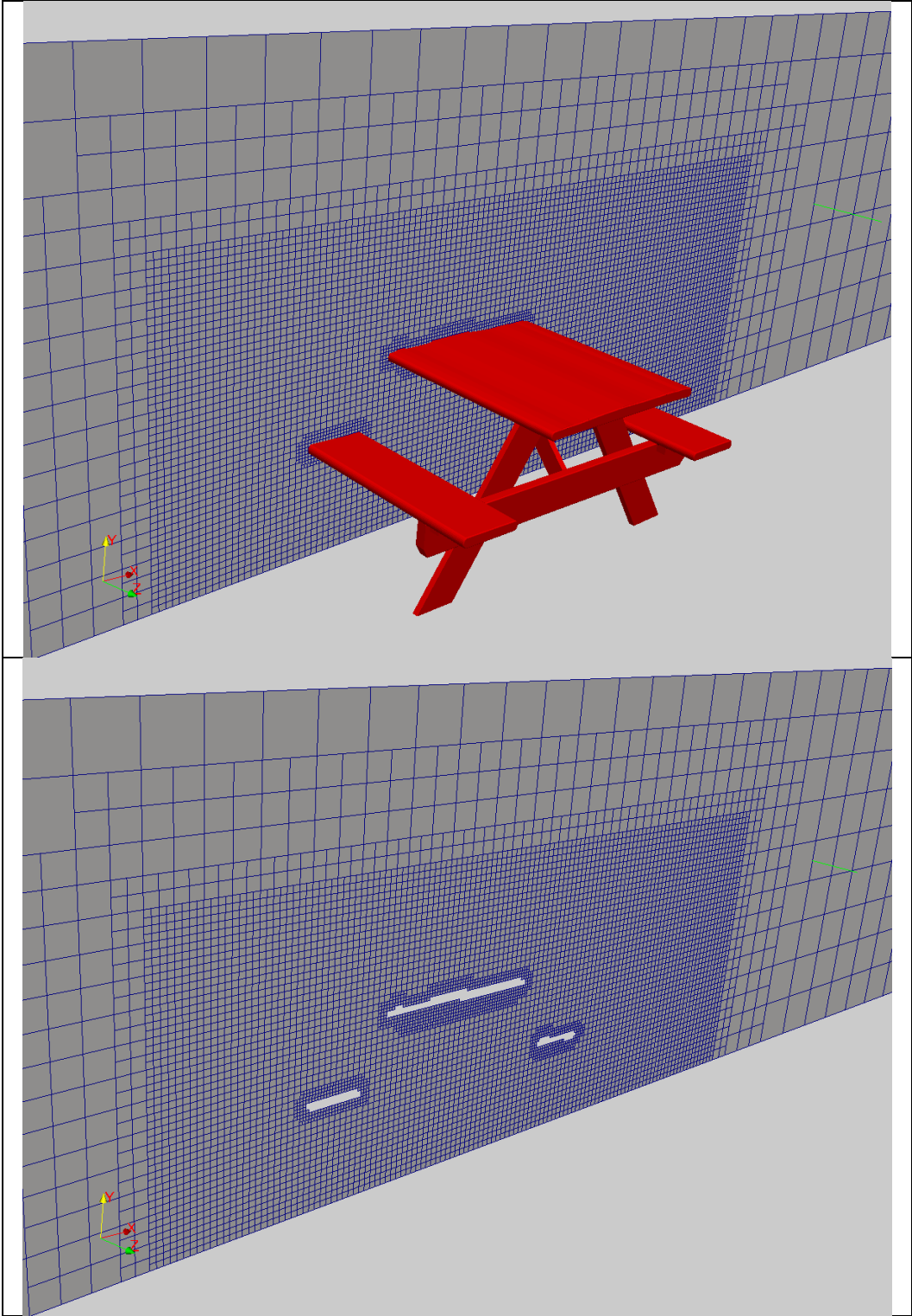


Figure 12. Castellated mesh with local mesh refinement and removal of mesh cells inside the picnic table

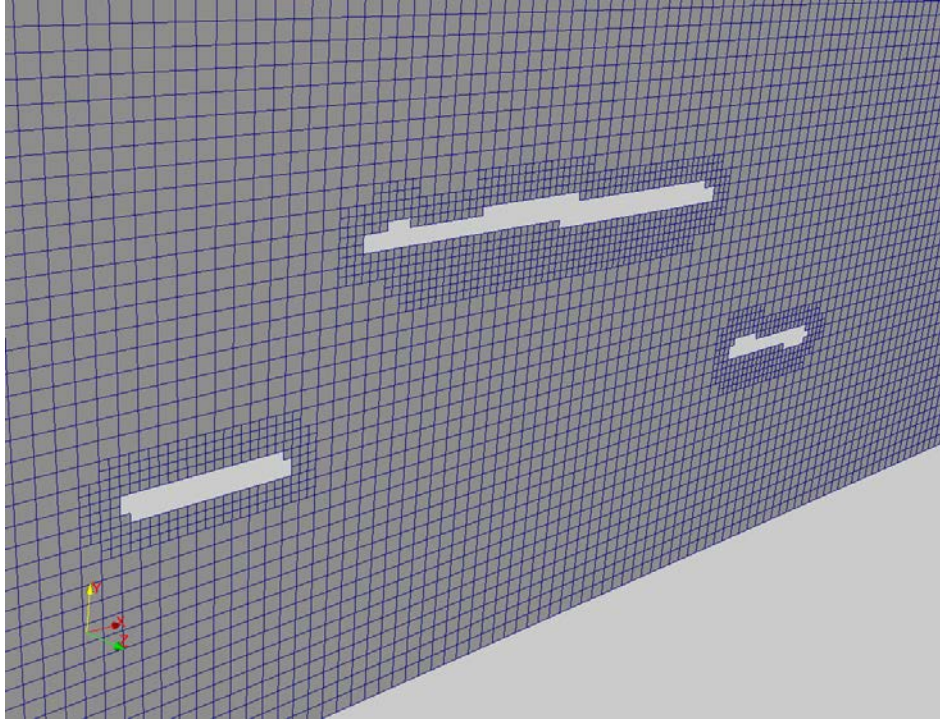


Figure 13. Zoom-in view of the castellated mesh; zigzag stair case cells are clearly seen around the table

### 7.4 Mesh Snapping

The castellated mesh can be further improved to eliminate stair-case representation of the object surfaces. It is achieved by “moving” mesh points near the object onto the STL surface so that a boundary-conforming mesh is obtained. The process of moving nodes near the surface onto the STL geometry is called “mesh snapping.” Snapping is carried out iteratively within SHM as follows:

- Nodes close to the STL surface are moved onto the surface;
- Relaxation of the internal mesh nodes is performed so that the mesh quality may be improved;
- If the quality criteria of any cells cannot be met during relaxation, the displacement of the violating nodes will either be reduced or not performed at all.

Snapping transforms the stair-case mesh around the surface into a geometry-conforming mesh so that the mesh is more faithfully representing the surface. The benefit of using the smooth boundary mesh is that bed shear stress may be computed more accurately than the stair-case mesh. However, snapping is

achieved by deforming the original mesh, which may or may not be possible and may have other unwanted consequences.

As a demonstration, mesh snapping is applied to the picnic table case. After mesh snapping a 3D boundary-conforming mesh is obtained as shown in Figure 14 and the zoom-in view is in Figure 15. Note that the initial background mesh is very coarse. Therefore, local mesh refinement is used to represent the picnic table in sufficient details around the table. Further, mesh snapping moves the mesh onto the surface. The actual refined and snapped mesh for the table surface is shown in Figure 16.

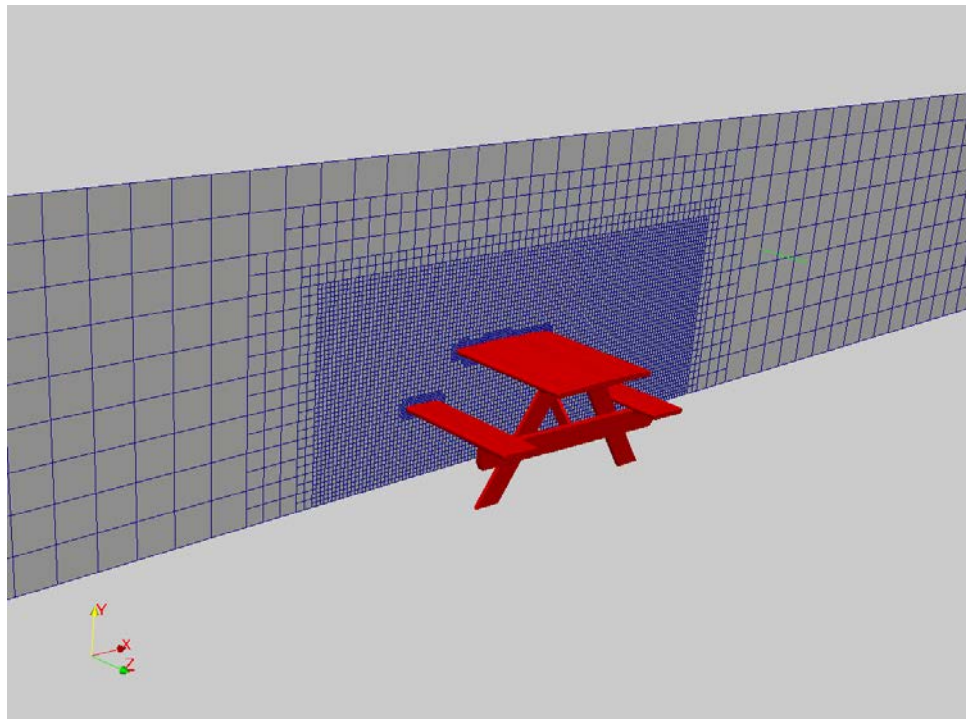


Figure 14. The 3D mesh generated for the flow around the picnic table after mesh snapping

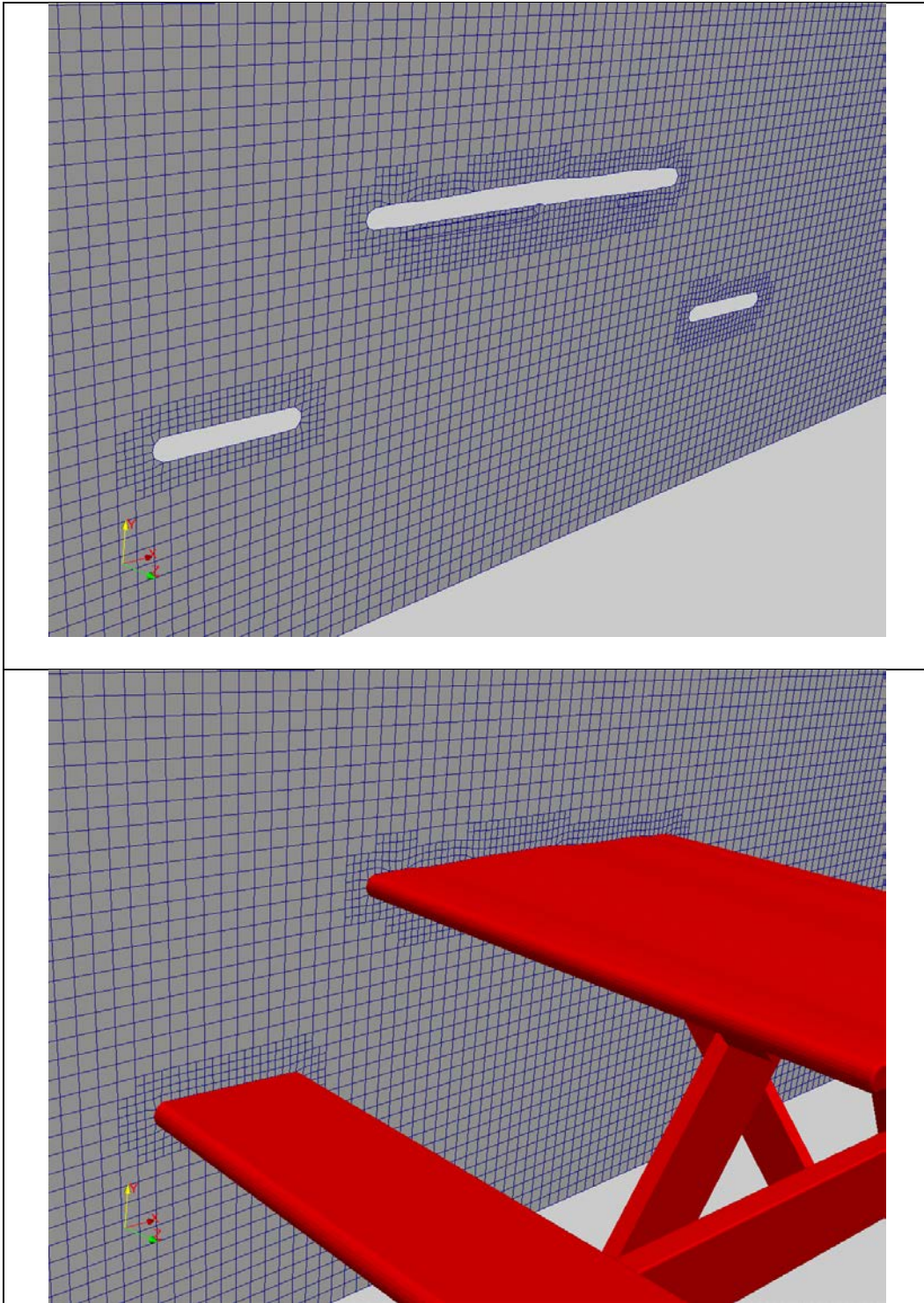


Figure 15. Zoom-in views of the 3D mesh after mesh snapping

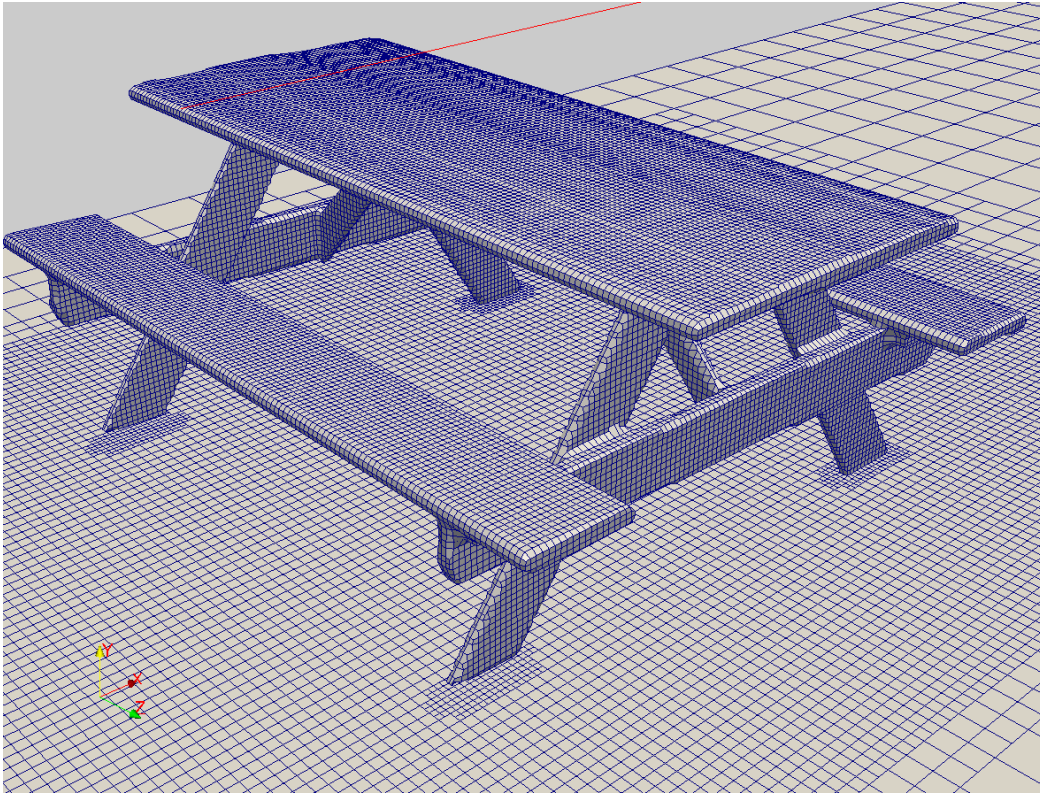


Figure 16. Refined mesh on the surface of the picnic table, along with the mesh at the bottom of the solution domain

## 7.5 Surface Mesh Layer Addition

SHM offers a further step to modify the mesh to better represent the flow field: Mesh Layer Addition. Using this procedure additional thin mesh layers may be added near solid surfaces or boundaries so that flows near the boundaries may be computed more accurately. Multiple layers may be added to user selected boundary patches with a user-specified layer thickness. The added surface layers are (supposedly) hexahedral and is carried out as follows:

- The mesh is projected back away from the specified boundary patch with a given thickness;
- Relaxation of the internal mesh is performed so that nodes are moved;
- The projection thickness will be reduced or not performed if the mesh quality criteria are not met;
- Mesh layers are added between the boundary patch and the projected layer; and
- A final mesh quality check is performed and inserted layers are removed if the quality is not met.

## Quantitative Modeling Tools for Large Wood

Mesh layer addition is performed with the picnic table case. Three thin layers are added near the bottom boundary of the solution domain. The resultant mesh is shown in Figure 17.

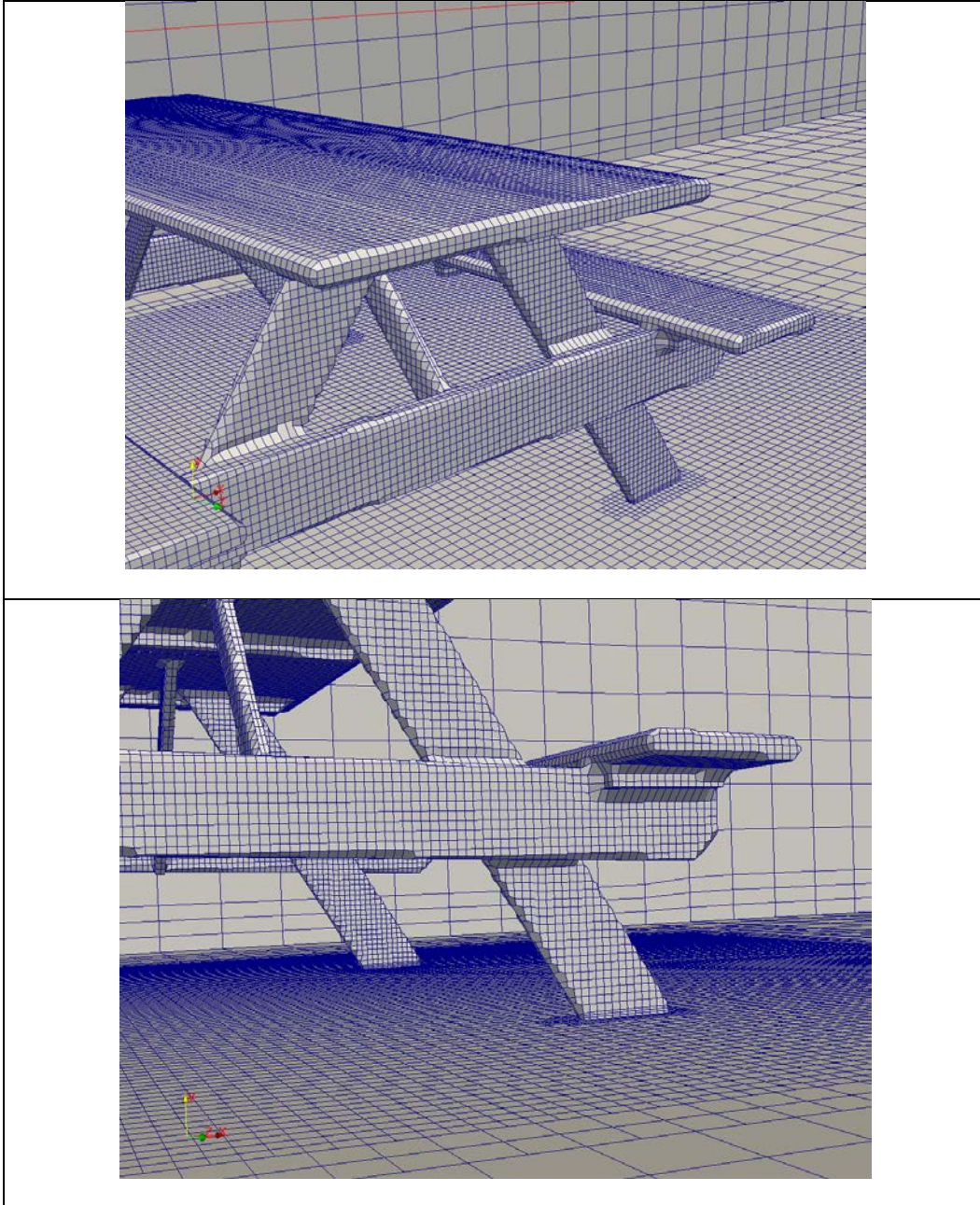


Figure 17. The 3D mesh for the picnic table case when three additional layers are added to the bottom boundary of the solution domain

## 7.6 Potential Problems

A number of potential problems have been reported in using snappyHexMesh and we have also discovered some limitations in using SHM. They are listed below. It is possible that future versions may eliminate some of the problems listed below as snappyHexMesh is continuously under revision and improvements.

- A good quality STL surface is very important for the success of mesh generation with SHM.
  - SHM itself can only define surfaces of cylinder, box and sphere; so other CAD programs are needed for generating STL surfaces.
  - The “surfaceCheck” utility, within the OpenFOAM package, may be used to check the geometry supplied with STL. Common problems include “non-closed STL” (i.e., with holes on the surface) or there are overlapping triangles. STL has to be repaired before SHM can proceed further for mesh generation.
- Edges with right angles may be deformed on the final mesh. For example, the circular edge of the cylinder is not represented accurately for the example in Figure 18. New versions may offer ways to get around this. For example, feature edges may need to be explicitly included using .eMesh files to instruct SHM that point on these edges should not be moved. The .eMesh file may be generated using the utility “surfaceFeatureExtract.” But these new features make SHM hard to apply.

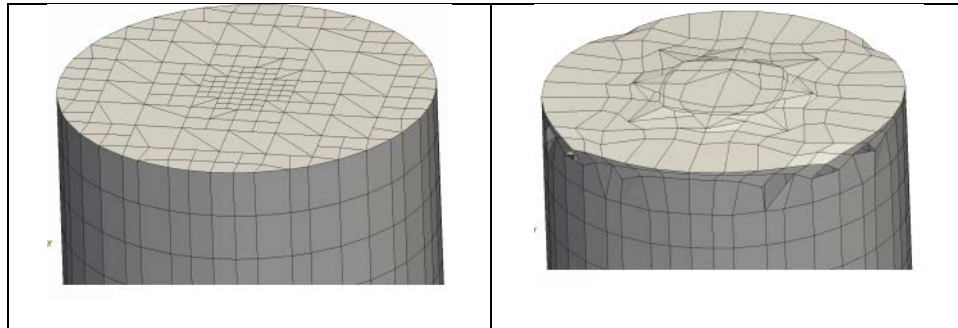


Figure 18. Potential edge problem with the snappyHexMesh

- Layer addition is hard to apply, particularly near the end of the STL surface, leading to unacceptably small layers or none at all.

Mesh quality control parameters may be set to change the mesh generation process discussed above. Different selection may impact the mesh generation process significantly. There is little documentation of how the parameters should be set. A few parameters are listed below based on our experience so far:

## Quantitative Modeling Tools for Large Wood

- Maximum non-orthogonality (maxNonOrtho):
  - Value 0 leads to only castellation step performed;
  - Values between 4 to 12 leads to castellation and snapping steps performed but snapped mesh quality may be poor;
  - Values between 13 and 43 leads to castellation and snapping performed with a reasonably good mesh.
  - Values between 44 to 180 leads to all steps activated (including layer addition).
  - Use of 180 will disable the quality check and is recommended to generate the mesh for river modeling with U2RANS.
- Maximum face skewness (maxBoundarySkewness and maxInternalSkewness):
  - The highest values that still allow surface layer addition are 1.10 and 0.45 respectively.

## 7.7 A Sample Use for River Flow

A sample use of SHM is presented below for modeling of flow through a section of the Sacramento River. SHM may be used to generate a boundary-conforming Z-mesh, called BCZ mesh in this report. BCZ mesh differs from the traditional Z-mesh in that (a) BCZ mesh has no requirement that mesh points have to be on the same horizontal plane and (b) mesh points are placed on the river bed (so called boundary-conforming) without the use of stair-case mesh cells. With BCZ mesh, fewer vertical points are used in shallow areas and the potential distortion of mesh cells on highly sloped river bed is alleviated in comparison with the sigma mesh. The traditional Z-mesh uses stair-case cells to represent the river bed. It leads to high uncertainty in shear stress computation. Shear stress is a key parameter in sediment transport modeling. This issue may be resolved by the use of BCZ mesh.

The confluence between the Sacramento River and the Georgiana Slough divergence channel near Walnut Grove, California, is selected for BCZ mesh generation using SHM. Detailed discussion of the site is presented in Chapter 7.

A background mesh is developed first as a multi-block structured mesh having hexahedral shapes. The main constrain is that it covers the horizontal extent of the study area. The vertical extent is sufficient so that the lowest point of the terrain and the highest point of the free surface are covered. For the background mesh generation, a list of points and curves are defined representing the model boundaries. Curves may be formed from points and 3D surface patches are then formed from the defined curves. The 3D hexahedral background meshes may then be generated from six surface patches forming a mesh block. A special option is under development with U2-Mesh in which a multi-block 2D quadrilateral mesh may be generated first and the 2D mesh is then extruded vertically to generate a 3D mesh. The extrusion method may be useful for many river simulation cases.

## 7. 3D Mesh Generation

The generated background mesh for the confluence of the Sacramento River and Georgiana Slough is shown in Figure 19; the solution domain and the final generated background mesh are shown. Zoom-in views of the mesh near the Georgiana Slough channel are plotted in Figure 20.

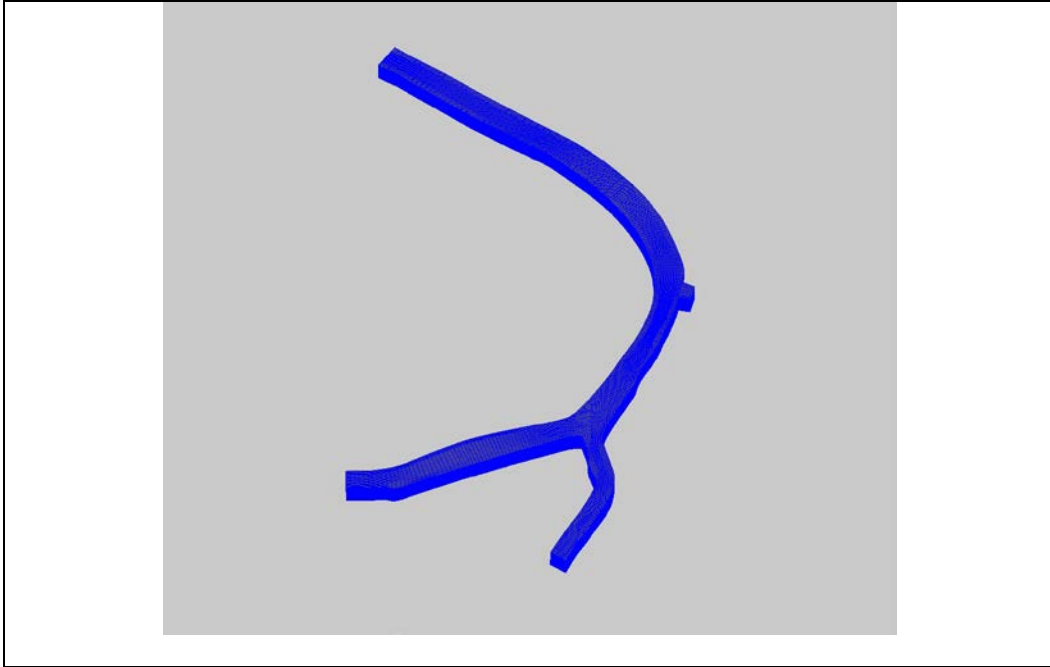


Figure 19. The 3D multi-block structured hexahedral meshes as the background mesh

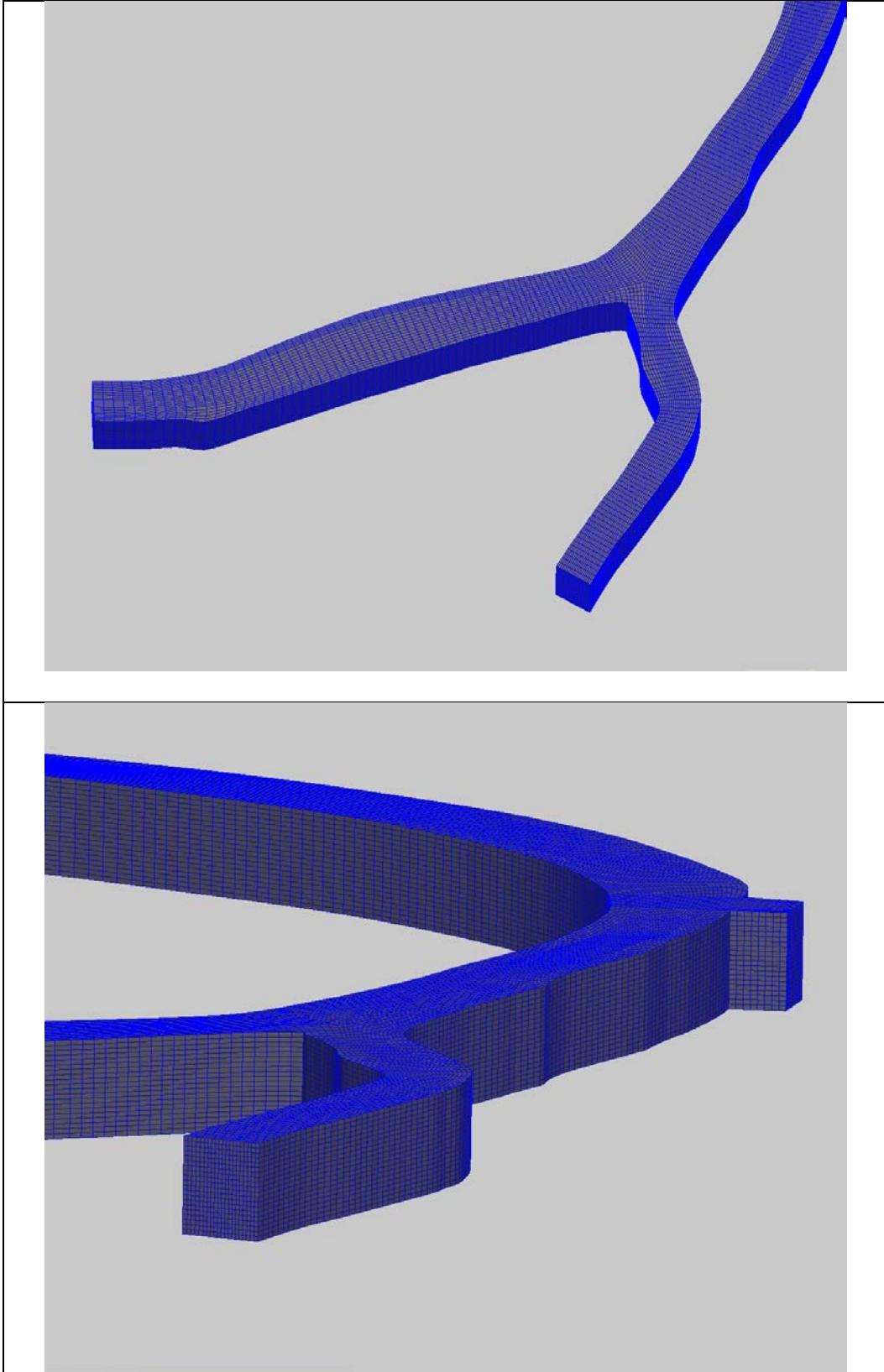


Figure 20. Zoom-in views of the 3D background mesh near the juncture

Next is to generate a new 3D mesh that conforms to the bed terrain and free surface within the model domain. If the bed and free surface elevations are available along each vertical mesh line, a new 3D mesh may be developed using SHM.

For the example, the bed terrain is available from Lidar and terrain survey data while the free surface elevation is available from the SRH-2D results. The survey terrain and free surface elevation are interpolated onto a horizontal triangulated mesh which has a domain covering the entire horizontal extent of the background mesh. The triangular mesh with terrain and free surface information is then converted into STL format. The STL is used as an input to the SHM along with the background mesh. Finally, SHM is used to generate a castellated 3D mesh as shown in Figure 21. Note that the background mesh is not only cut from the bottom by the bed terrain STL; it is also cut from the top by the free surface STL.

Finally, mesh nodes near the bed with the stair-case feature is moved onto the bed using the mesh snapping of SHM. The operation leads to the BCZ mesh as shown in Figure 22. It is clearly shown that the BCZ mesh has a smooth bed while the castellated mesh is stair-cased.

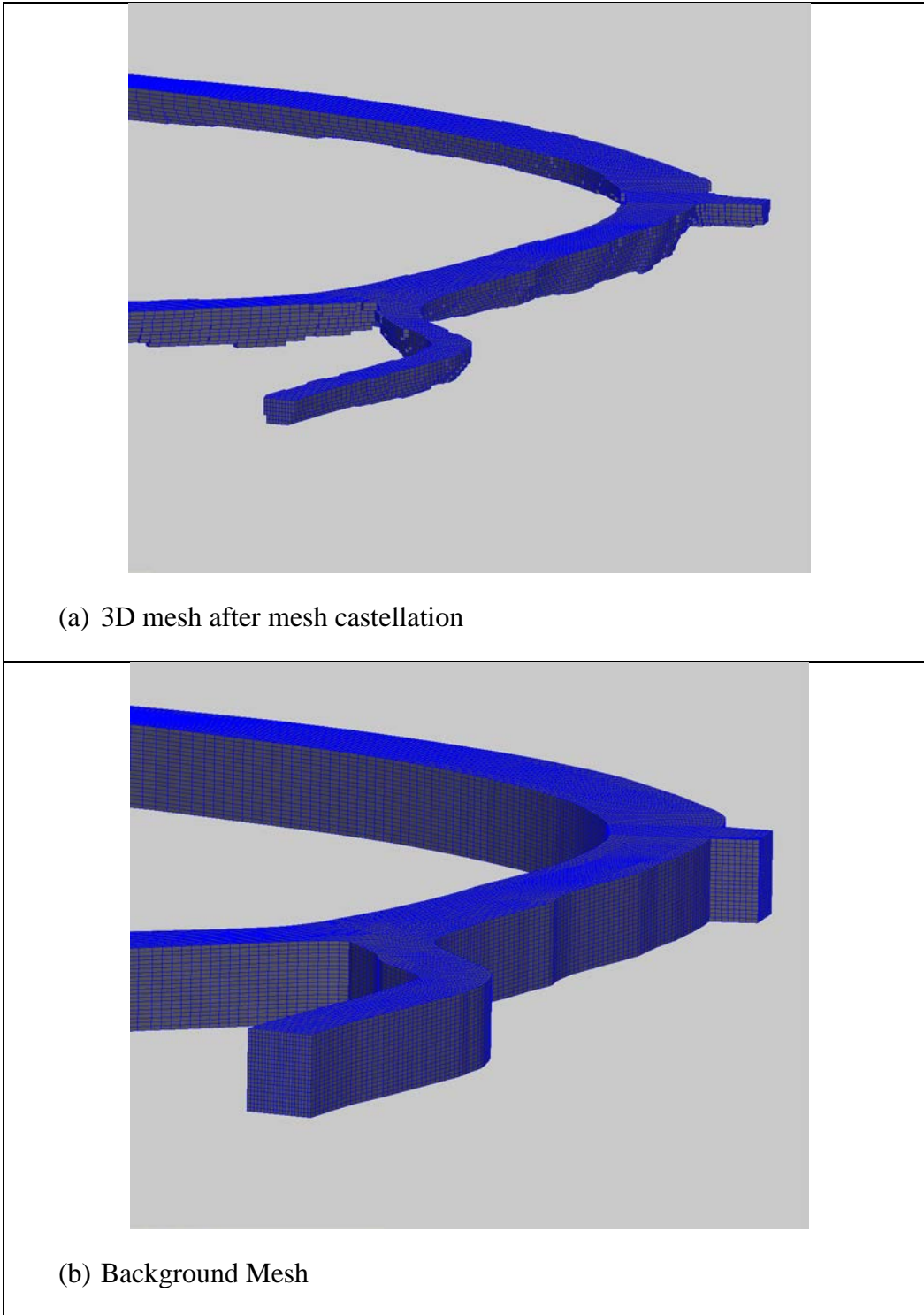
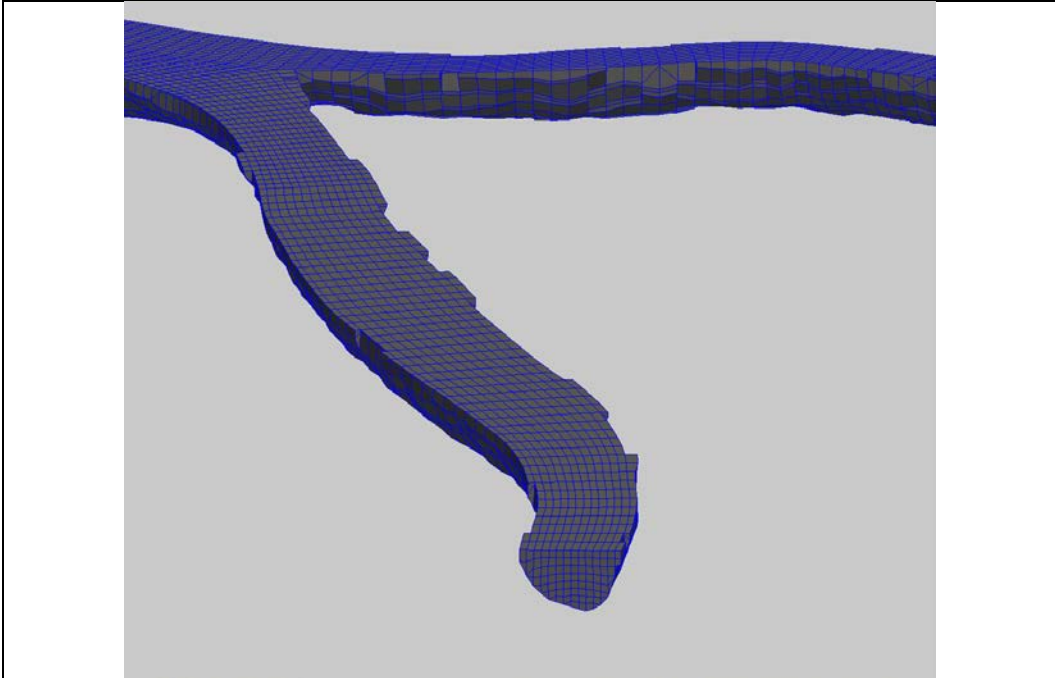
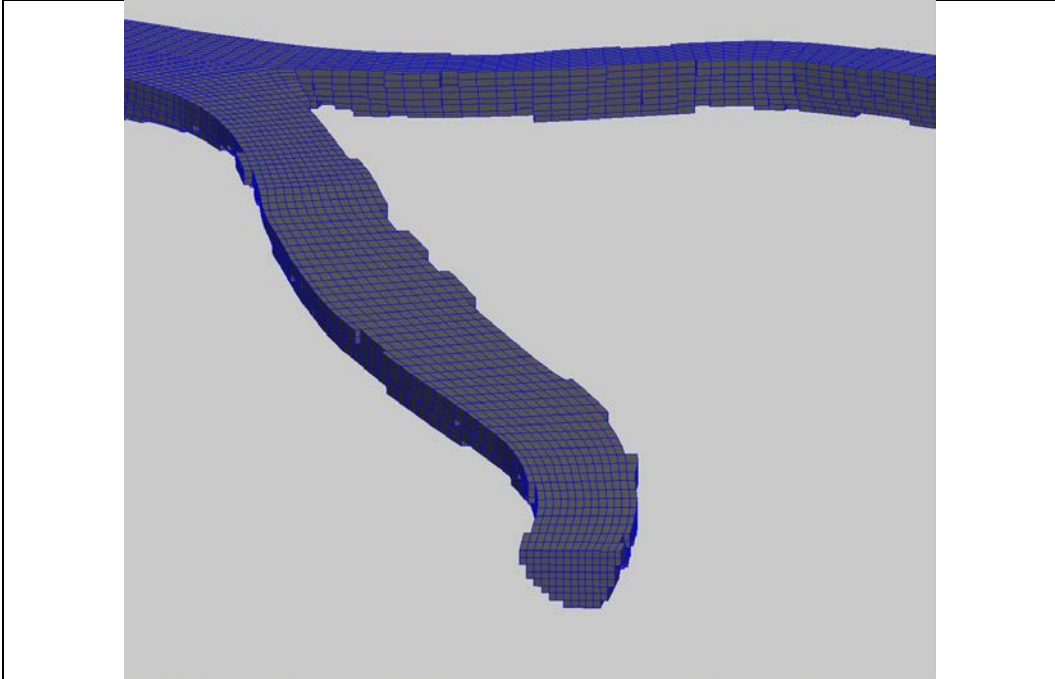


Figure 21. Comparison of the background mesh and castellated mesh



(a) BCZ Mesh after Snapping



(b) Staircase Z-mesh after Castellation

Figure 22. Comparison of castellated mesh and the snapped mesh

## 8. Flow Module Results

The flow module extension and enhancements have been carried out based on the previous model U2RANS of Lai et al. (2003). The following new features have been added to U2RANS:

- U2RANS is extended to read the meshes generated by SHM which may include any number of faces with a mesh cell as well as a cell with only part of its faces having mesh refinement.
- The flow module has been made to operate on an arbitrary hexahedron with even highly deformed and non-orthogonal cells. Module test and verification have been carried out to ensure that the module works properly and correctly.
- An option is added so that the U2RANS can simulate flows using the unstructured physical-coordinate (UPC) sigma mesh which has been discussed in a separate report about SRH-3D development. UPC sigma mesh can be automatically generated giving an initial 2D unstructured mesh and the free surface elevation from SRH-2D or SRH-3D results. This option alleviates the complex mesh generation process and is often adequate for many river engineering projects. This work also paves the way to use the decoupled method to treat the free surface. Field cases have been used to validate this new capability.
- An unsteady simulation option is developed and added into the model.
- Model results can be output to a format used by ParaView. The graphical post-processing software ParaView is an open-source, multi-platform application designed to visualize data sets of varying sizes from small to very large. It has an open, flexible, and intuitive user interface. Furthermore, ParaView is built on an extensible architecture based on open standards. Our test of ParaView showed that it is competitive with any available commercial software and is recommended for use to view the U2RANS results. ParaView can be freely downloadable at the following website: <http://www.paraview.org/>. A nice capability is that ParaView supports the polyhedron mesh cells.
- The new TECPLOT 360 format is also added in order to support the display of polyhedron mesh cells for those who already have TECPLOT 360 license.

A number of test and validation cases have been carried out with the new flow module. They are documented below as model verification cases.

## 8.1 Flow over a Picnic Table

The new flow module is used to solve the sample flow over the picnic table whose mesh has been generated in Chapter 6 as a demonstration of the new features. The 3D mesh is generated using SHM and used as one of the inputs.

The simulation is carried out by assuming the following: the flow velocity at the front is 1.0 m/s; turbulence is simulated with the two equation  $k-\epsilon$  model. The predicted pressure field, velocity magnitude and velocity vector are shown in Figure 23, Figure 24 and Figure 25.

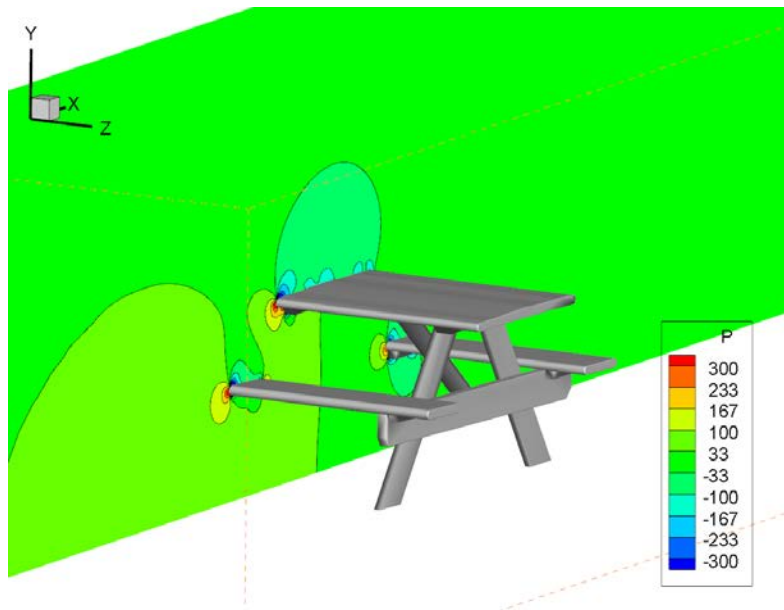


Figure 23. Predicted pressure field in Pascal on the mid-plane of the solution domain

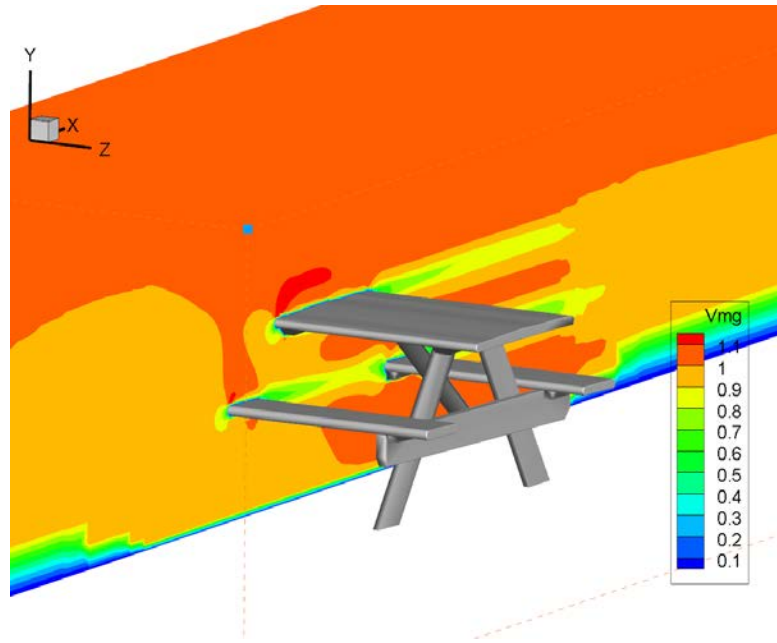


Figure 24. Predicted velocity magnitude (m/s) distribution on the mid-plane of the solution domain

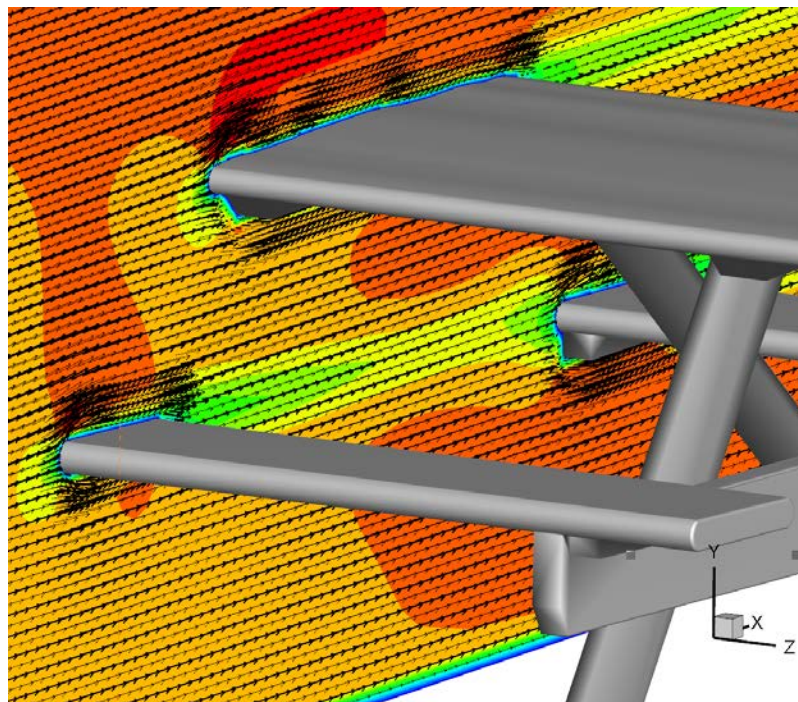


Figure 25. Predicted flow velocity vector (m/s) near the table on the mid-plane of the solution domain

### 8.2 Flow over a Tree with Rootwad

The next challenge is to demonstrate the tools for flow modeling with very complex geometry. For this purpose, flow over a tree with a rootwad is selected.

The motivation for the case is that large wood (LW) has been widely used in stream and watershed restoration projects as studies have found that flow and habitat complexity is positively correlated with habitat quality (Smith et al., 2006). Its popularity is linked to many ecological and morphological benefits it creates (Abbe and Montgomery, 2003). Engineered log jams (ELJ) using LW, for example, are an effective way of creating habitat complexity for aquatic species such as salmonids (Pess et al., 2013). LW has a strong influence on local channel morphology leading to pool and bar formation and sediment storage (Eaton et al., 2012). There is a need to better understand the flow and geomorphic processes induced by the placement of LW related to critical habitats using quantitative morphological assessments or structured design guidelines. There is also a need for more thorough understanding of flow field and morphological complexity related to eddies and velocity gradients that result from large wood, boulders, and other complex objects (Smith et al. 2010).

LW use in streams, however, has unresolved challenges with regard to its impact to stream morphology, safety and lack of design guidelines. Laboratory or field study of LW is difficult due to irregular nature of LW structures. CFD modelling, therefore, becomes an attractive alternative. At present, Reclamation is teaming up with engineers at the U.S. Corp of Engineers (USACE) to carry out a research on flows around LW. USACE will set up a laboratory study while Reclamation will conduct the CFD study. In the future, comparisons of CFD results with laboratory results will be made. Herein, we present a CFD computation using the developed tools as a demonstration.

Wood jams are extremely difficult to represent in computer modelling or laboratory experiments due to their complexity and irregular shapes. LW in rivers is typically found in chaotic forms with various orientation and sizes of logs, branches, roots, and slash materials forming an array of interwoven geometries. This collection of geometries presents a challenge when trying to replicate as a 3D solid model. With the recent advancement in laser scanners technologies the ability to capture complex objects in three dimensions is becoming feasible. Utilizing stationary terrestrial LiDAR scanners deployed in the field we are able to capture high resolution point cloud data made up of millions of 3D points of LW structures that were recently constructed for river restoration applications.

In this study, we have successfully scanned in a tree with a rootwad which was used for river restoration purpose on the Trinity River, California. The raw 3D point cloud is downloaded into the computer environment to serve as the foundational dataset for solid modelling. Figure 26 shows the trees in the field and the solid model representation of a particular tree after laser scanning.

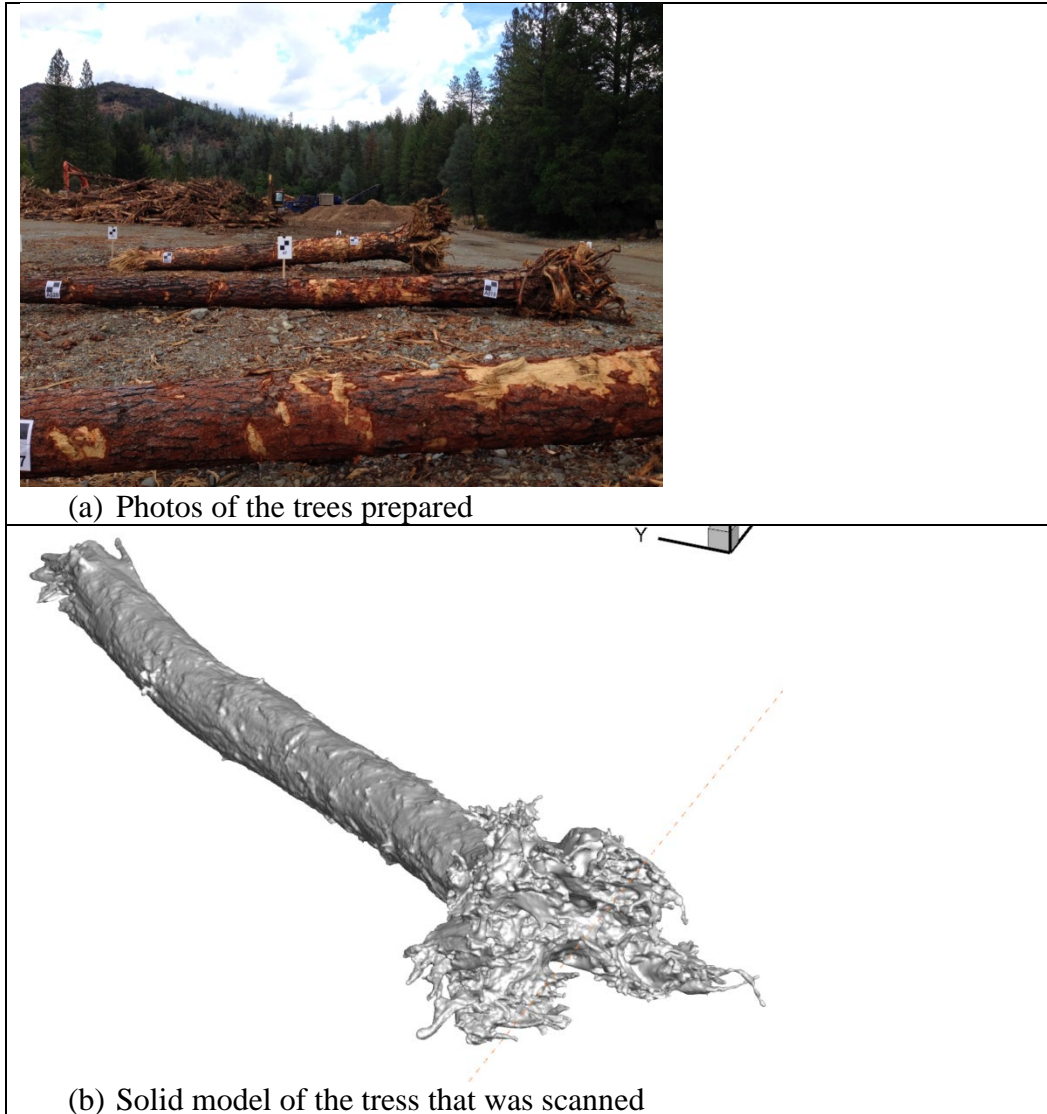


Figure 26. Complex trees with rootwad used for restoration on the Trinity River (a) and the solid model of one of the trees scanned using 3D laser scanner

The scanned tree surface is represented with a triangulated mesh network and its representation is saved to a file with the STL format. Figure 27 displays two close-up views of the tree represented by the STL. As shown, the presence of the rootwad makes the tree geometry very complex and generation of a mesh around such geometry can be a challenge.

Next, we use SHM to generate a suitable mesh around the tree in order to carry out the flow modeling. We generated a background hexahedral mesh using simply a rectangular box. The box has 10 meters in length (x direction), 2 meters in width (y direction), and 1 meter in height (z direction). The number of cells is 100 along

x, 20 along y and 10 along z. The STL represented tree is “placed” into the background mesh as shown in Figure 28. An automated local mesh refinement is applied around the tree and also in two subzones of the background mesh. The castellation and snapping are activated for the automatic mesh generation. The final SHM generated 3D mesh is shown in Figure 29, and a zoom-in view of the mesh is plotted in Figure 30.

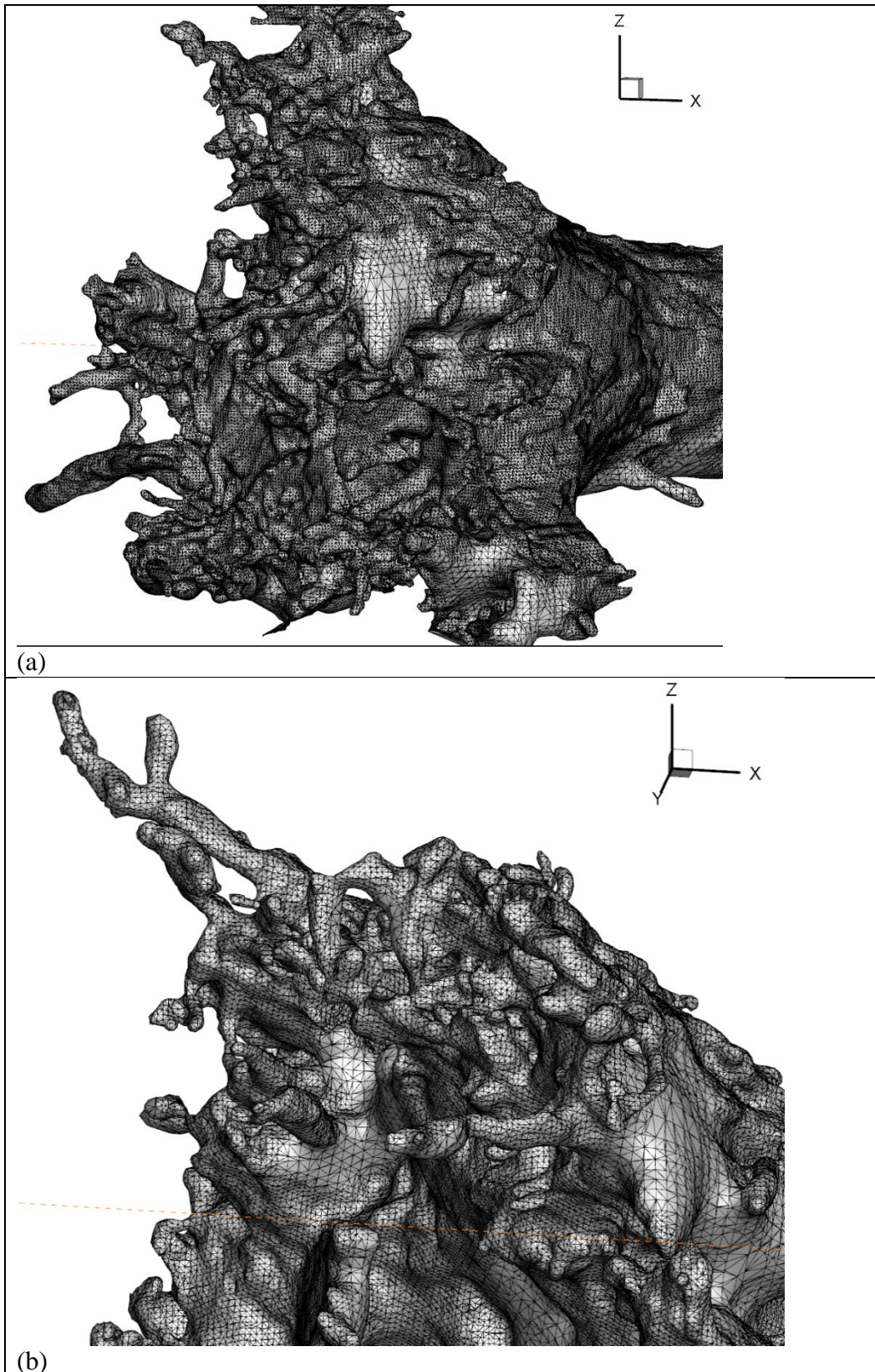


Figure 27. STL representation of the tree with rootwad

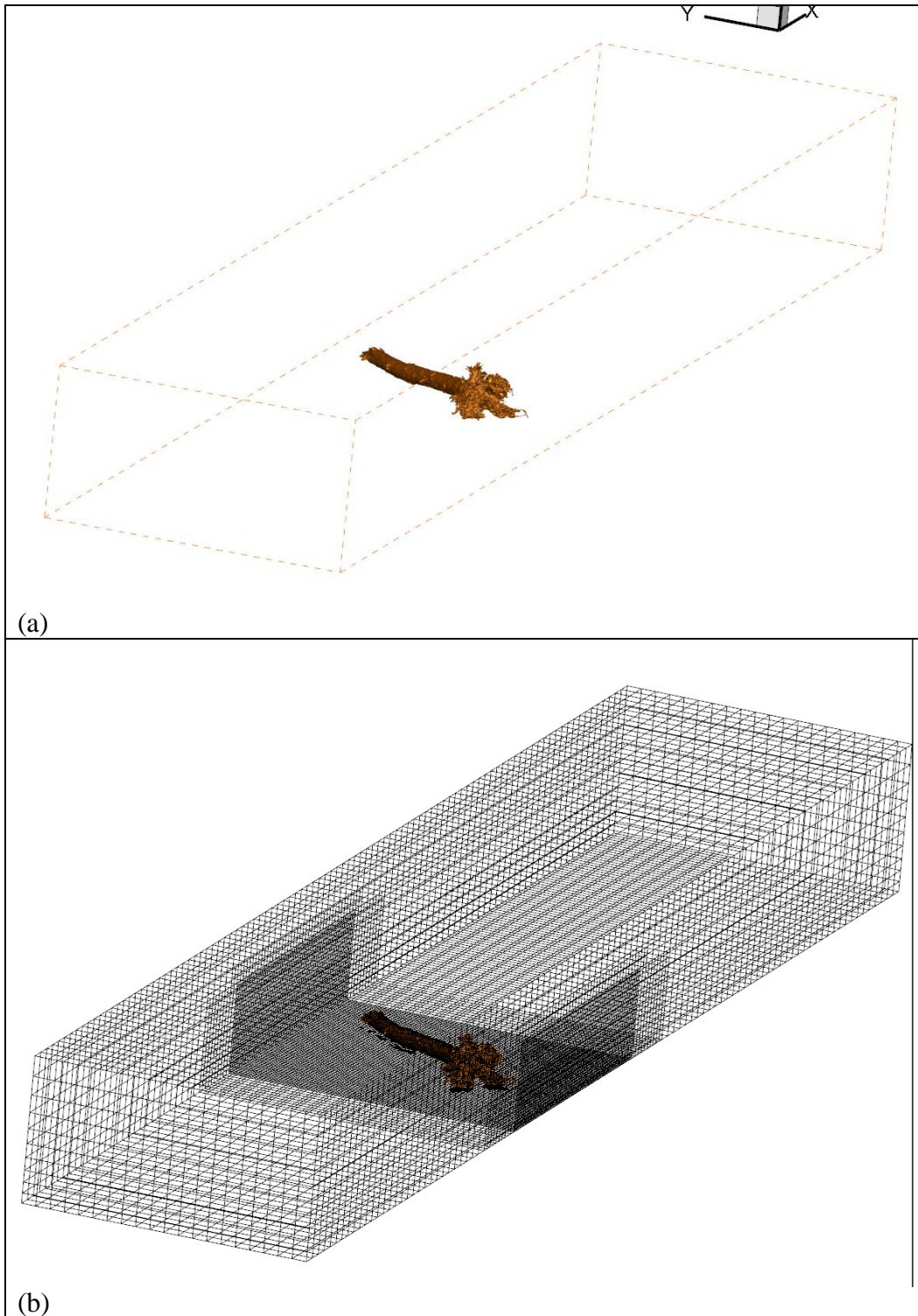


Figure 28. Background mesh and placement of the tree in the model domain

## Quantitative Modeling Tools for Large Wood

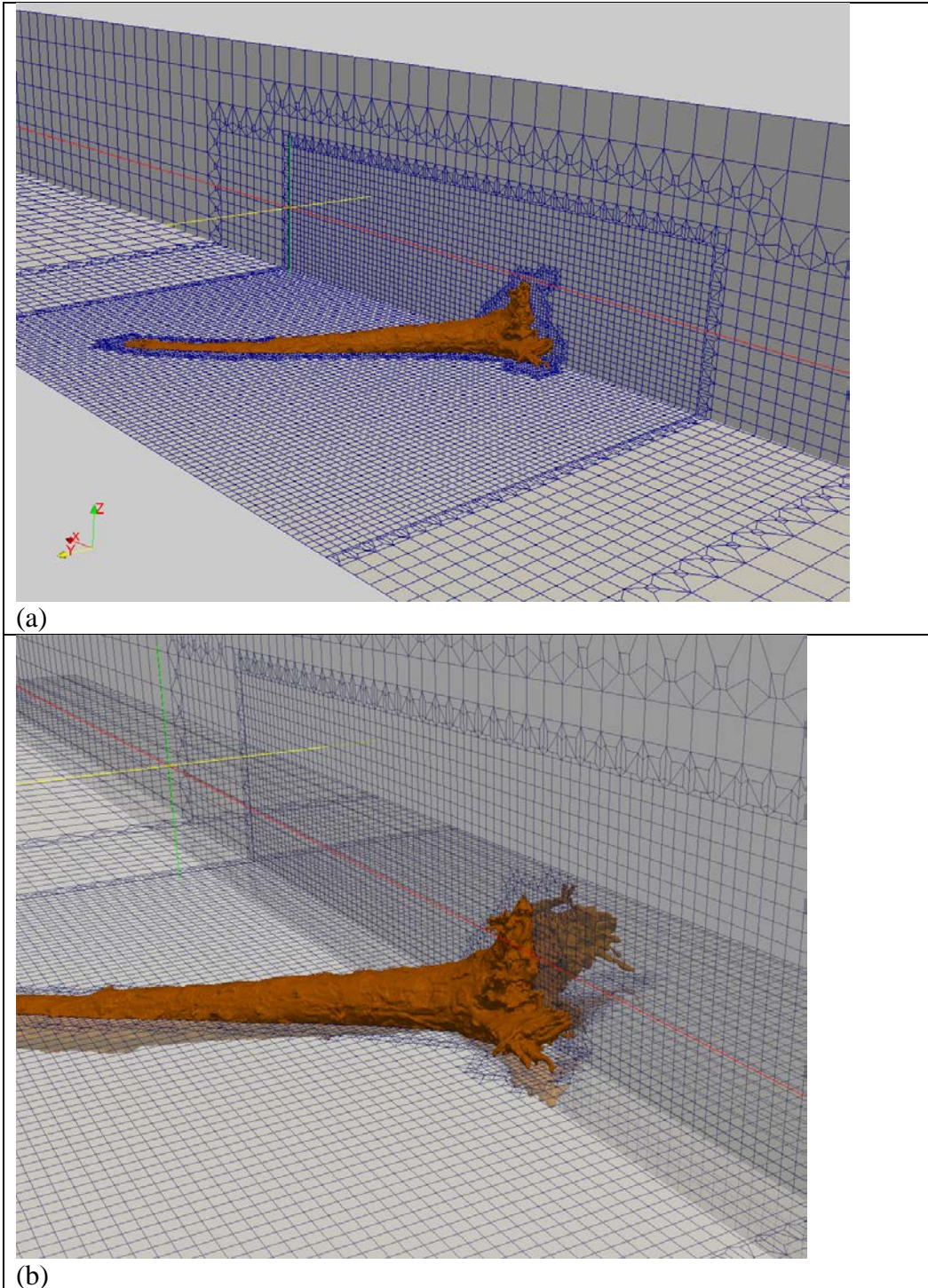


Figure 29. Two views of portions of the final 3D mesh

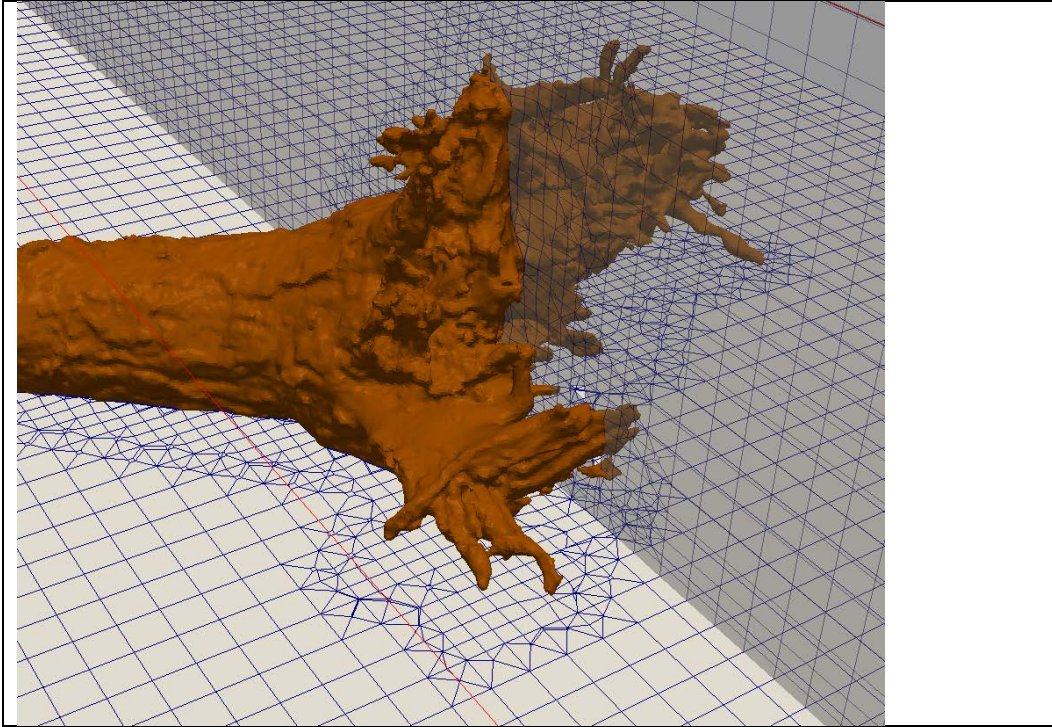


Figure 30. Zoom-in view of the mesh around the rootwad

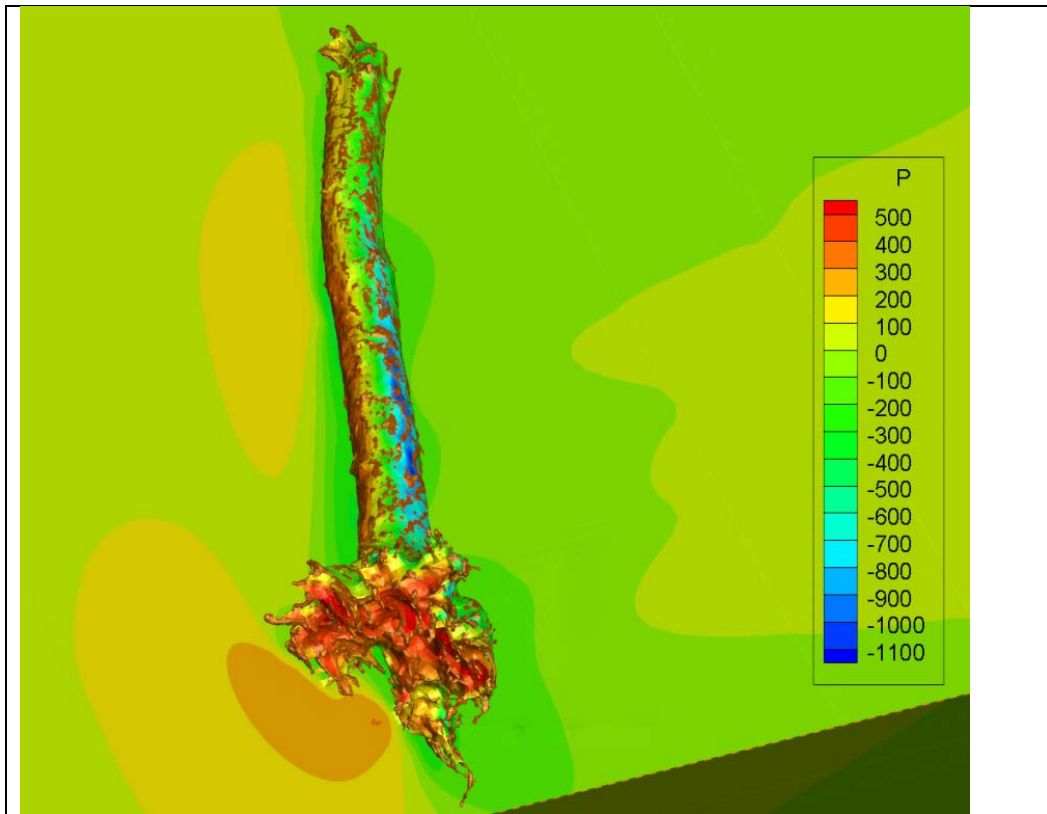
## Quantitative Modeling Tools for Large Wood

With the 3D mesh generated, flow modeling over the tree is finally carried out. We assume that the approaching flow has a uniform velocity of 1.0 m/s and two-equation  $k$ - $\epsilon$  model is used for turbulence.

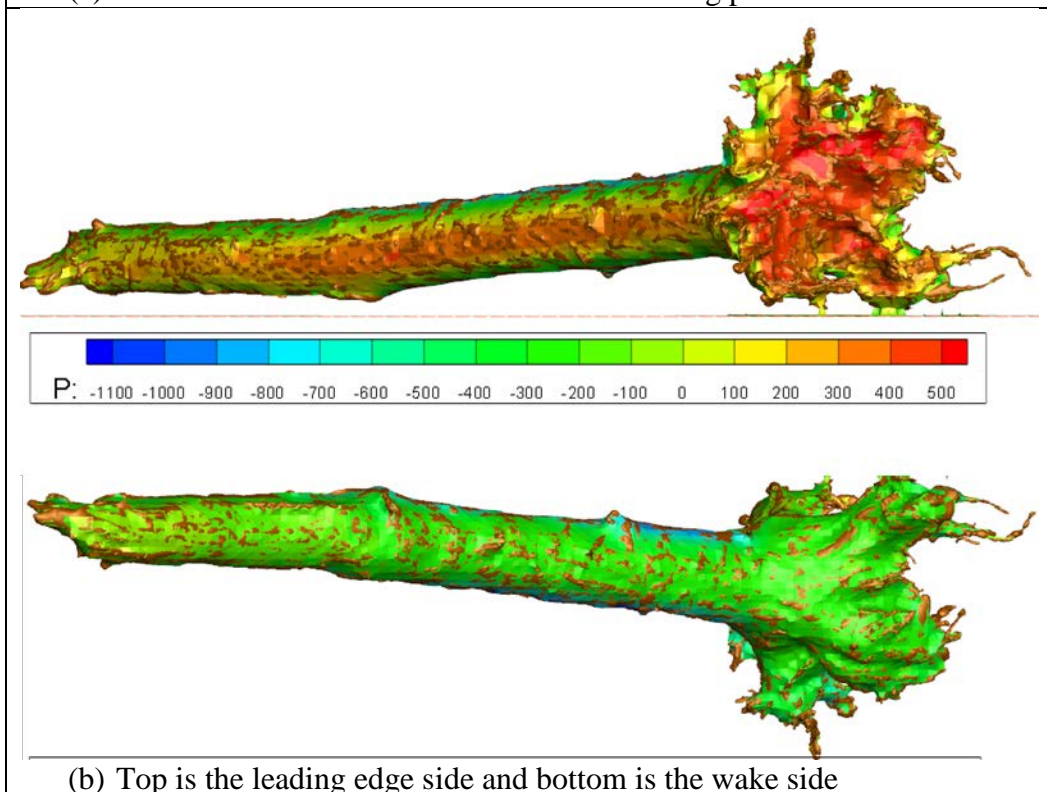
We can only discuss the model results qualitatively as no measurement data are available for model validation. Figure 31 shows the model predicted pressure on the tree surface. It is seen that the leading edge of the tree experiences higher pressure and wake side is lower, consistent with our expectation. In particular, the highest pressure is in the rootwad area. With pressure distribution, the total force and moments may be computed acting on the tree. Such information is useful to understand the stability of the woody structure placed in a stream.

The predicted velocity field around the tree is displayed in Figure 32, while the flow streamlines are plotted in Figure 33. From the vertical cutting plane, it is seen that the model predicts higher velocity on the top part and lower velocity in the wake region; it is consistent with the blockage effect of the tree. From the horizontal cutting plane, the model predicts that the flow is pushed against the bank with high velocity due to the presence of large rootwad. The rootwad has the highest impact on the flow and creates large wake zone behind. From the streamline plots, it is seen that the flow in the wake is very complex with multiple vortices which are expected to be important in terms of flow complexity for fish habitat.

USACE is planning to conduct laboratory experiments for flows around trees. Once lab data are available, we will perform more CFD modeling around trees so that the model results may also be validated.



(a) Around tree surface and on a horizontal cutting place



(b) Top is the leading edge side and bottom is the wake side

Figure 31. Simulated pressure distribution around the surface of the tree. Pressure is in  $N/m^2$ .

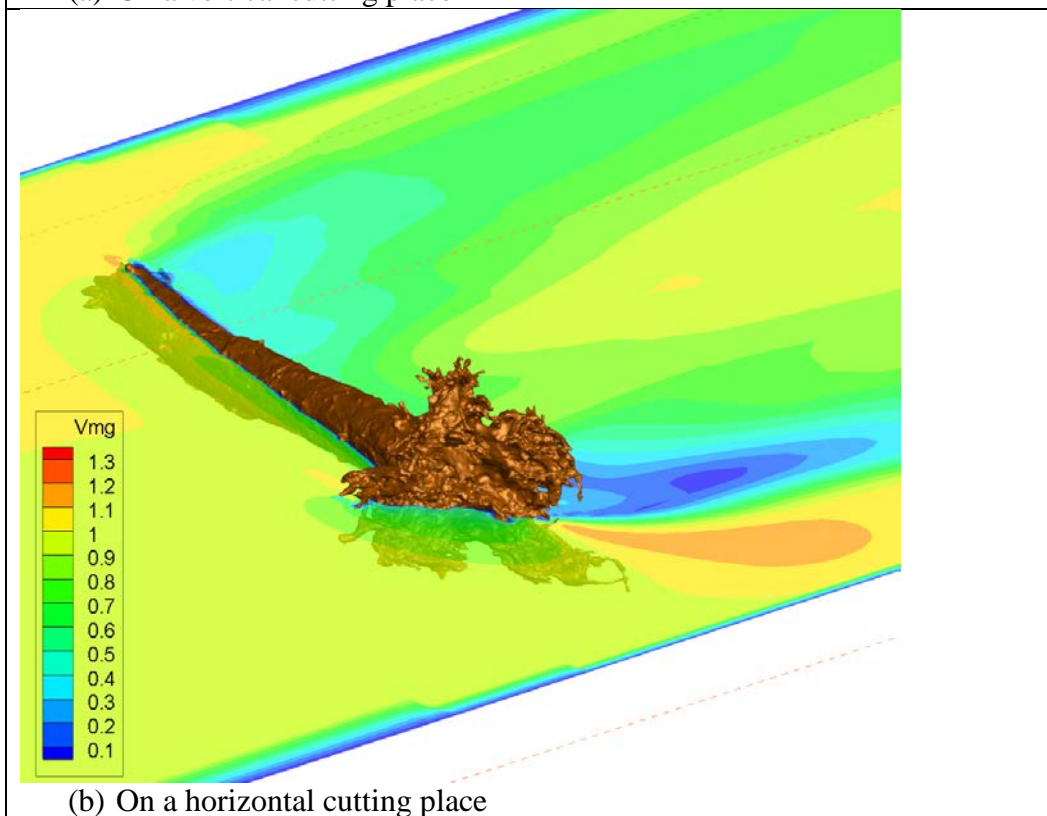
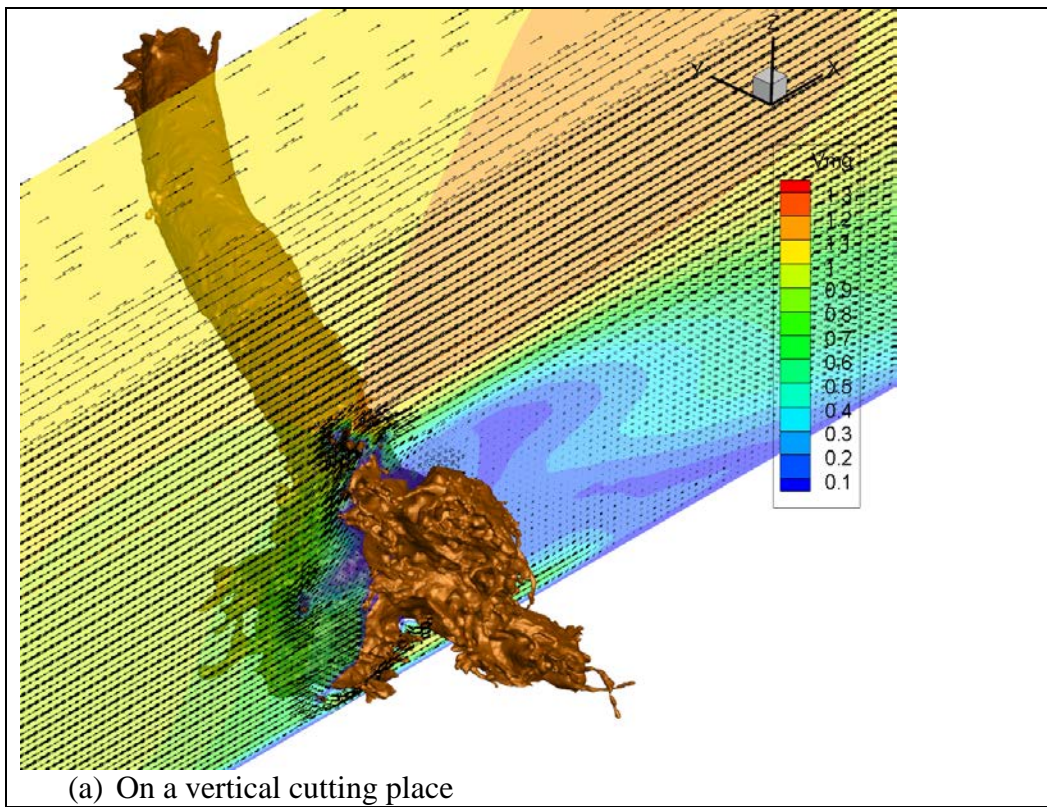


Figure 32. Simulated velocity field around the tree. Velocity is in m/s.

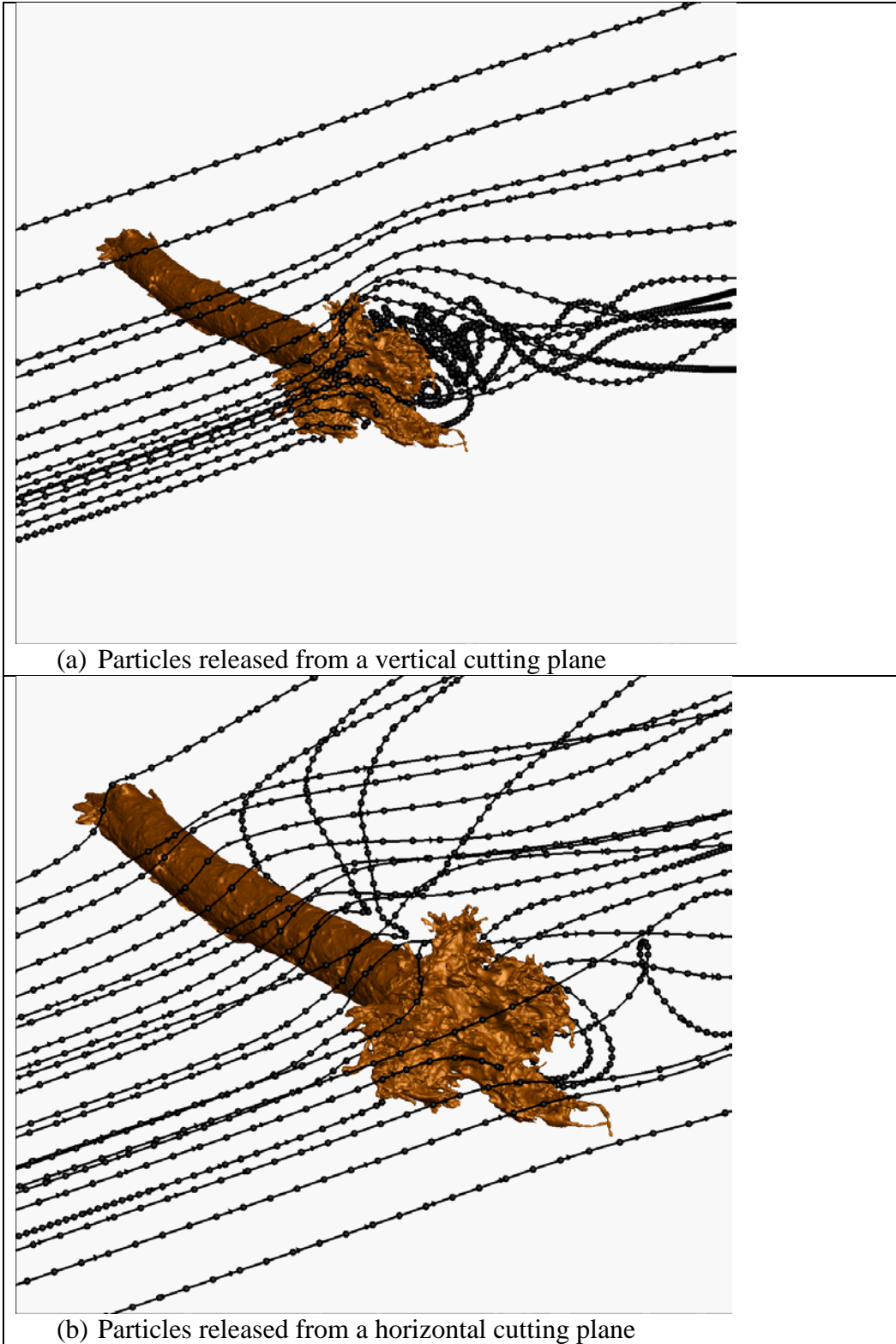


Figure 33. Simulated flow streamlines around the tree

## 8.3 Flow at the Junction of Sacramento River and Georgiana Slough Channel

We carried out an unsteady flow modeling on a reach of the Sacramento River using the flow module developed in this study. The case is typical of river flow applications of 3D models in the future and can serve as a good model validation study since field data are available for comparison.

### 8.3.1 Background

Juvenile salmonids can travel multiple routes to the Pacific Ocean as they out-migrate downstream through California's San Joaquin and Sacramento rivers. Engineering is sometimes used to prevent, or minimize these fish from entering routes associated with higher mortality (Bowen et al. 2009; Bowen and Bark 2010; Zielinski et al. 2014). Juvenile salmon that are routed through the interior delta may exhibit reduced survival from a number of stressors including: elevated predation, poor water quality, elevated water temperatures, and pumping facilities. Both physical and non-physical fish barriers have been engineered to deter fish from sub-optimal routes, yet measuring the effectiveness of different methods for guiding fish is still an emerging science. There are a number of factors that have been identified to influence effectiveness. The relative importance of many of these factors may vary spatially, temporally, and by the species of concern or the stage of life-cycle of the species. Definitive estimates of the extent to which barrier effectiveness varies as a function of these factors remain poorly understood. This is partially due to lack of science in understanding fish movement response and behavior. In turn, this hampers the development of reliable design criteria.

Field and computational studies have been initiated by agencies such as the U.S. Bureau of Reclamation, the California Department of Water Resources, the U.S. Army Engineer R&D Center, and the U.S. Geological Survey. Some of the results may be found in a number of reports (e.g., Bowen et al. 2009; Bowen and Bark 2010). One of the study goals is to advance the science in seeking whether computational models, such as the ELAM model (Eulerian-Lagrangian Agent Model) may be developed and used to predict fish movement behavior in response to local flow hydrodynamics as well as other variables (Nestler et al. 2011). With ELAM model, hydrodynamic and turbulence variables are needed and are computed by 3D CFD models.

In this study, we perform a 3D modeling of flows at the junction of the Sacramento River and the Georgiana Slough channel, near Walnut Grove, California. The 3D model is in support of the Eulerian-Lagrangian-Agent Method (ELAM) model in predicting fish movement patterns and statistics. Ultimately, the combined model tools may be used to assess the effectiveness of the fish barriers used in the field and model results may be compared with the fish tracking data deployed in the field. The flows at the junction are oscillatory and

complex due to tidal influence so the modeling is a challenging test to any CFD models.

### 8.3.2 Site Description and Available Data

The study site is the junction of the Sacramento River and the Georgianna Slough channel near Walnut Grove, California (see Figure 34). The Sacramento River flows southeast from the upstream and turns towards west through a bend. Flow diversion to the Georgianna Slough is on the south side of the bend. Flow at this junction area is oscillatory due to tidal influence and displays complex eddy patterns.

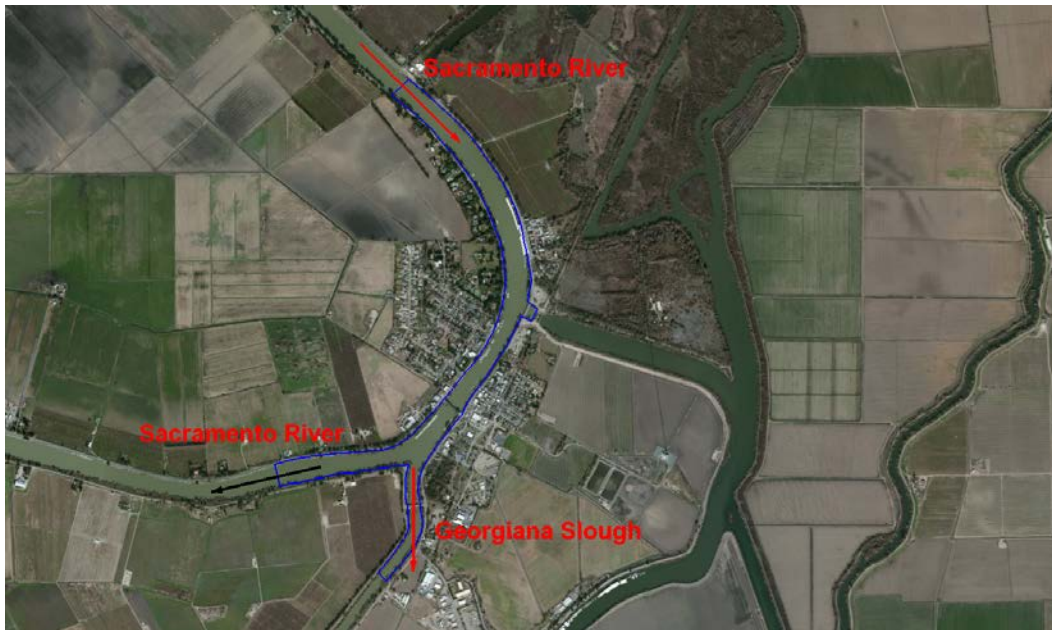


Figure 34. Aerial photo of the study site at the confluence of the Sacramento River and Georgianna Slough, Walnut Cove, California

The bathymetric data of the study site was collected by DWR's North Central Region Office (NCRO) using multibeam on three separate trips in 2013 and 2014. The dates of data collection are shown in an overview of the project area in Figure 35. The data was collected with equipment both on land and water before, during and after the barrier experiment and was positionally corrected with RTK GPS to conform with the NAD83 California State Plane Zone II coordinate system and NAVD88 datum.

Field calibration tests (including multibeam patch tests, sound velocity readings, and RTK GPS observations) were regularly performed in order to ensure data quality and positional accuracy. Multibeam data were collected aboard an Oquawka 2072 Vessel and recorded using Hypack Hydrographic Survey software (Hypack). Data were processed using either Caris or Hypack, exported as XYZ

## Quantitative Modeling Tools for Large Wood

text files, and imported as a raster in a geodatabase using ArcGIS software. The bed elevation contours surveyed on June 16-17, 2014 are plotted in Figure 36.

In addition, LiDAR data in the DEM form (5m by 5m resolution) are also available in the study area (see Figure 37 for the coverage area); they were collected in 2007. The data set was obtained by DWR and used to represent the bank and floodplain area.

The LiDAR data was combined with the 2014 bathymetric data to create a composite terrain used for the present modeling study.

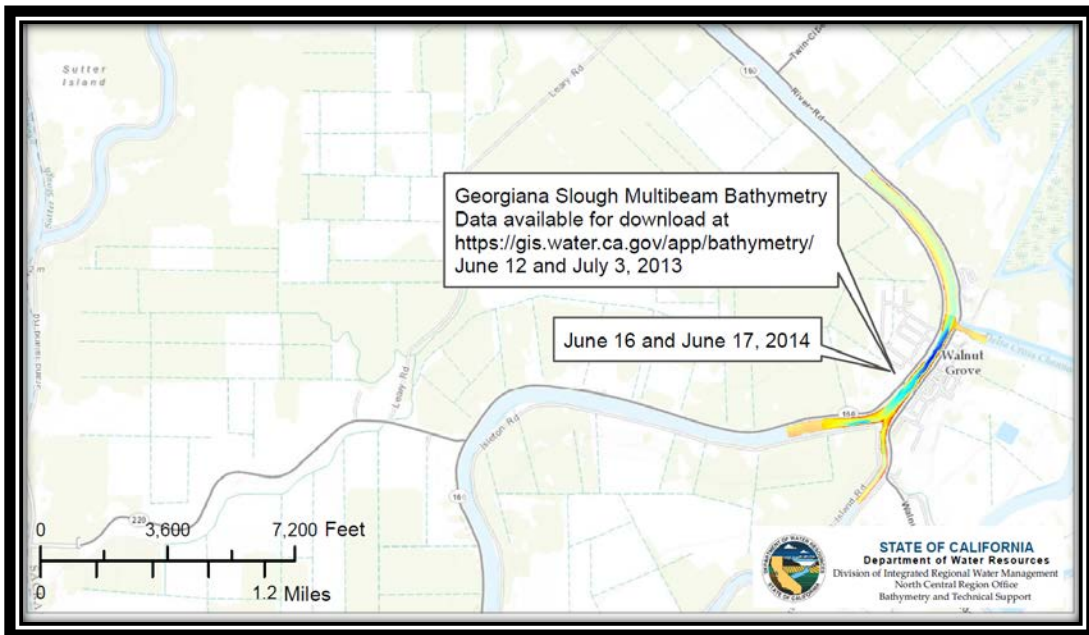


Figure 35. Coverage area and survey dates of multibeam bathymetric data conducted by DWR NCRO

## 8. Flow Module Results

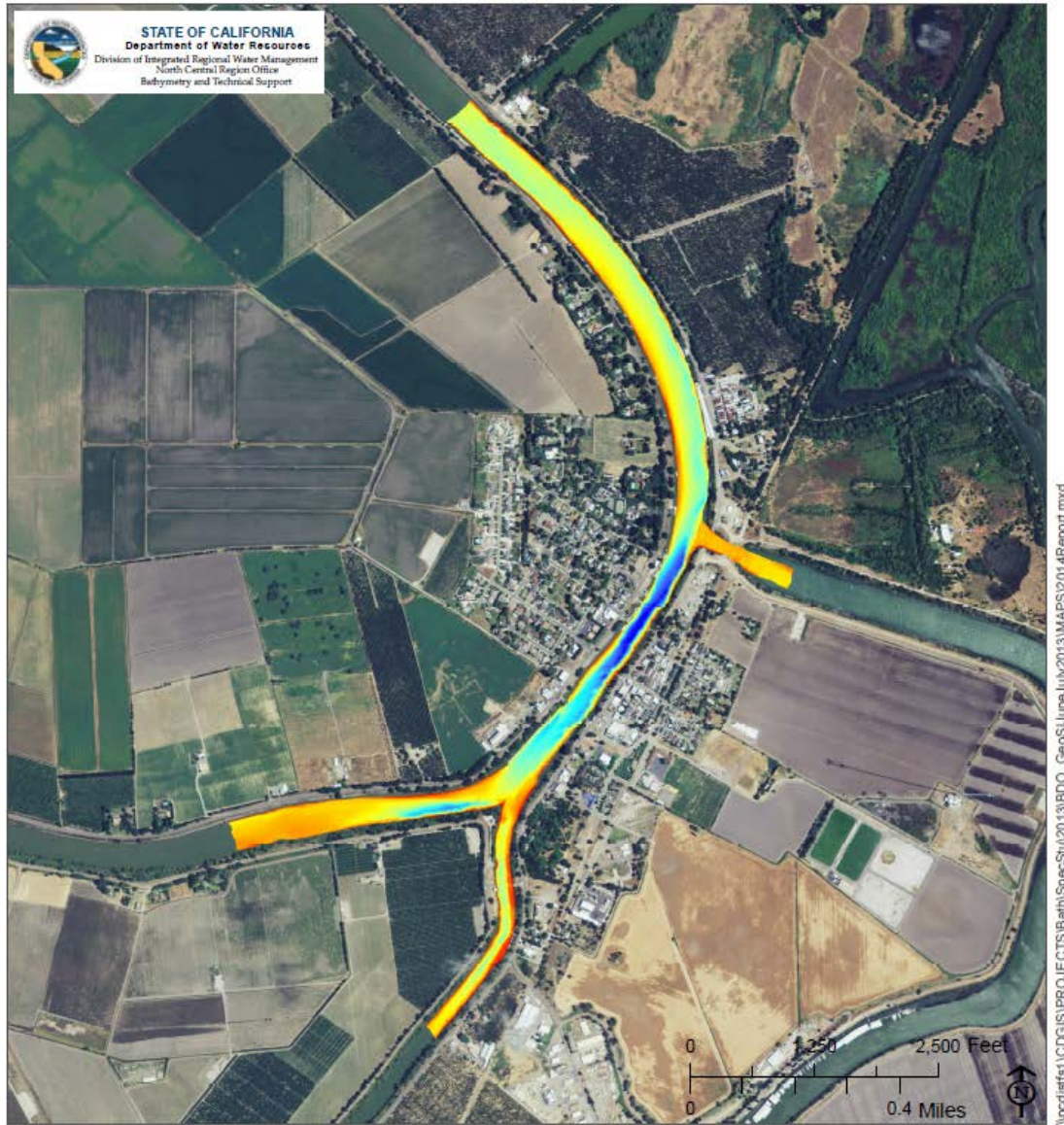


Figure 3

Survey Date: June 16-17, 2014  
Collection Method: RTK GPS and Multibeam Echo Sounder  
Collected by: Scott Flory  
Processed by: Lisa Sawyer  
Reviewed by: Shawn Mayr  
Coordinate System: California State Plane Zone II  
Projection: Lambert Conformal Conic  
Datum (horizontal): NAVD83  
Base Map: NAIP Imagery 2009 4 Band  
Map Author: Amy Zuber

### Georgiana Slough Bathymetry Summer 2014 ( Post Barrier )

Elevation (NAVD88, Feet)



Figure 36. Bed elevation as measured on June 16-17, 2014

## Quantitative Modeling Tools for Large Wood

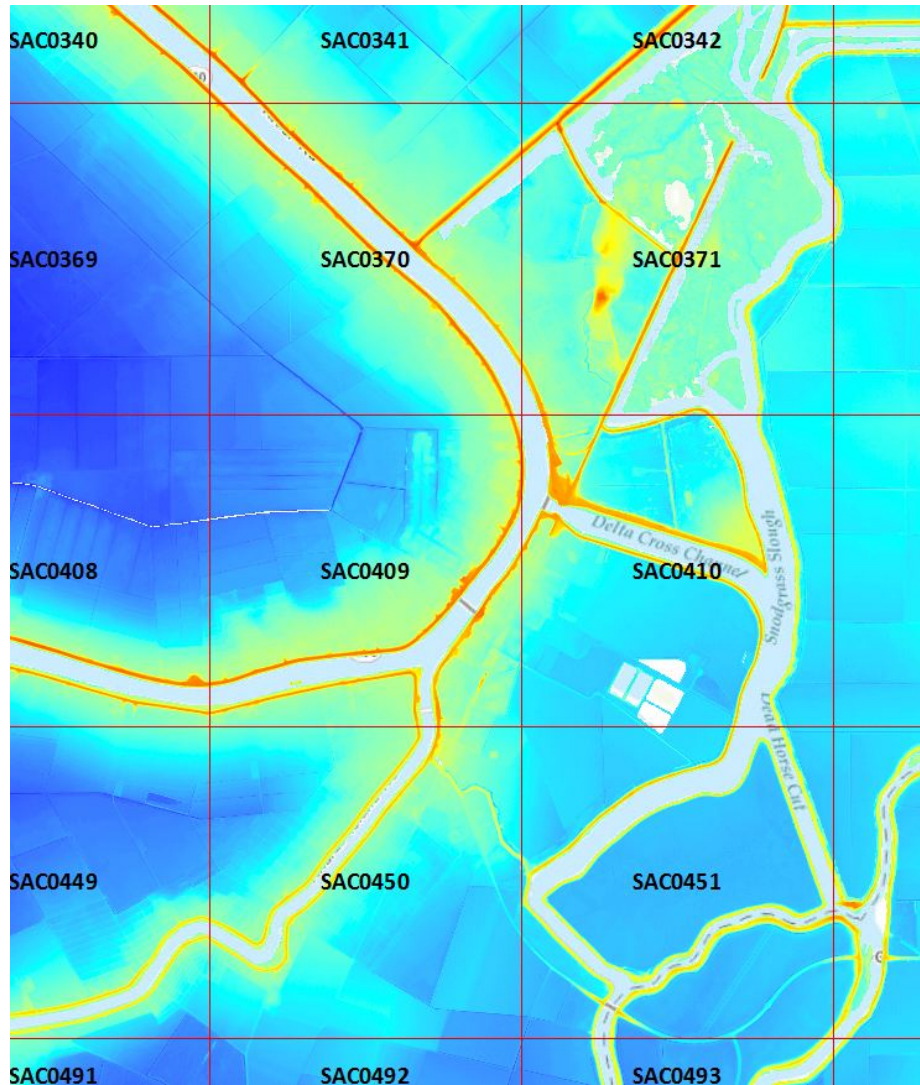


Figure 37. Coverage area of the available Lidar data for the study site

Another set of valuable survey data is the ADCP measurements carried out by USGS engineers for a number of years. The ADCP survey provides 3D velocity at selected cross sections and at different times. So they are used for model validation.

For example, a set of ADCP data were obtained in 2008 on a number of river transects shown in Figure 38. Repeated surveys were performed at a transect to compute the averaged velocity (e.g., Figure 39). The raw velocity data also has to be properly processed to obtain the secondary flow patterns at a transect. The USGS team used VMT software (<http://hydroacoustics.usgs.gov/movingboat/VMT/VMT.shtml>) to process the velocity data; the approach was described by Parsons et al. (2013).

## 8. Flow Module Results

Different data processing approaches may lead to quite different results. This will be discussed when specific comparisons of CFD results and ADCP data are presented later.



Figure 38. Repeat transect survey was carried out in 2008 at the study site



Figure 39. Six (6) boat paths were used for the transect at the confluence

### 8.3.3 Model Domain and Mesh

3D CFD modeling is carried out for flows at the junction site and the results are used to understand the fish movement behaviors and inputs to the fish movement ELAM model.

The selected model domain is shown in Figure 40. The domain covers the reach of Sacramento River with about 4.6 km in length.

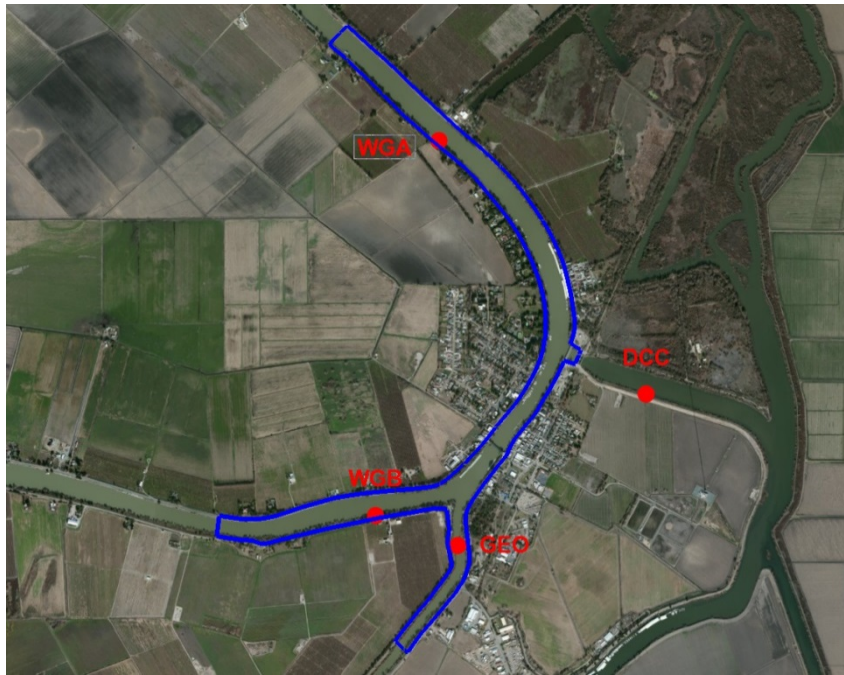


Figure 40. Model domain selected for the 3D modeling

A 2D mesh is generated first using SMS as shown in Figure 41. The 2D mesh consists of 36,362 cells and 37,138 nodes and it is used to compute the water surface elevation with SRH-2D model. The 3D mesh is automatically generated by U2RANS with the UPC sigma mesh approach given the water surface elevation at each time (from SRH-2D) and the number of vertical cells (user input). The initial 3D mesh at time zero is displayed in Figure 42; it has a total of 1,336,968 nodes and 1,272,670 cells. In generating the UPC sigma mesh, 36 vertical points are specified.

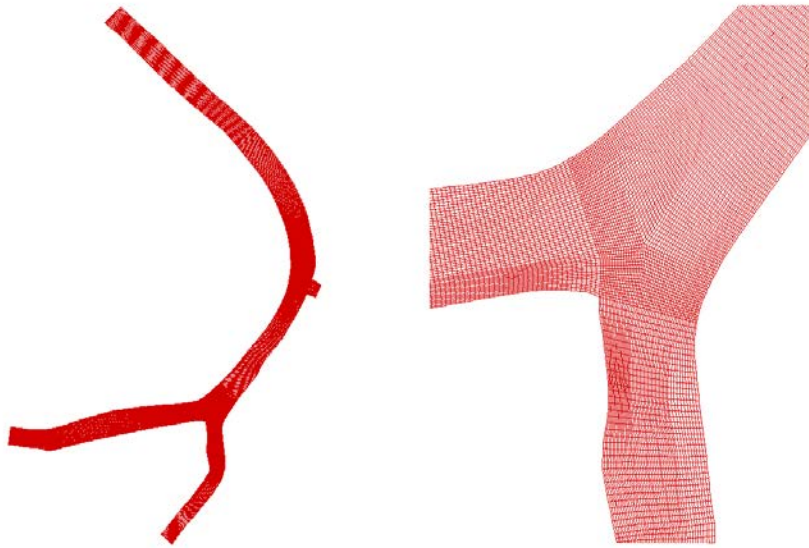


Figure 41. The 2D mesh developed for the model domain; left is an overview and right is the zoom-in view of the junction



Figure 42. Generated 3D sigma mesh at time zero; top is an overview and bottom is the zoom-in view (vertical distortion of 4:1 is used)

### 8.3.4 Boundary Conditions and Other Model Inputs

There are four open boundaries of the model domain and boundary conditions are needed at the four locations. For the study site, flow discharge and water surface elevation data are available as four gauge stations are nearby. The locations of the four gauges are displayed in Figure 43. For report convenience, the four gauges are labeled as in Figure 40 and they are WGA (Walnut Grove gauge A), WGB (Walnut Grove gauge B), GEO (Georgiana Slough gauge), and DCC (Delta Cross Channel). The recorded discharge and water elevation at these gages are plotted in Figure 44 for the time period of December 8, 2006 to February 4, 2007, as well as the period of November 5, 2008 to March 1, 2009. In the model setup, we choose to use the discharge data as the boundary condition at WGA, WGB and DCC open boundaries and the water elevation as the boundary condition at the GEO open boundary. Note that flow may reverse its direction at these boundaries. The model uses positive discharge as flow into the model domain and negative discharge as flow out of the domain.

A preliminary model run is performed with SRH-2D in order to calibrate the appropriate Manning's roughness coefficient. It also provides the water surface elevation. We first obtain the average discharge and water elevation at the gages over the time periods in Figure 44. Such obtained average discharge is 8,412 cfs at WGA, -2,835 cfs at GEO, and -757 cfs at DCC; and the average water elevation is 4.627 ft at WGB (NAVD 88). A steady state run is performed using the above average values as the boundary conditions. The Manning's coefficient is calibrated by matching the computed water elevation at WGA to the average recorded elevation over the same time periods as the boundary conditions (the average water elevation is 4.722 ft at WGA). The calibrated Manning's coefficient is 0.033, very close to the expected value for a gravel bed river such as the Sacramento River. With this calibrated Manning's coefficient, water elevation of 4.720 ft is predicted by SRH-2D at WGA, compared with the average value of 4.722 ft.

After calibration, an unsteady simulation is carried out for a 24 hour period on January 16, 2009. This particular day is chosen for model validation as a good set of ADCP data is available for model comparison. Flow discharges recorded at gages on January 16, 2009 are shown in Figure 45. They are used as the boundary conditions. At GEO, a fixed pressure boundary condition is applied with the 3D modeling while water elevation is used with the SRH-2D simulation.

Figure 45 clearly shows that the flow at the study site is oscillatory and complex due to strong influence of the tides. River flow direction reversed twice near WGB station and once at the WGA station.

The initial condition of the unsteady simulation is based on the model results obtained with a separate steady-state solution at time zero.

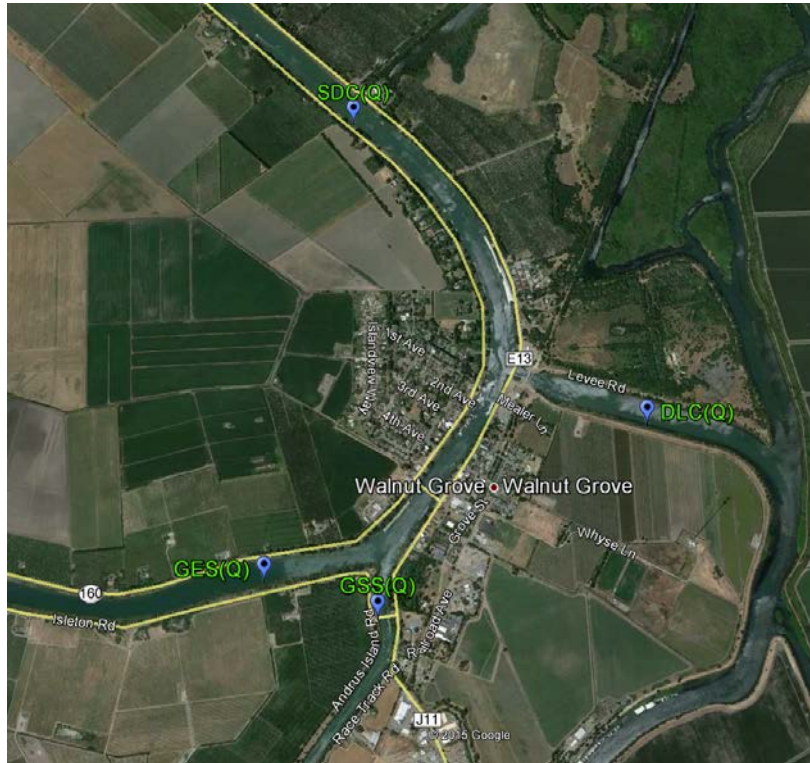


Figure 43. Aerial map and the four gauge locations of the study area

## Quantitative Modeling Tools for Large Wood

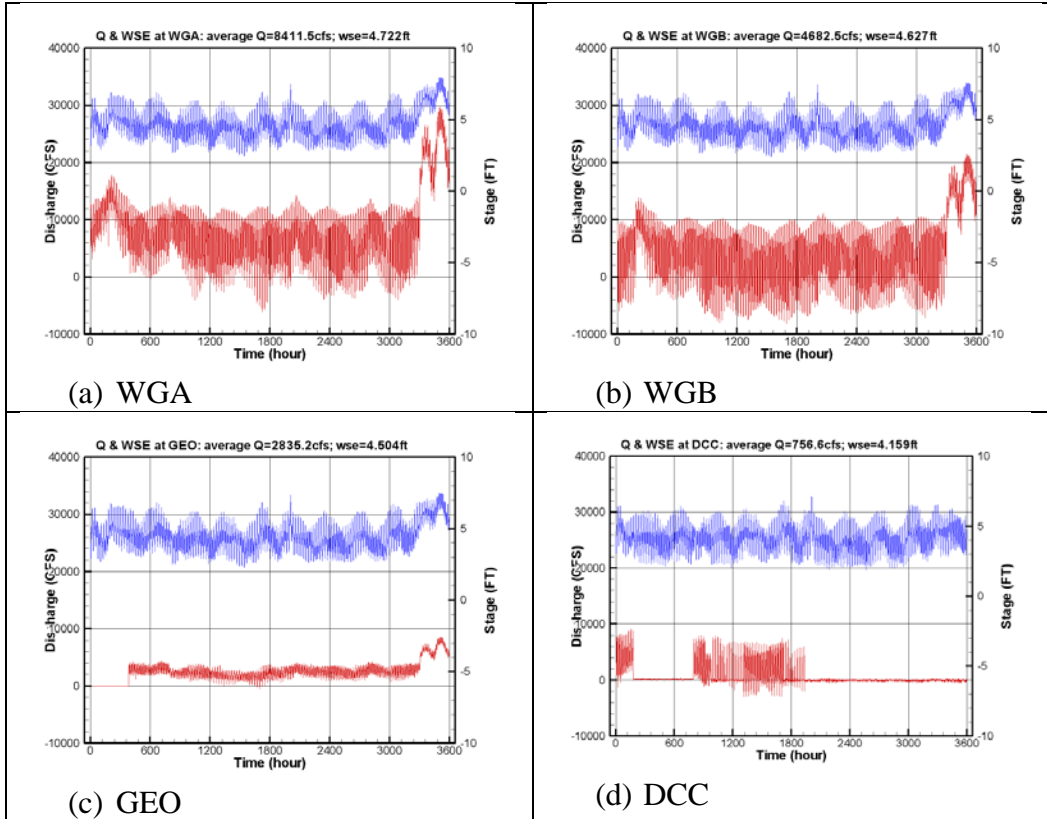


Figure 44. Recorded discharge and water elevation at four gages during December 8, 2006 to February 4, 2007 and November 5, 2008 to March 1, 2009

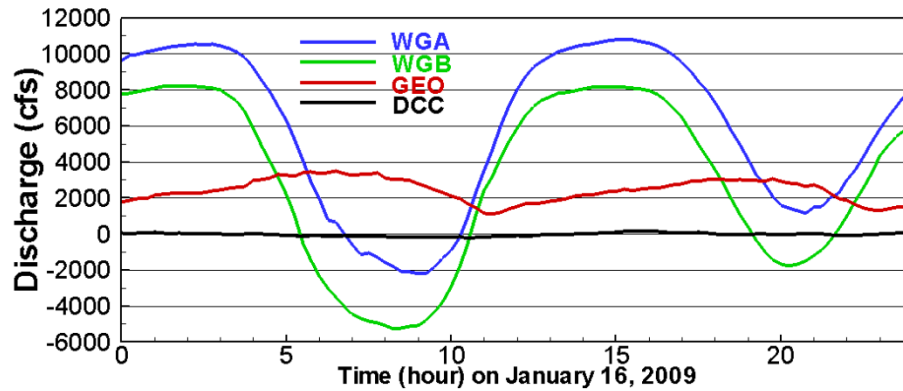


Figure 45. Flow discharges at the four gages during January 16, 2009

### 8.3.5 Model Results and Discussion

Unsteady 3D modeling of the site has been performed for January 16, 2009. The predicted velocity and flows patterns are shown in Figure 46 and Figure 47 at two times of the day. The flow patterns at the two times are quite different. At hour 3.5, the flow moves downstream along the Sacramento River, but the flow reverses its direction at hour 8.15.

At the junction, complex vortices and eddies are generated and they are changing rapidly in time. We have created the animation of the flow patterns over the time period and the fish tracking data is also added. The effort is carried out by USACE engineers to discern whether the fish movement is correlated to the flow patterns. Snapshots of the animation at three times are shown in Figure 48, Figure 49 and Figure 50. The results show clearly that multiple vortices are generated at the junction when flow reverses and they are closely correlated to the fish movement. The results are being analyzed by USACE engineers and may be available in the future.

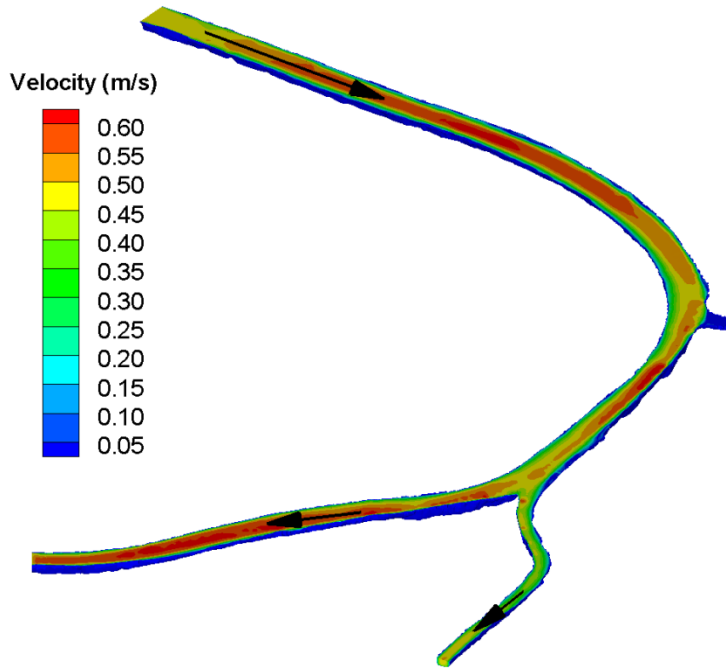


Figure 46. 3D model predicted velocity and flow pattern at hour 3.5

## Quantitative Modeling Tools for Large Wood

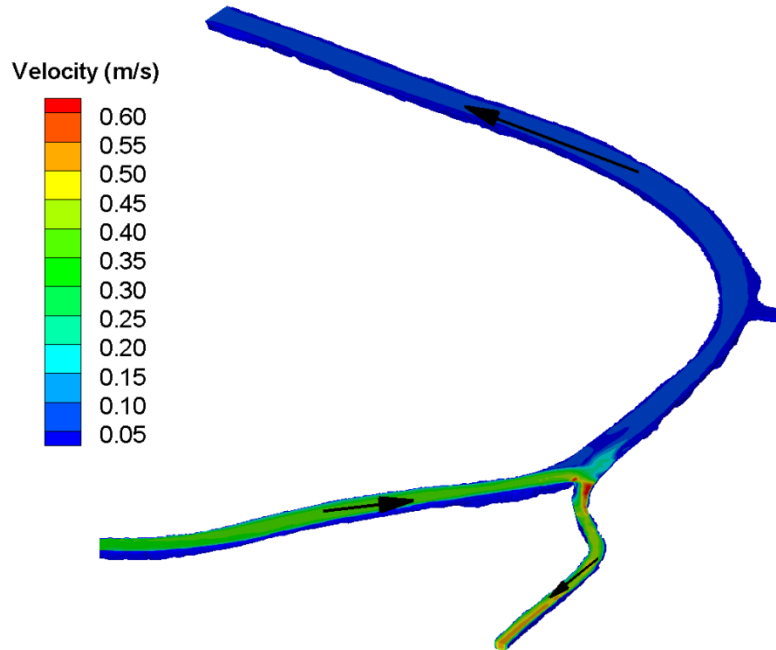


Figure 47. 3D model predicted velocity and flow pattern at hour 8.15

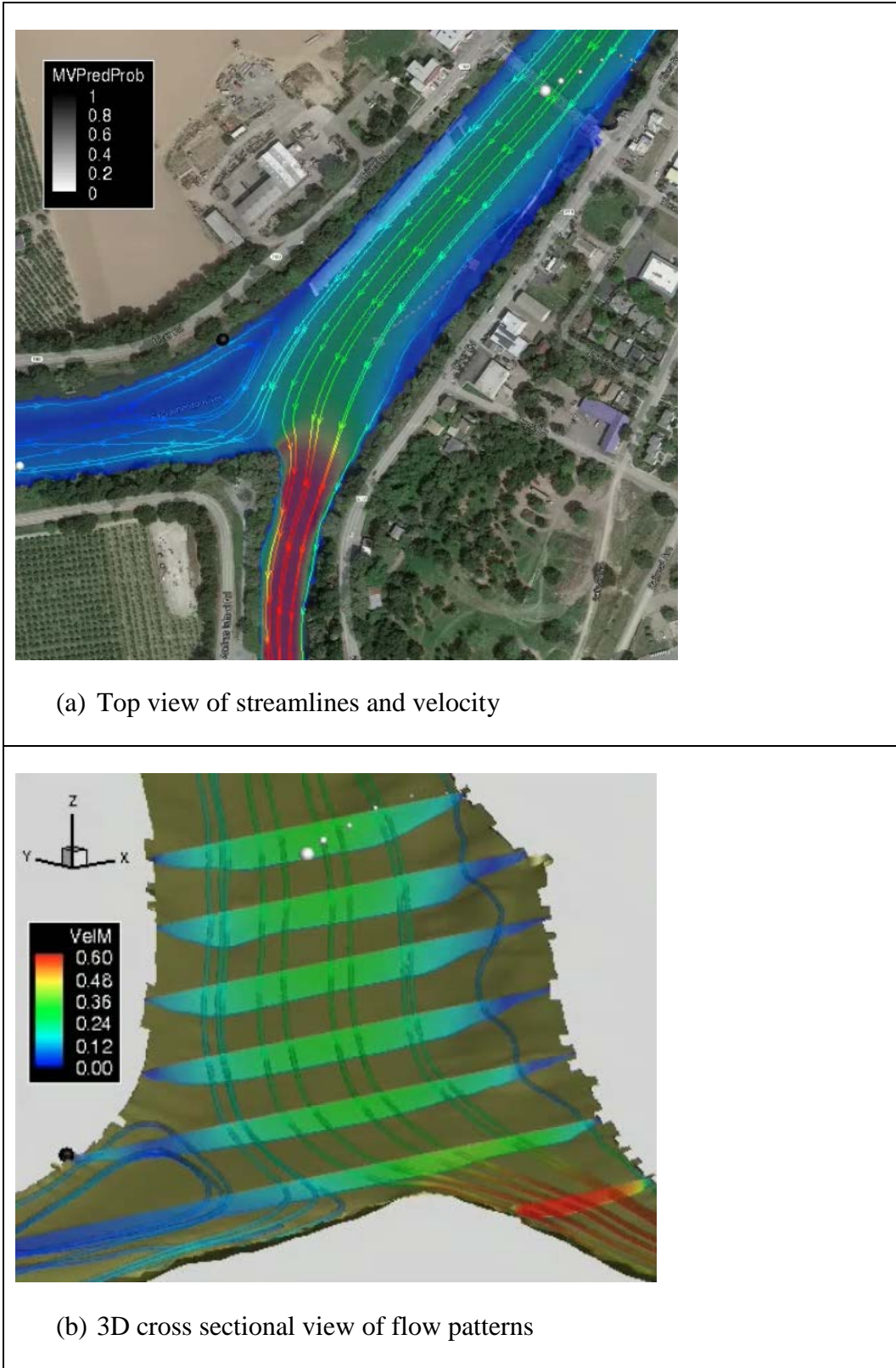


Figure 48. Flow patterns and variables at time 5:20am, January 16, 2009

## Quantitative Modeling Tools for Large Wood

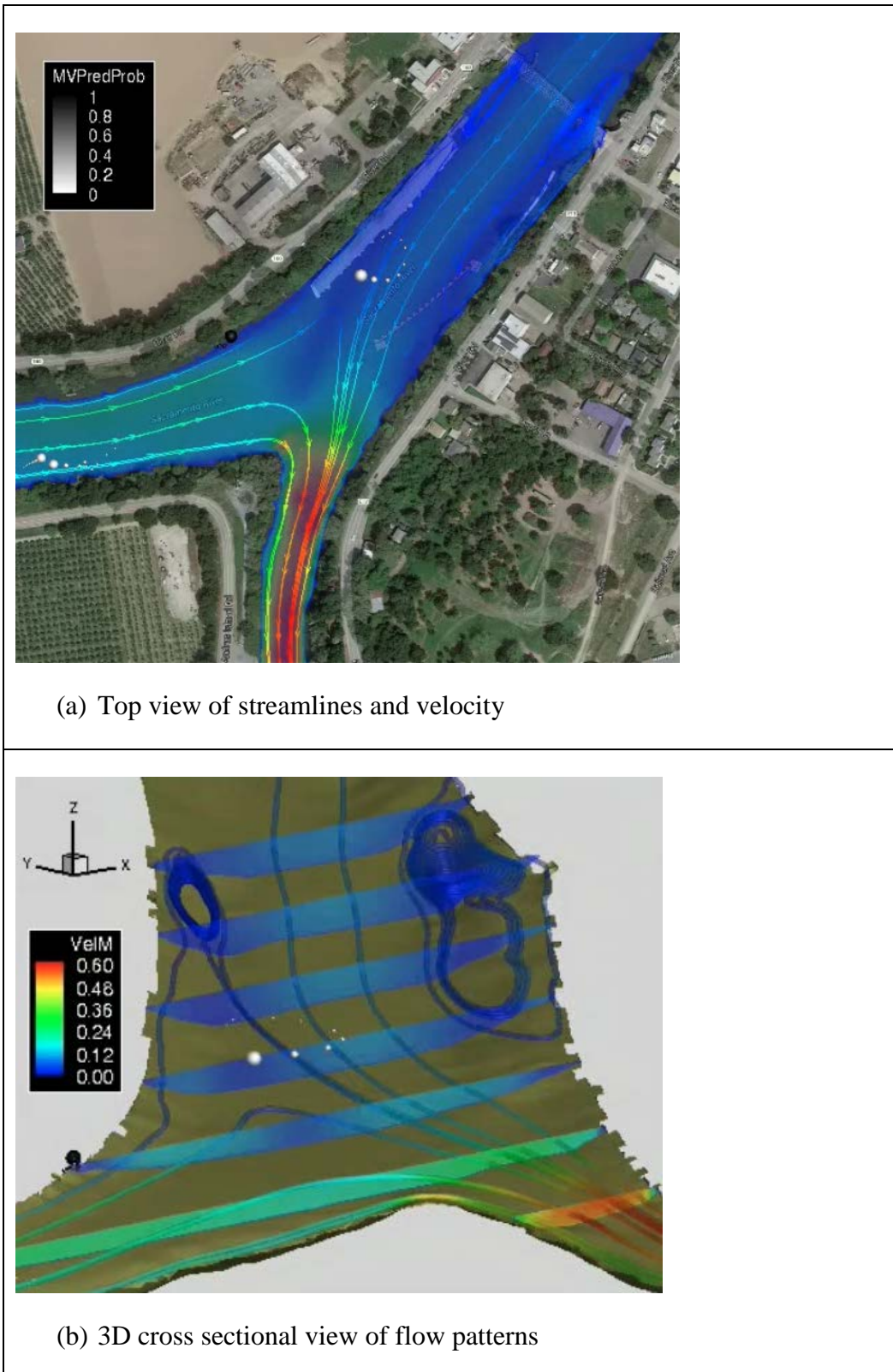


Figure 49. Flow patterns and variables at time 6:17am, January 16, 2009

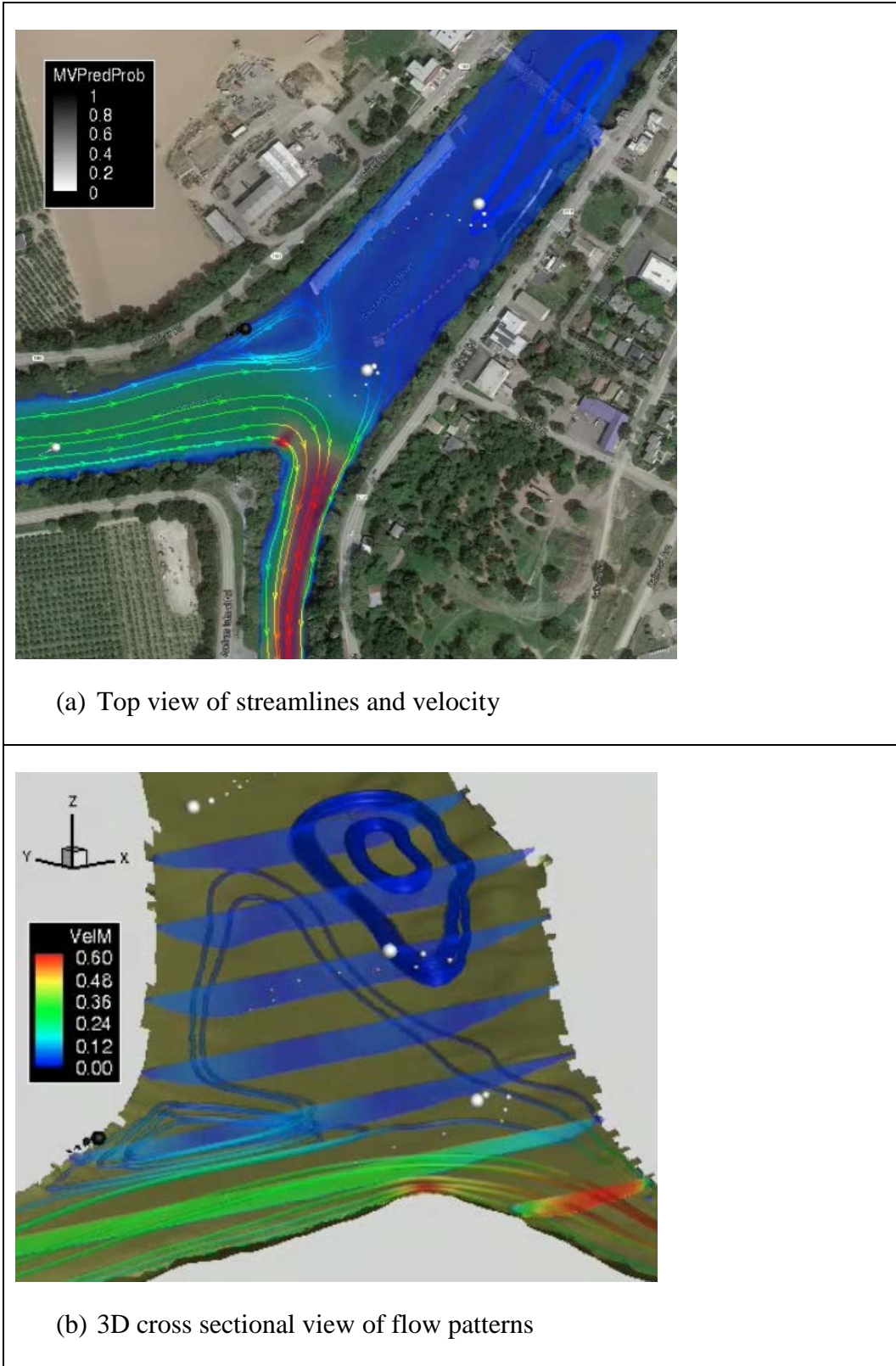


Figure 50. Flow patterns and variables at time 6:53am, January 16, 2009

## Quantitative Modeling Tools for Large Wood

Next, the CFD model results are compared with the ADCP velocity data at two transects shown in Figure 51. One is named GEO9 and another is GEO22. Multiple boat sweeps were used during the survey so that reliable ADCP velocity data may be obtained through spatial averaging.

Plan-view velocity is compared between the 3D model result and ADCP data. Figure 52 is the comparison at GEO9 and time 3.5 hour and Figure 53 is at GEO22 and time 8.15 hour. The ADCP data was an average between 3:28:43 and 3:35:32 at GEO9 and between 8:04:48 and 8:14:15 at GEO22. Visual inspection shows the numerical model results are in good agreement with the ADCP data. The major discrepancy is at the tip of GEO22 and can be explained by the high uncertainty of bathymetry used and the potential vegetation impact of the flow velocity.

Secondary flows are compared at the two transects. Secondary flows are difficult to measure in the field and also difficult to model numerically. Much research and effort have been conducted on how to process the raw ADCP data so that reliable secondary flow patterns may be extracted. A number of methods were discussed and a particular method was proposed by Parsons et al. (2013). Herein, only a summary is given.

The ADCP data on a transect with multiple boat sweeps was processed using the VMT software as reported by Parsons et al. (2013). A description of VMT can be found at: <http://hydroacoustics.usgs.gov/movingboat/VMT/VMT.shtml>. The averaging procedure used by VMT was carried out as follows:

- Step 1: an average cross section is obtained using least-square data fit; a grid is then setup on the average plane.
- Step 2: measurement data is projected onto the average cross section using orthogonal translation.
- Step 3: projected data is interpolated to the grid of the average plane.
- Step 4: Arithmetic averaging of velocity components is performed at each grid point of the average plane.

The above four steps are illustrated in Figure 54.

The predicted and measured secondary flow patterns are compared in Figure 55 at GEO9 and time 3.5 hour, and in Figure 56 at GEO22 and time 8.15 hour. In the plots, three different ways of ADCP data processing for secondary flows are shown: “No Rotation” means the data are obtained as field measured and no velocity vector rotation is applied; “ZNSFDM” means that secondary flow is obtained by applying an extra constraint so that the net secondary discharge is zero; and “Rozovskii” means that the method of Rozovskii was applied in obtaining the secondary flow. Comparison in the two figures shows that the 3D model prediction is in qualitative agreement with the measured secondary flow data. In general, measurement of secondary flows has high uncertainty and it is

## 8. Flow Module Results

particularly true in the field. Data processing method itself has introduced high uncertainty as shown with the present data. High variability is seen in the secondary flow patterns with the three methods. In view of the high uncertainty in obtaining secondary flows, quantitative comparison is not feasible.



Figure 51. Two transects, GEO9 and GEO22, where repeated ADCP velocity measurement were made

## Quantitative Modeling Tools for Large Wood

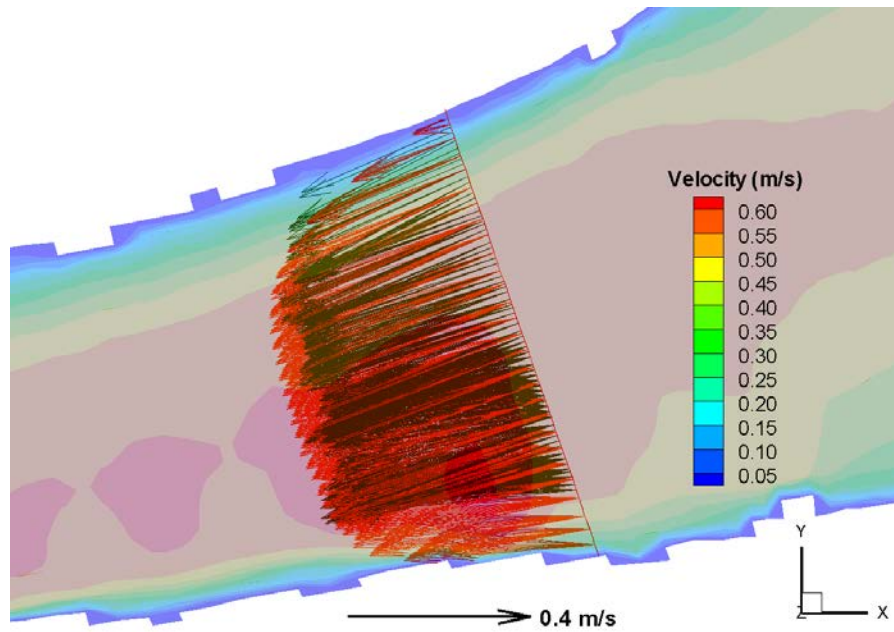


Figure 52. Comparison of predicted (red) and ADCP measured (black) velocity at cross section GEO9 at time 3.5 hour, on January 16, 2009

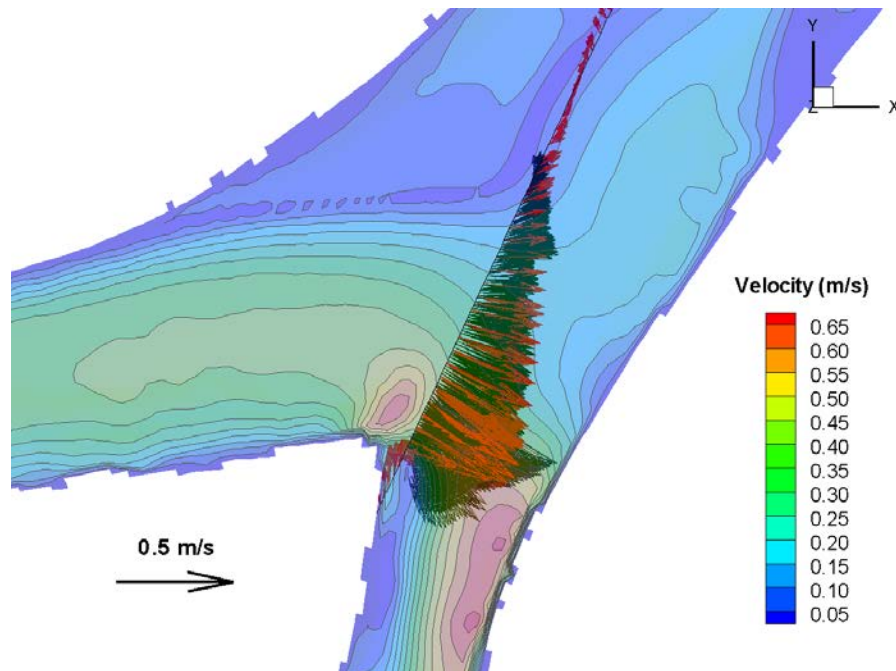


Figure 53. Comparison of predicted (red) and ADCP measured (black) velocity at cross section GEO22 at time 8.15 hour, on January 16, 2009

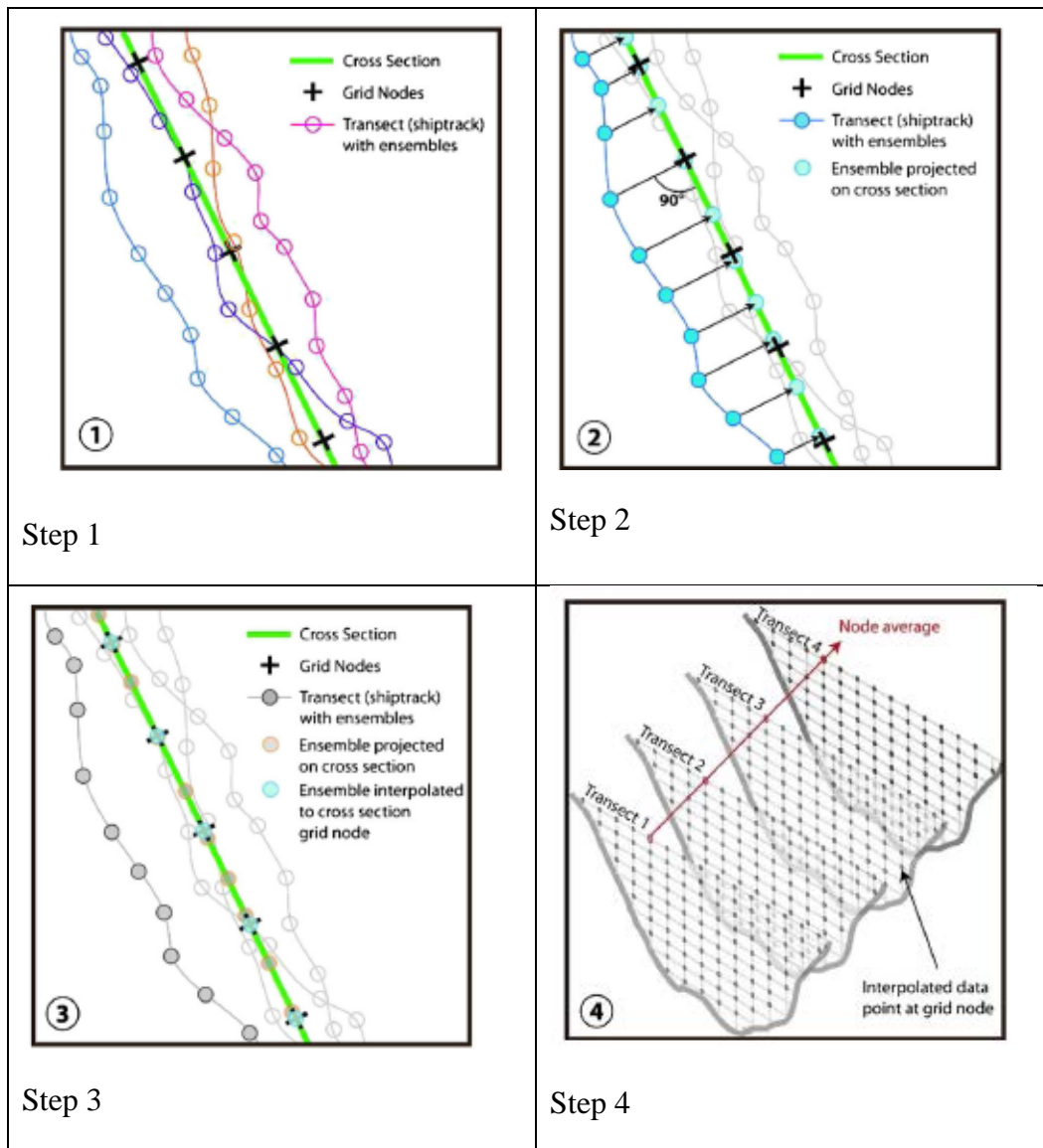
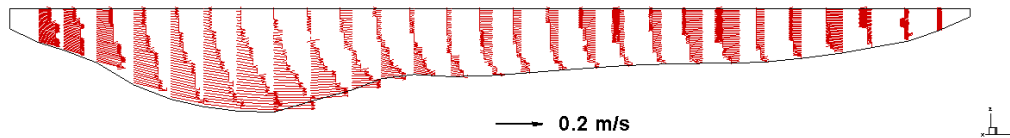


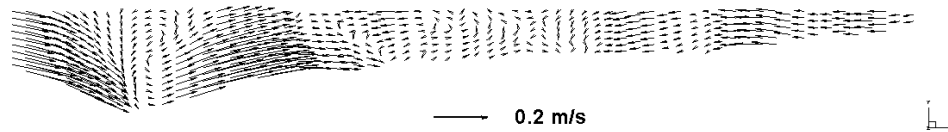
Figure 54. Four steps used for processing the raw ADCP velocity data to obtain the average data at the cross sections (source: Parsons et al. 2013)

## Quantitative Modeling Tools for Large Wood

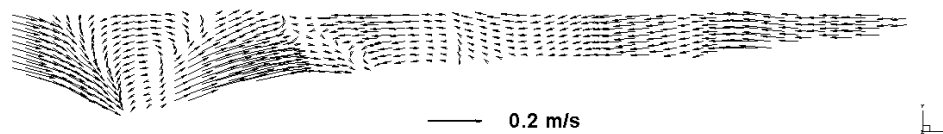
U2RANS Prediction



ADCP No Rotation



ADCP ZNSDM



ADCP Rozovskii

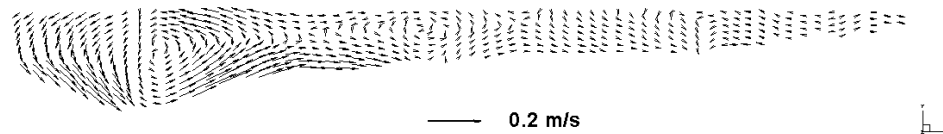


Figure 55. Comparison of predicted (red) and ADCP measured (black) secondary flow velocity at cross section GEO9 at time 3.5 hour, on January 16, 2009

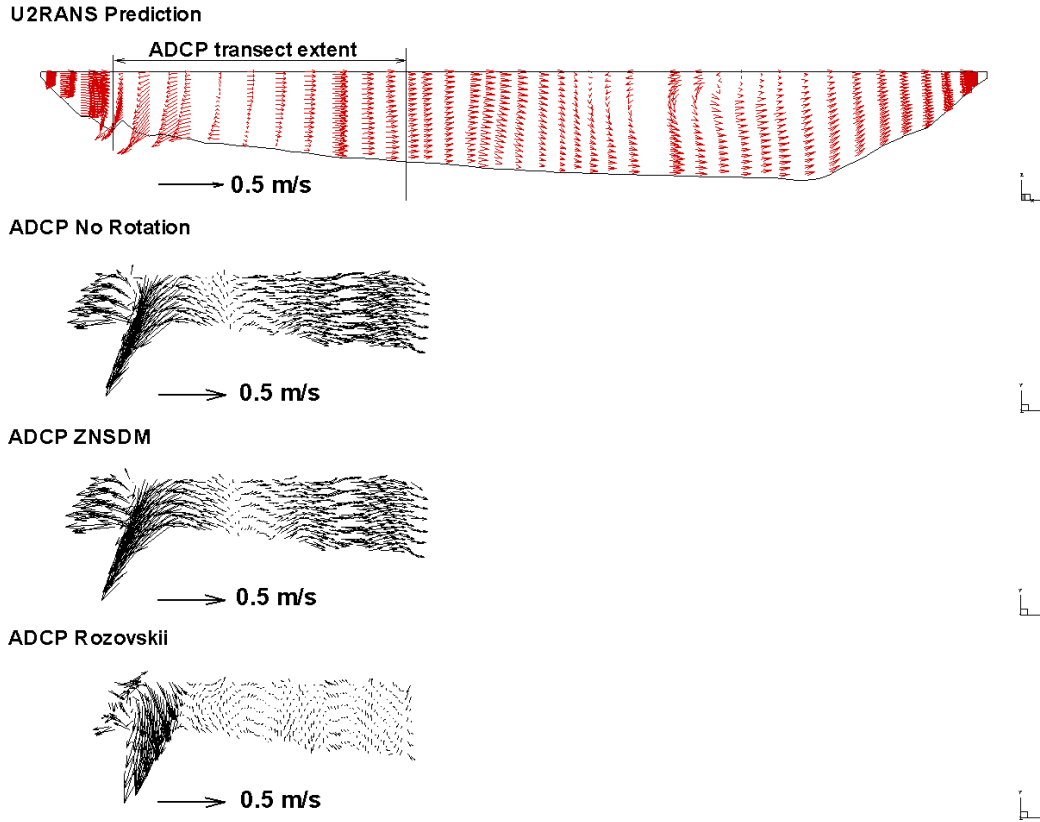


Figure 56. Comparison of predicted (red) and ADCP measured (black) secondary flow velocity at cross section GEO22 at time 8.15 hour, on January 16, 2009

Finally, the depth-averaged velocity at the two survey transects is compared between the CFD results and the ADCP data at various times of the 24 hour period simulated. These results are shown in Figure 57 through Figure 65. The digital ADCP data was not available to us at the time; so the comparison is only with plots generated by the USGS surveyors and no quantitative comparison is possible.

## Quantitative Modeling Tools for Large Wood

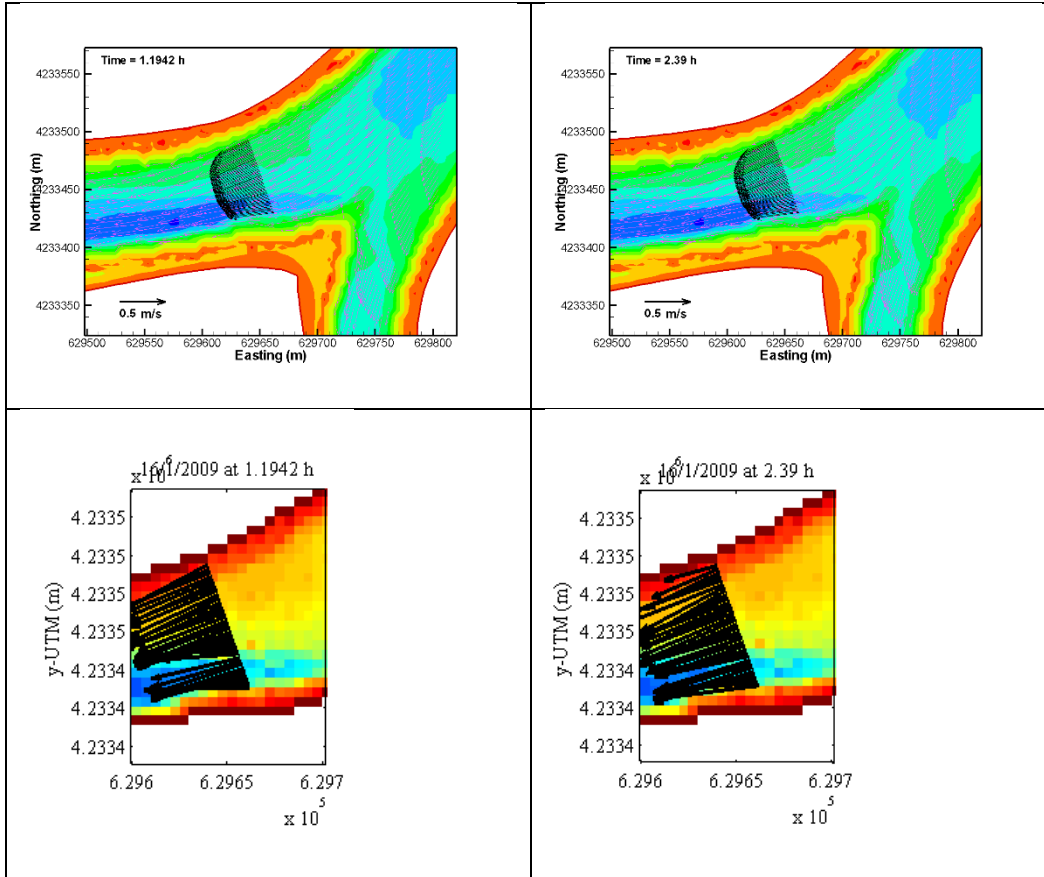


Figure 57. Comparison of predicted (top) and ADCP measured (bottom with horizontal axis Easting) velocity at cross section GEO9 from 1 to 3 hours on January 16, 2009

## 8. Flow Module Results

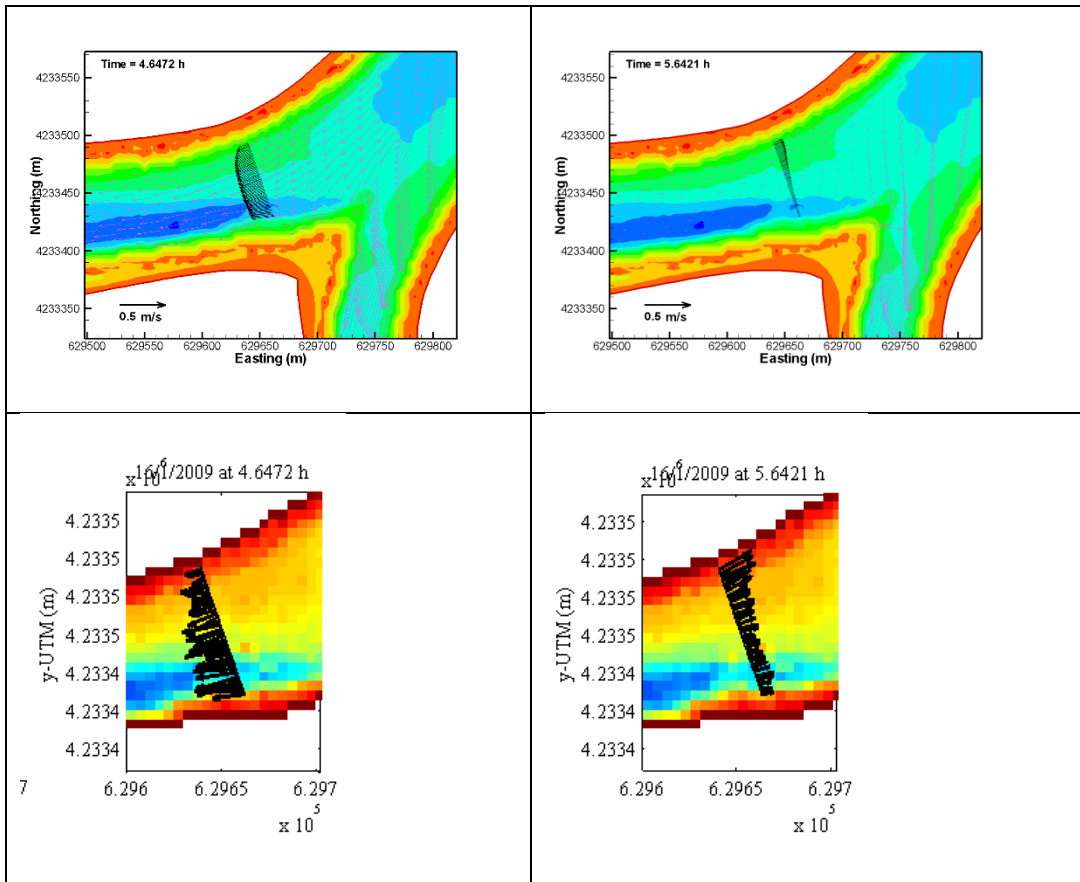


Figure 58. Comparison of predicted (top) and ADCP measured (bottom with horizontal axis Easting) velocity at cross section GEO9 from 4 to 6 hours on January 16, 2009

## Quantitative Modeling Tools for Large Wood

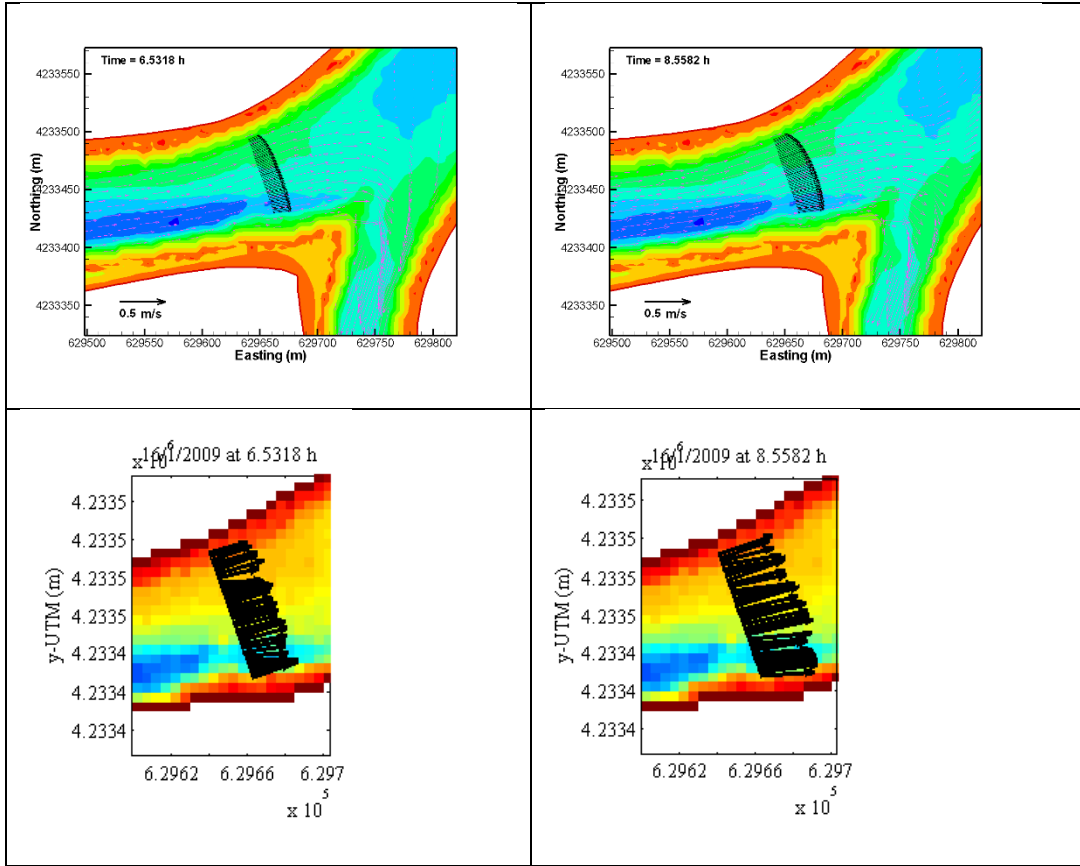


Figure 59. Comparison of predicted (top) and ADCP measured (bottom with horizontal axis Easting) velocity at cross section GEO9 from 6 to 9 hours on January 16, 2009

## 8. Flow Module Results

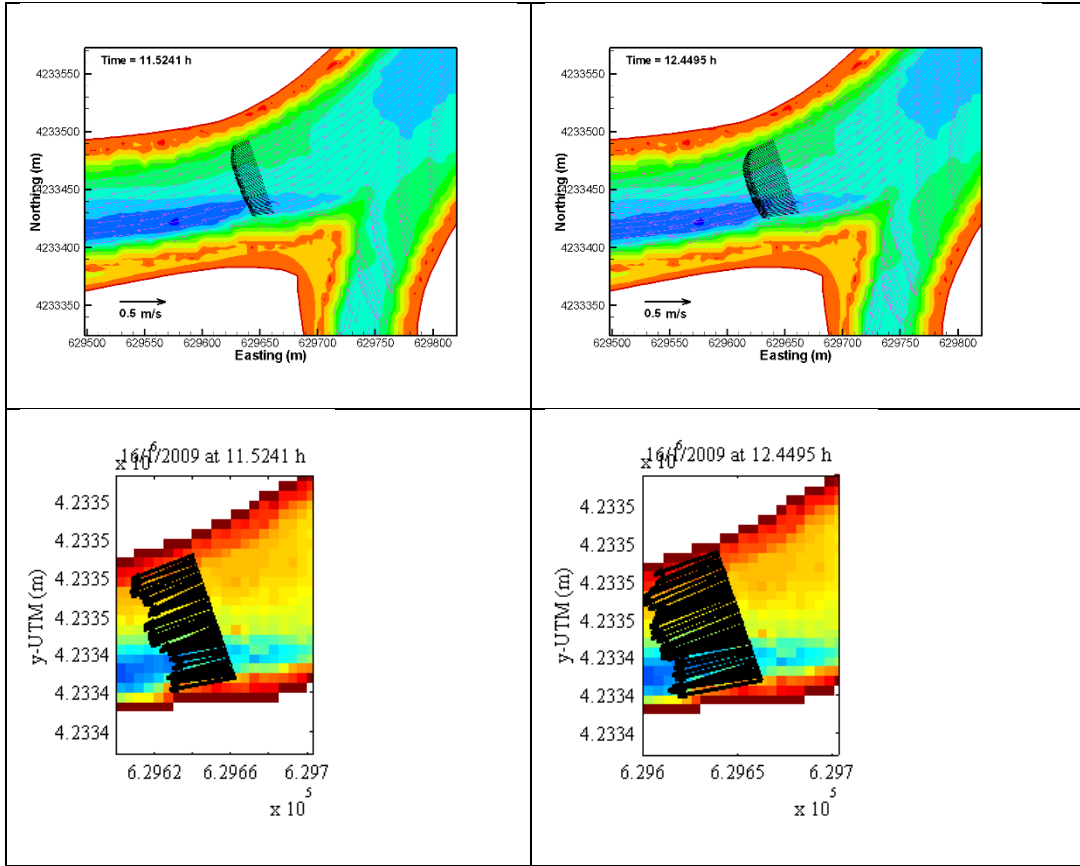


Figure 60. Comparison of predicted (top) and ADCP measured (bottom with horizontal axis Easting) velocity at cross section GEO9 from 11 to 13 hours on January 16, 2009

## Quantitative Modeling Tools for Large Wood

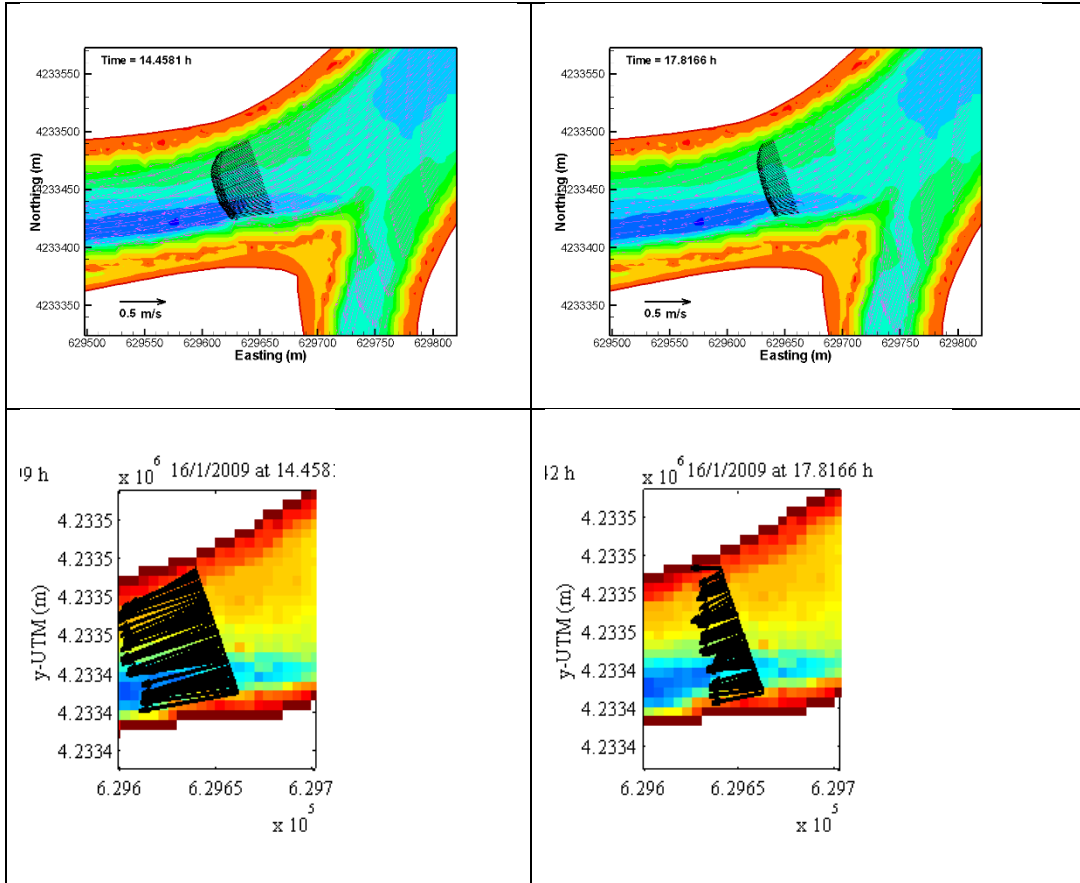


Figure 61. Comparison of predicted (top) and ADCP measured (bottom with horizontal axis Easting) velocity at cross section GEO9 from 14 to 18 hours on January 16, 2009

## 8. Flow Module Results

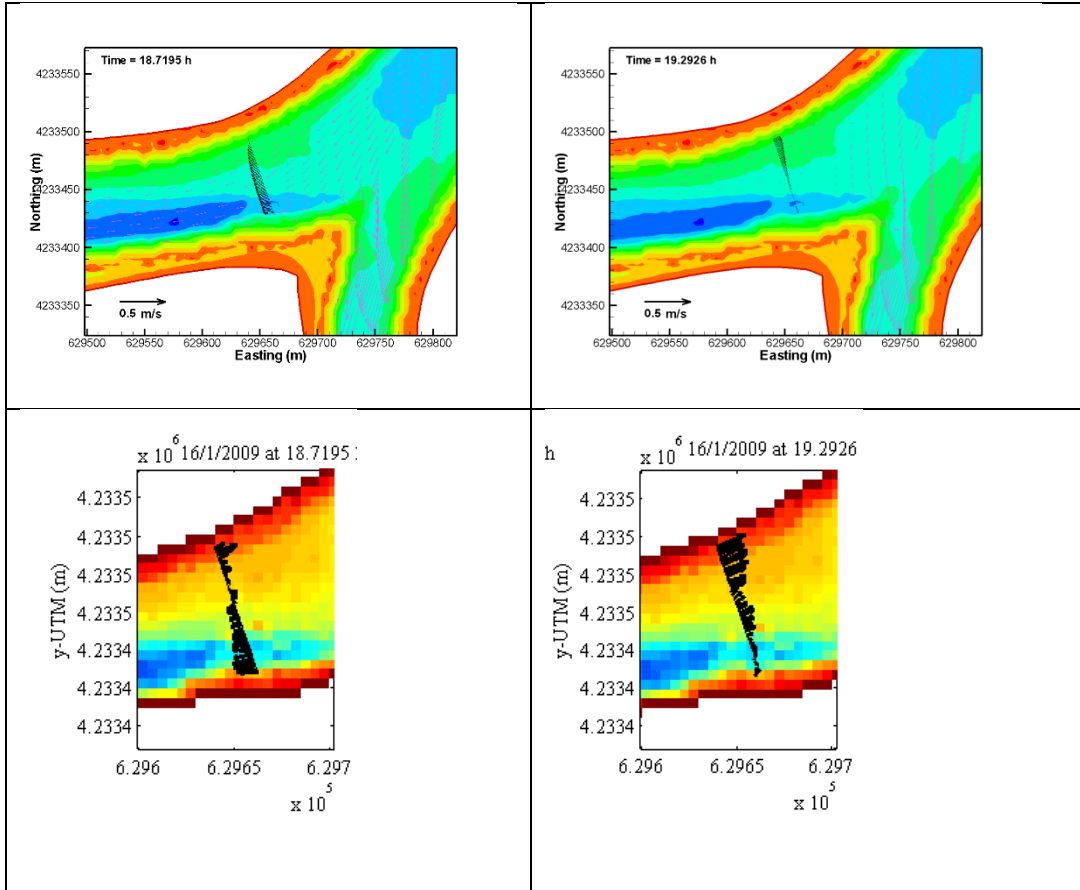


Figure 62. Comparison of predicted (top) and ADCP measured (bottom with horizontal axis Easting) velocity at cross section GEO9 from 19 to 20 hours on January 16, 2009

## Quantitative Modeling Tools for Large Wood

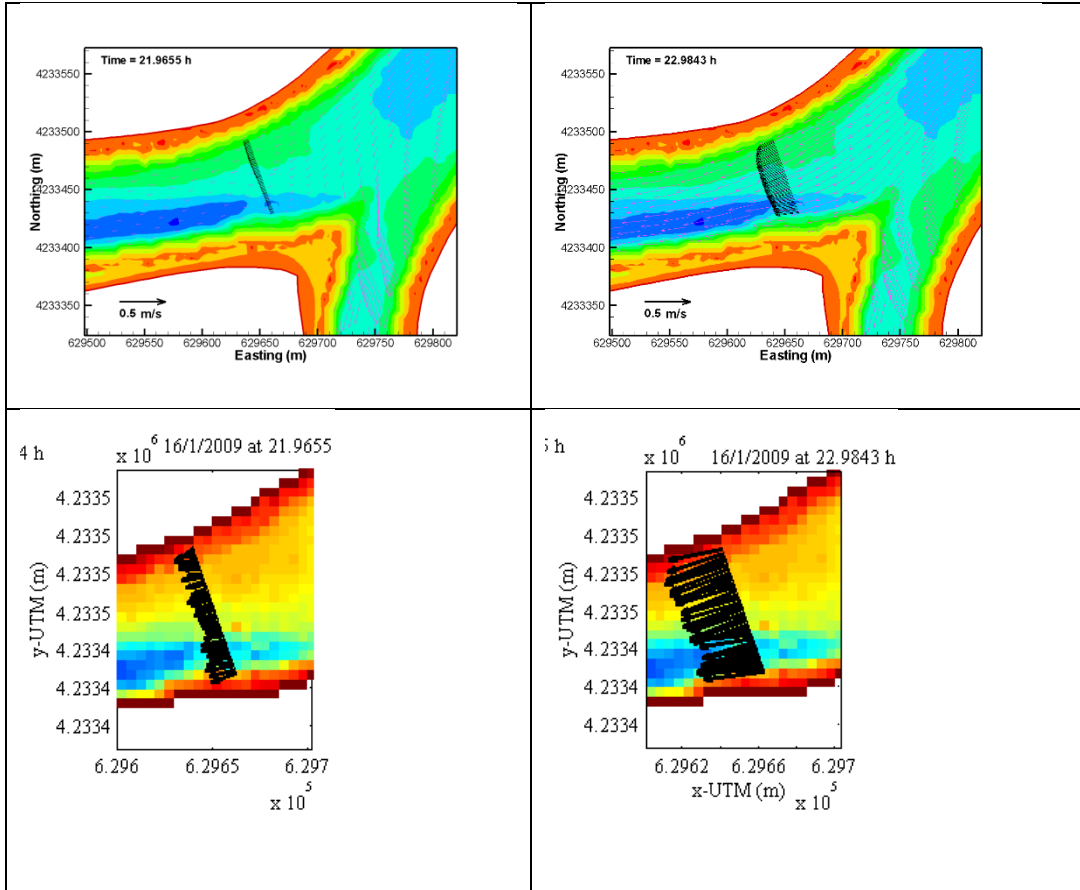


Figure 63. Comparison of predicted (top) and ADCP measured (bottom with horizontal axis Easting) velocity at cross section GEO9 from 21 to 23 hours on January 16, 2009

## 8. Flow Module Results

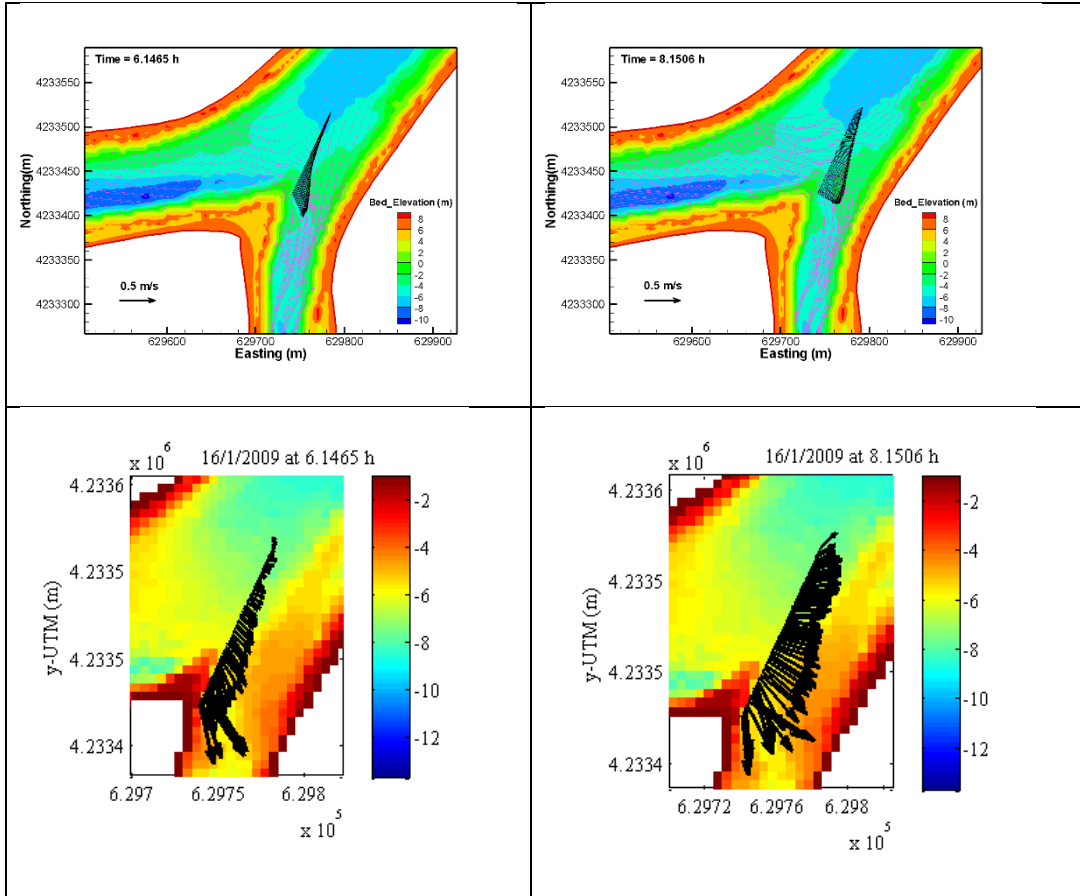


Figure 64. Comparison of predicted (top) and ADCP measured (bottom with horizontal axis Easting) velocity at cross section GEO22 from 6 to 9 hours on January 16, 2009

## Quantitative Modeling Tools for Large Wood

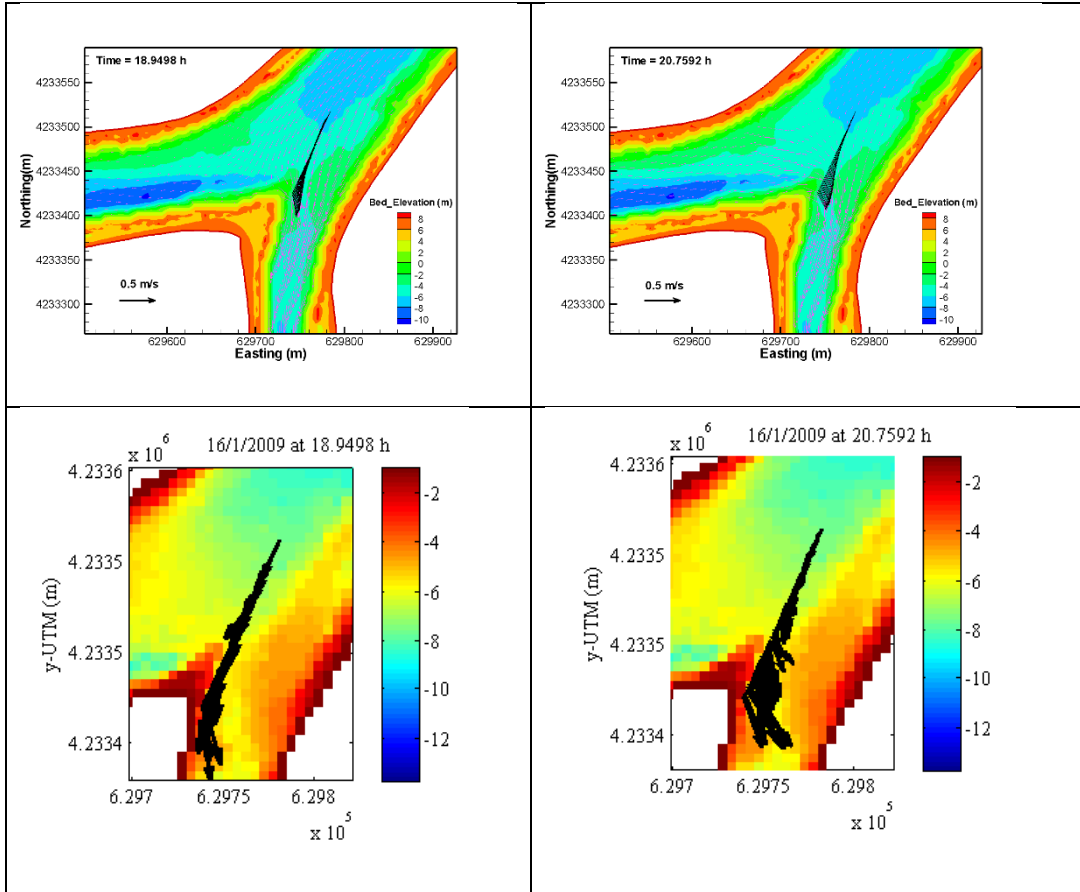


Figure 65. Comparison of predicted (top) and ADCP measured (bottom with horizontal axis Easting) velocity at cross section GEO22 from 18 to 21 hours on January 16, 2009

## 8.4 Flow at the Fremont Weir Section of Sacramento River

The modeling is part of a larger effort related to the Yolo Bypass EIS/EIR study for fish survival. Participants include Reclamation Bay Delta Office, Department of Water Resources (DWR) of California, USACE ERDC, and USACE Sacramento District.

U2RANS 3D simulation is carried out to predict flow hydrodynamics along the Fremont Weir section of the Sacramento River, California. Flow hydrodynamic variables have a significant impact on fish movement behaviors. Therefore, CFD model results are generated by this study to support the Eulerian-Lagrangian Agent Method (ELAM) modeling of fish movement at the study site. The fish movement modeling portion of the study is to be carried out by engineers at the U.S. Army Corps of Engineers (USACE). ELAM model takes hydrodynamic flow and turbulence data, coupled with bioenergetic data for specific species, to make probabilistic estimates of fish movement in an aquatic environment. In addition, CFD results may also be used in conjunction with the telemetry fish tracking data in the field to discern the fish behaviors and statistical patterns in relation to flow characteristics. Further, CFD model results may also play an important role in Fremont Weir notch design in that the desired flow characteristics beneficial to fish migration may be obtained.

The study site is the section of the Sacramento River along the Fremont Weir as shown in Figure 66. The primary interested area of the study covers about 10 km (about 6 miles) section of the Sacramento River with the downstream cross section located at the Verona station.

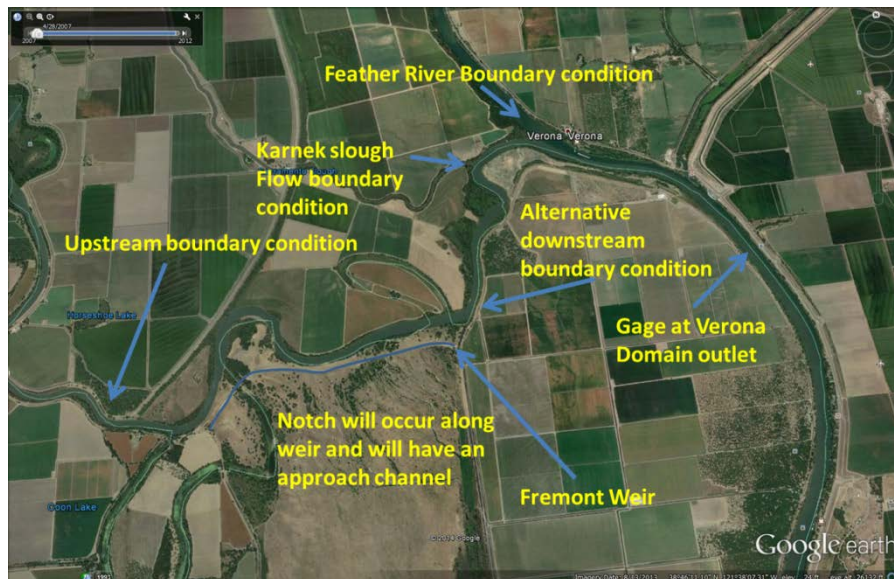


Figure 66. Study area near Fremont Weir, Sacramento River, California

### 8.4.1 Model Domain and Field Data

The model domain developed in this study is shown in Figure 67. The model starts from Knight Landing at the upstream and ends at Verona gauge station at the downstream. The approximate longitudinal length of the model domain is about 18 km (10.8 miles). High-Res-3D model includes five open boundaries: Knights Landing inflow, Feather River inflow, Verona outflow, and small inflows from Sacramento Slough at Karnak and Natomas Cross-Cut. The boundary conditions at these five open boundaries are discussed later.



Figure 67. High resolution model domain used for U2RANS modeling of the Sacramento River near Fremont Weir, the Sacramento River, California

The field data set corresponds to the period of December 2014 to April 2015. The data include the following:

- 2015 bathymetric data at selected transects and longitudinal sweeps, which are used to develop the proper river model;
- 2014/2015 flow and stage (water elevation) data at some gauge locations in the period; and
- 2015 ADCP velocity data on a number of transects at selected days of the period.

The bathymetric data was collected by the Department of Water Resources (DWR), California for the 2015 Fremont Weir fish behavior Study; the data collection time is between January 21 and 27, 2015 for the cross sections and April 8, 2015 for three longitudinal profiles. The bathymetric data points from the survey are displayed in Figure 68. The data set covers about the last 10 km (6 miles) of the model domain. The bathymetry upstream of the survey, about 8 km (4.8 miles), is based on previous data by Hammack et al. (2013b) (terrain data



### 8.4.2 Model Development

In general, river flow modeling includes the following steps:

1. Selection of the model domain;
2. Mesh generation for the solution domain;
3. Topography and flow roughness representation on the mesh and initial and boundary conditions;
4. Model calibration and, if applicable, model verification; and
5. Model application.

Step 2 and 3 are described below for the present study below. Step 1 has already discussed in the above.

The mesh is developed in two stages. First, a 2D mesh is obtained covering the model domain using SMS. An overview and two close-up views of the mesh are shown in Figure 70 through Figure 72. This 2D mesh consists of 35,701 mesh cells of mixed quadrilaterals and triangles (7,444 triangles and 28,257 quadrilaterals). The mesh is used for SRH-2D modeling to provide the initial condition for the U2RANS modeling. Next, the 3D mesh is developed using either the sigma-mesh approach carried out automatically by U2RANS or the sophisticated mesh generator snappyHexMesh. The results from both meshes are found to be very close. With the sigma-mesh, a total of 20 vertical cells are used resulting in a total of 714,020 3D mesh cells comprising both hexahedrons and prisms. The 3D mesh has been developed under the existing condition without considering the Fremont Weir area as well as the weir notch design. The current model is used primarily for model validation by comparing results with the ADCP data and to provide flow inputs to the ELAM model for fish movement modeling.

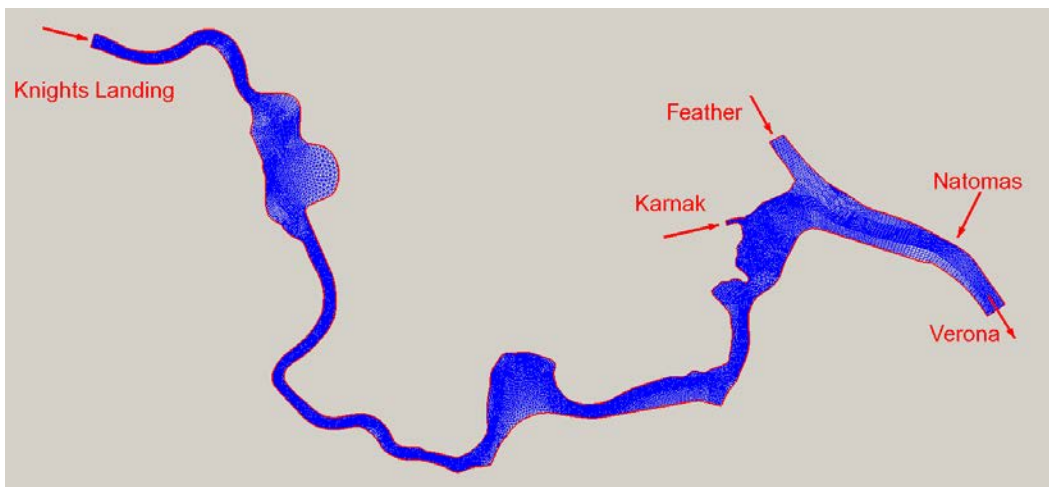


Figure 70. An overview of the 2D mesh developed for the High-Res-3D model

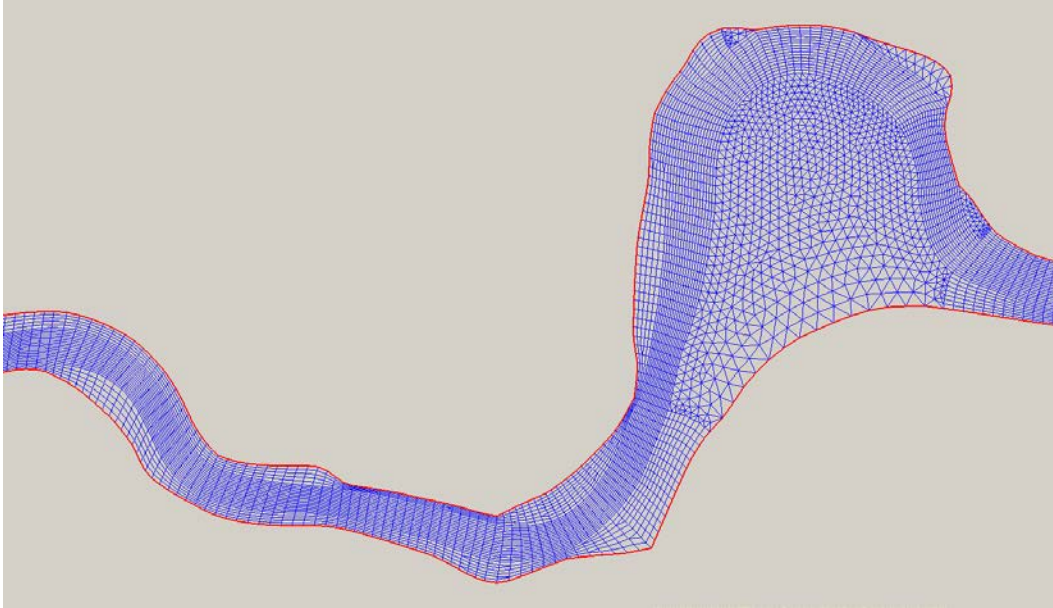


Figure 71. A close-up view of the High-Res-3D mesh at the big bend area of the Fremont Weir section

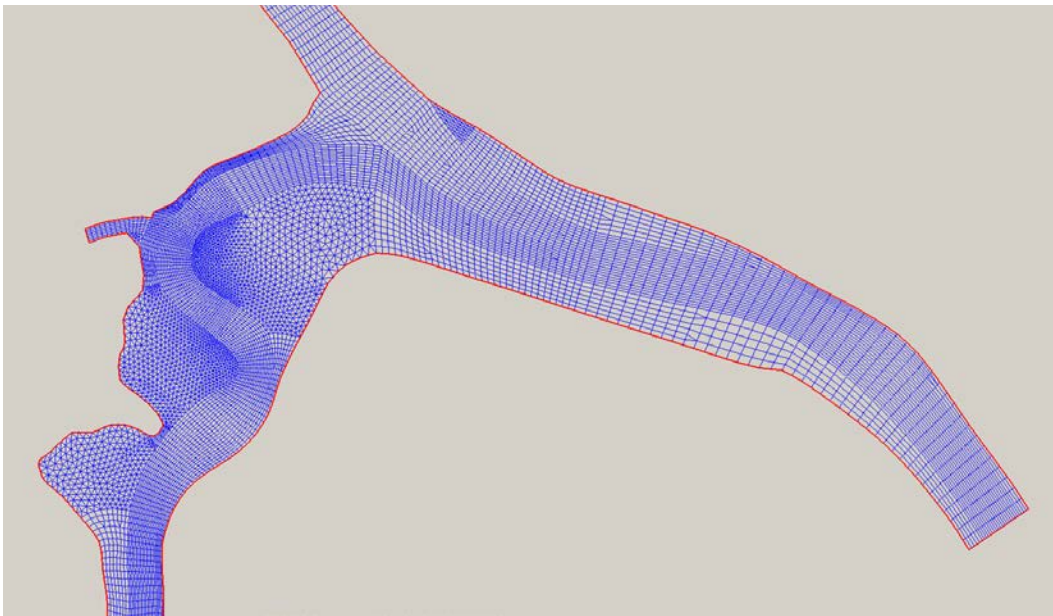


Figure 72. A close-up view of the High-Res-3D mesh at the confluence of the Sacramento River and the Feather River

The 2015 terrain was interpolated onto the 3D mesh to represent the river accurately. The terrain represented by the 3D mesh is shown in Figure 73. 3D close-up views of the terrain at the big bend area of the model are displayed in Figure 74 and Figure 75.

## Quantitative Modeling Tools for Large Wood

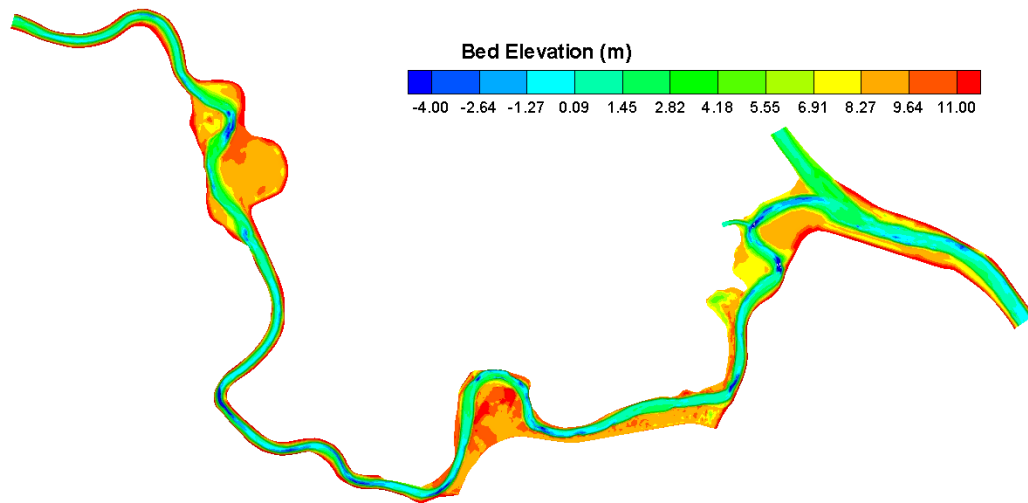


Figure 73. 2015 terrain represented by the High-Res-3D mesh: entire domain view

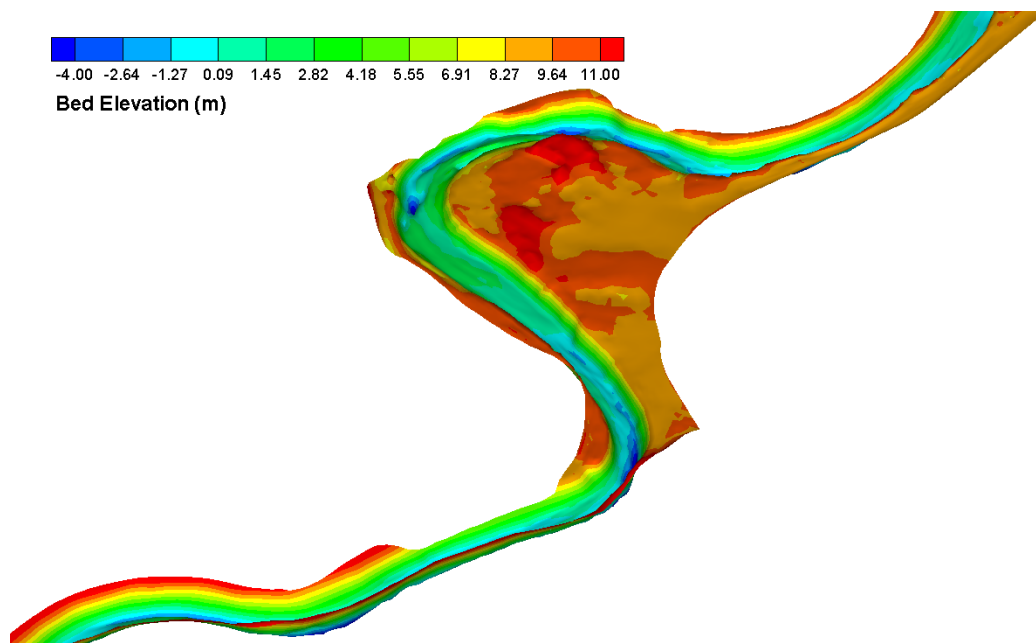


Figure 74. 2015 terrain represented by the High-Res-3D mesh: the upstream section at the big bend area (1:5 vertical distortion)

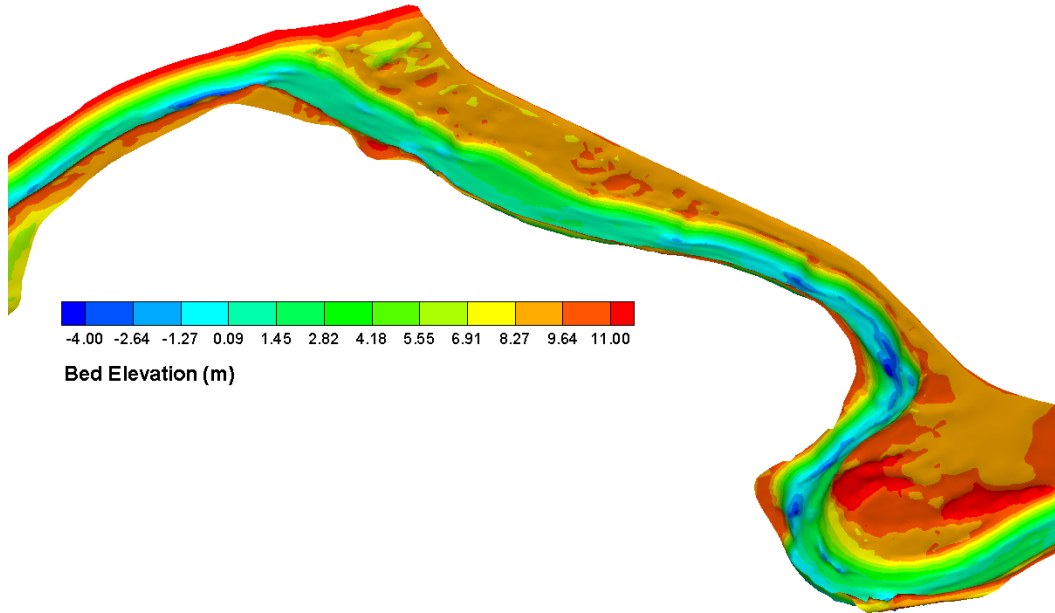


Figure 75. 2015 terrain represented by the High-Res-3D mesh: the downstream section of the big bend area (1:5 vertical distortion)

#### 8.4.3 Boundary Conditions

There are five open boundaries that need boundary conditions for the 3D model (see Figure 67). They are discussed next.

At the upstream (Knights Landing), the discharge is estimated using the discharge at Verona gauge, subtracted by the discharges at the Feather River, Natoma boundary and Karnak Slough. Such derived discharge is shown in Figure 76 and it is used as the upstream boundary condition at the Knights Landing. Such derived discharge work well for low flow scenario. For high flows, e.g. on February 11, 2015, the estimated discharge through the Fremont Weir area is over-estimated, due possibly to an under-estimate of the flow in the Feather River. Adjustment is made for the 3D modeling on February 11, 2015 as discussed later.

The Feather River into the Sacramento River is based on a 2D large-domain model. The flow hydrograph such obtained is shown in Figure 76. As discussed above, the flow in the Feather River may be under-estimated during high flow.

Other inflows to the Sacramento River include: those from the Sutter Bypass, 800 meters upstream of the Feather River confluence, via the Sacramento Slough near Karnak, and from the Natomas Cross-cut downstream of the Feather River confluence but above the Verona station. The Natomas flow is estimated to be 30% of the Bear River flow and is found to be very small and insignificant to the model results. The flow hydrographs from the Karnak Slough and the Sutter Bypass are shown in Figure 77.

## Quantitative Modeling Tools for Large Wood

Finally, the stage (water elevation) at Verona is based on the recorded gauge data and it is used at the downstream boundary condition. The stage data is plotted in Figure 78 for the period of December 1, 2014 to March 31, 2015.

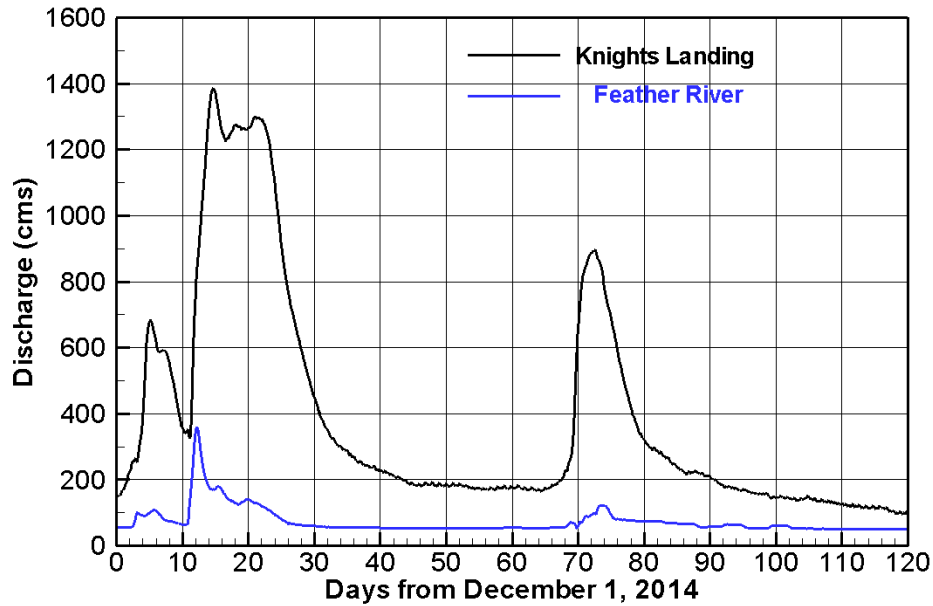


Figure 76. Flow discharges at the Knights Landing and Feather River for the period of December 1, 2014 to March 31, 2015

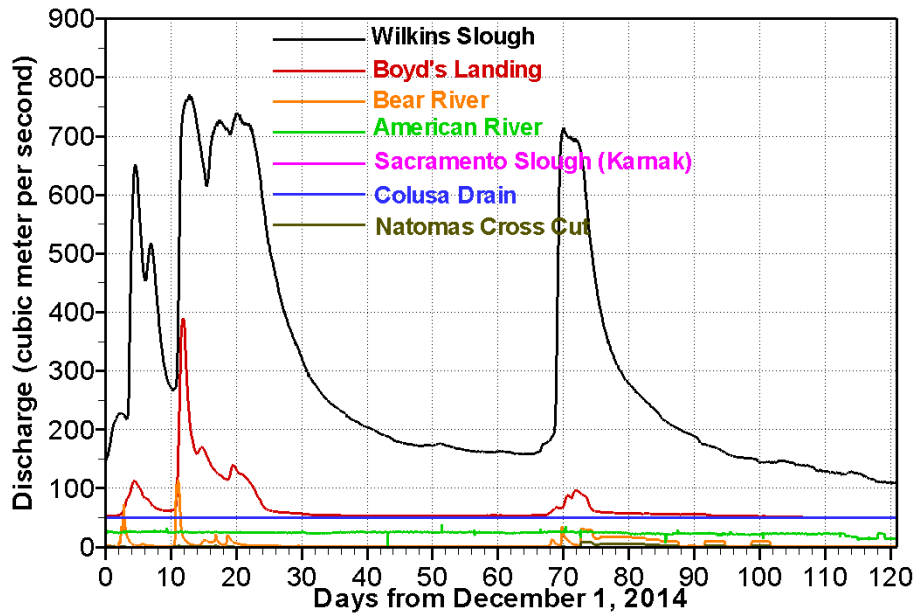


Figure 77. Flow hydrographs at seven inflow boundaries of the large-domain 2D model from December 1, 2014 to March 31, 2015

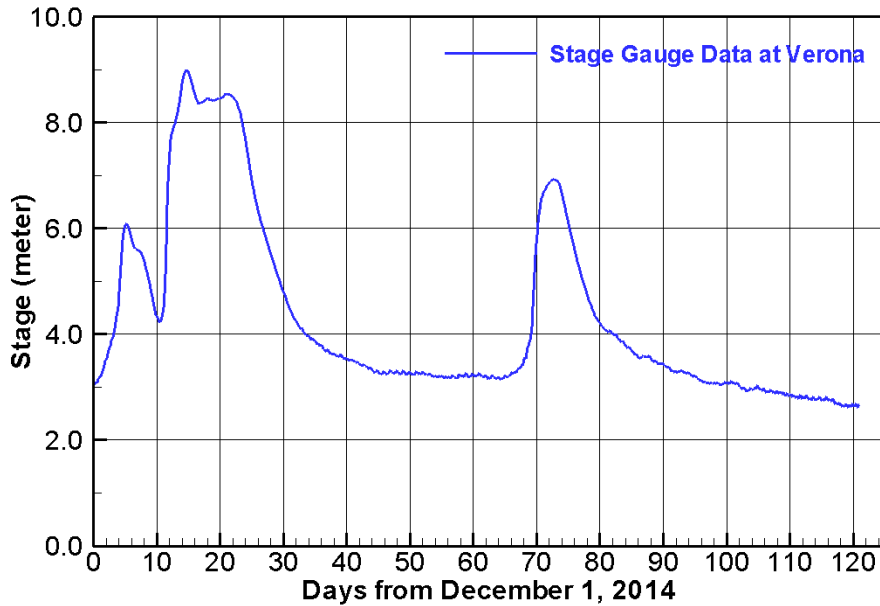


Figure 78. Stage at Verona gauge for the period of December 1, 2014 to March 31, 2015

ADCP data was collected by the DWR survey crew on three dates: January 26, February 11, and February 18, 2015. The daily discharge at Verona station is 232, 995, and 423 cubic meters per second, respectively, for the three days. Survey was carried out at ten river transects along the Fremont Weir section of the river as shown in Figure 79.



Figure 79. Ten (10) transects where the ADCP measurement was carried out in January to February, 2015

Two dates are selected for High-Res-3D modeling: January 26 and February 11, 2015. The January 26 represents a typical low flow condition (232 cubic meets

## Quantitative Modeling Tools for Large Wood

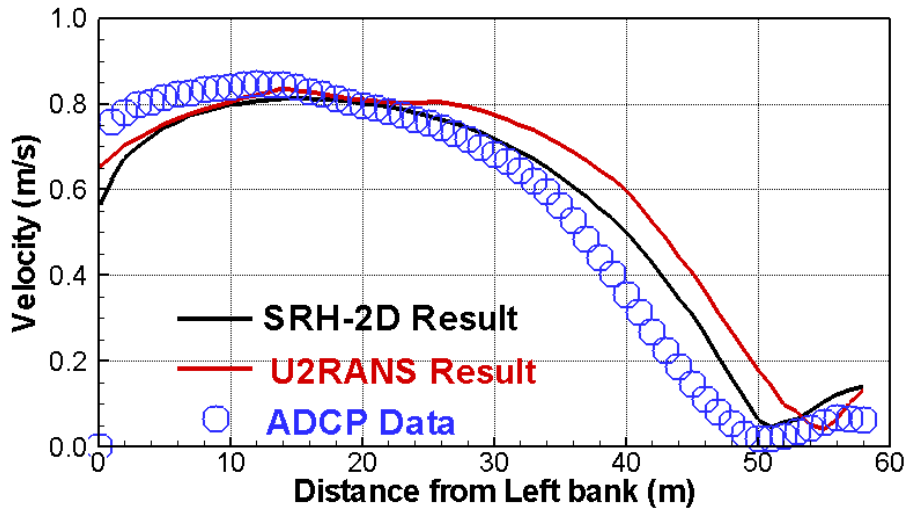
per second), while February 11 is a relatively high flow condition (995 cubic feet per second). The two High-Res-3D runs are named Low-Q and High-Q runs, respectively. Validation using both low and high flows lends credence to the accuracy of the 3D model.

### 8.4.4 Low Discharge Results and Comparison with ADCP Data

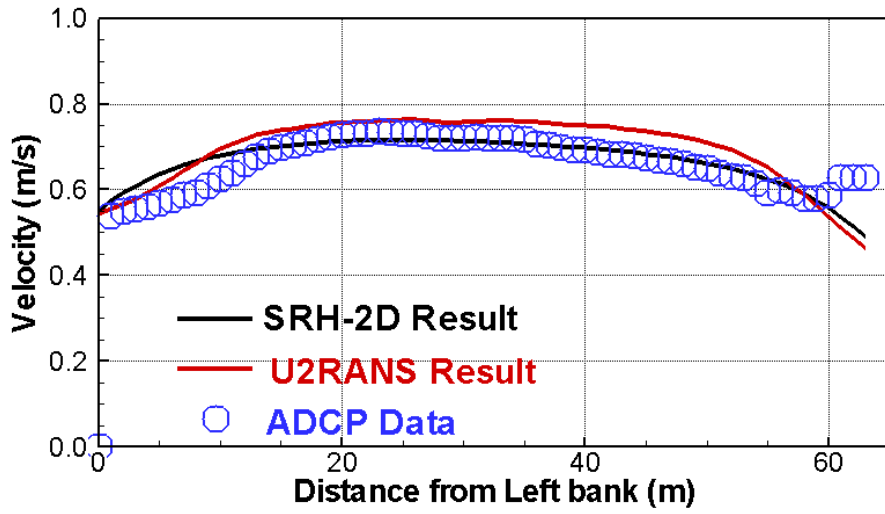
The Low-Q run corresponds to January 26, 2015 flow conditions. The 3D (also SRH-2D) model results are compared with the ADCP data for the depth-averaged velocity at ten ADCP transects in Figure 80.

First, it is shown that 2D and 3D model results agree very well with the ADCP velocity data at most transects except for Transect 8. At Transect 8, the models predict that the maximum velocity remains near the left bank but the ADCP data shows that the maximum velocity has been shifted towards the center and the right bank. The probable cause for the mismatch is the high uncertainty of local river bathymetry used by the numerical models. This will be discussed next when the secondary flow patterns are compared later.

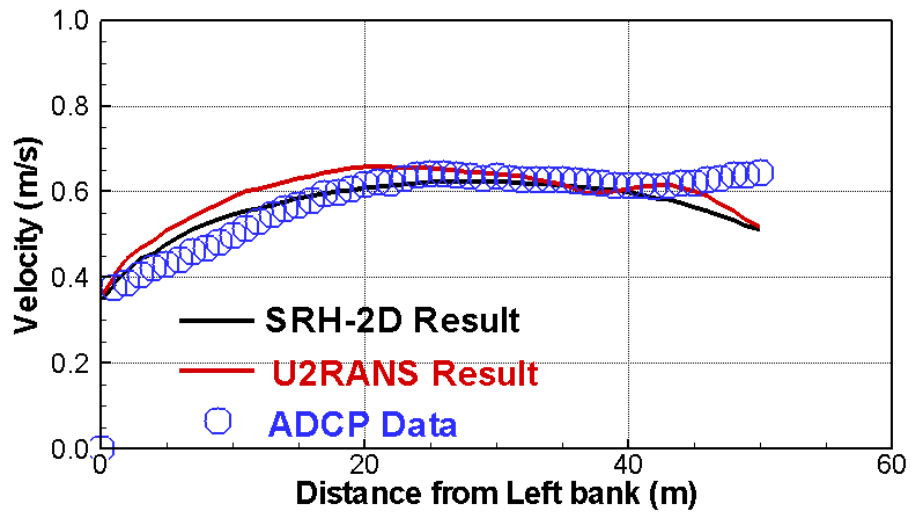
Second, it is found that 3D and 2D model results are very similar in most locations. This is a confirmation that 2D depth-averaged model is a very reliable tool in predicting the depth-averaged velocity for natural channels. If engineers are interested in the depth-averaged velocity only and if there are no major in-stream geometrical features that may cause significant local flow changes, a 2D model may be sufficient for flow prediction of a natural channel. A 3D model is needed only when there are in-stream structures in the model domain or one is interested in secondary flow patterns.



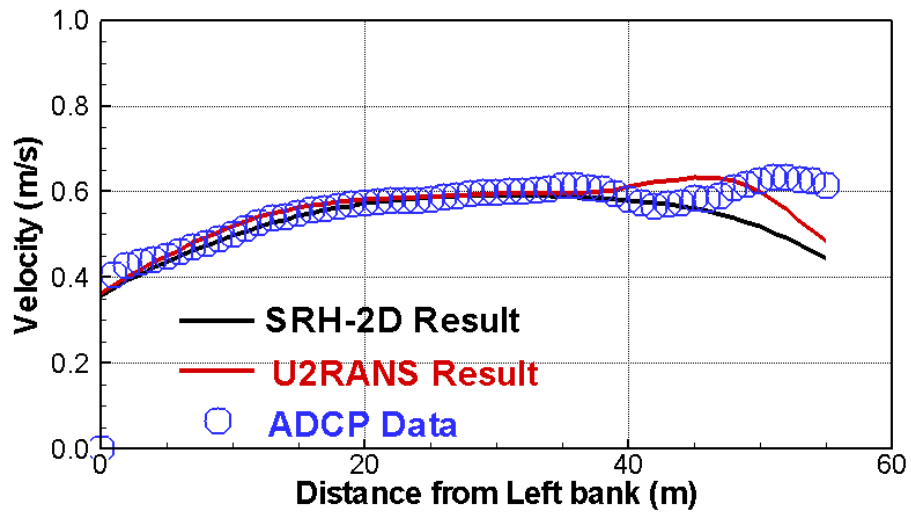
(a) Transect 1



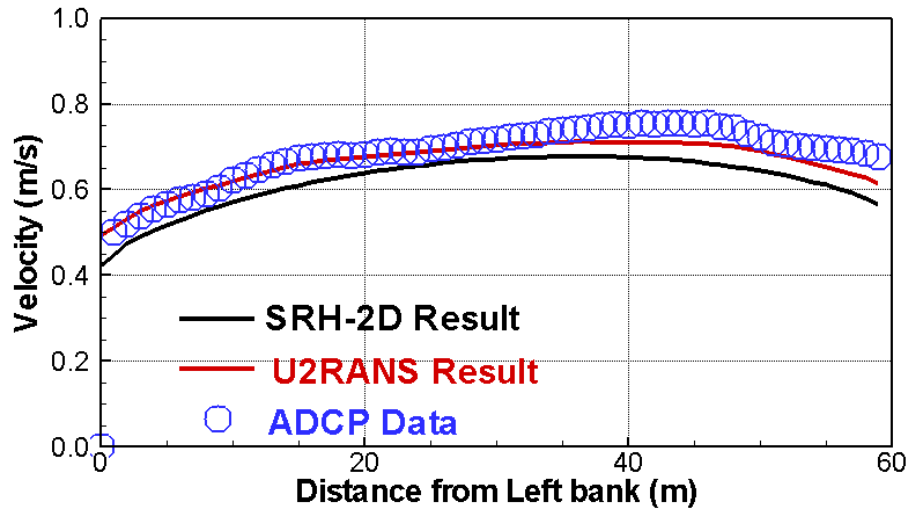
(b) Transect 2



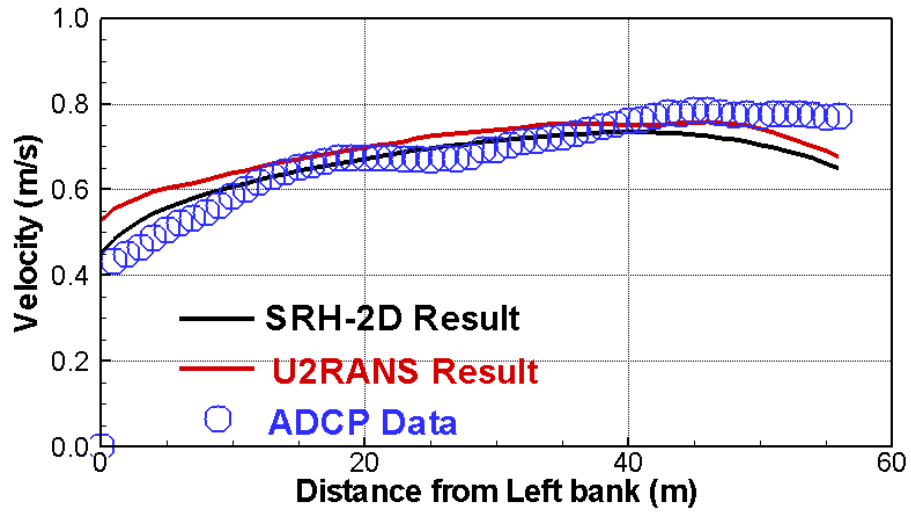
(c) Transect 3



(d) Transect 4

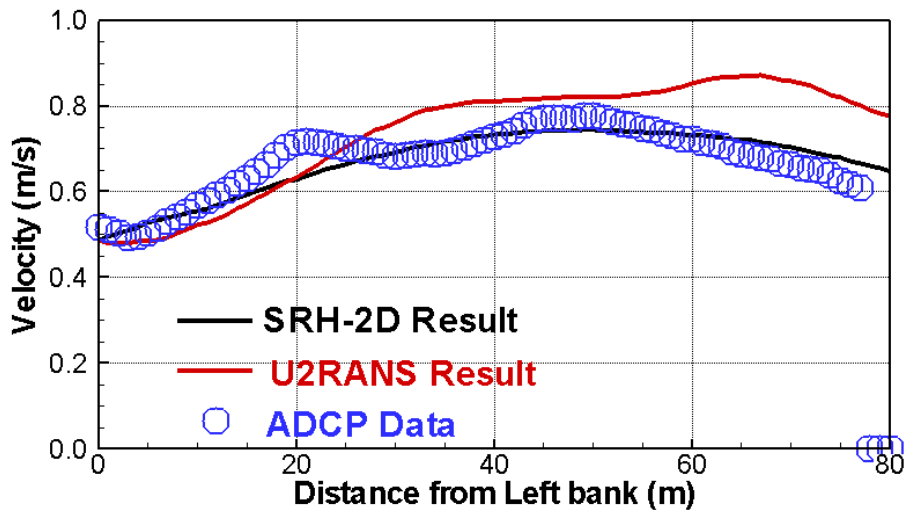


(e) Transect 5

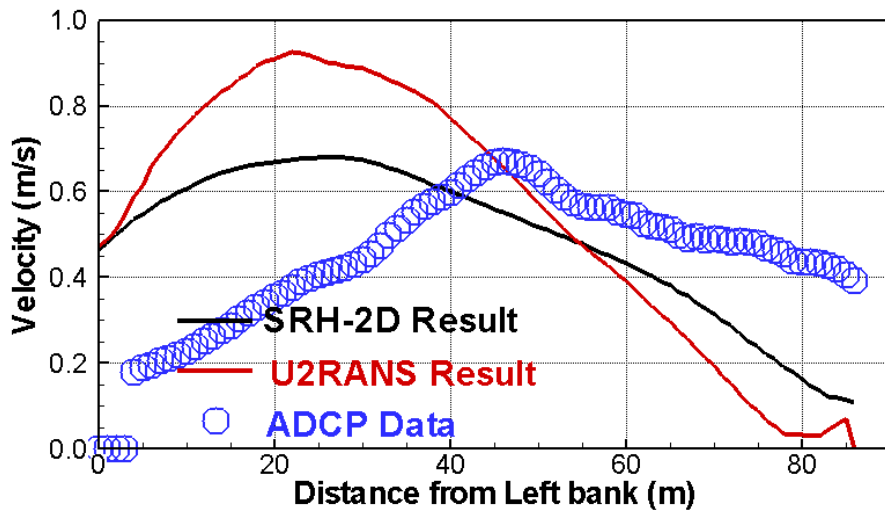


(f) Transect 6

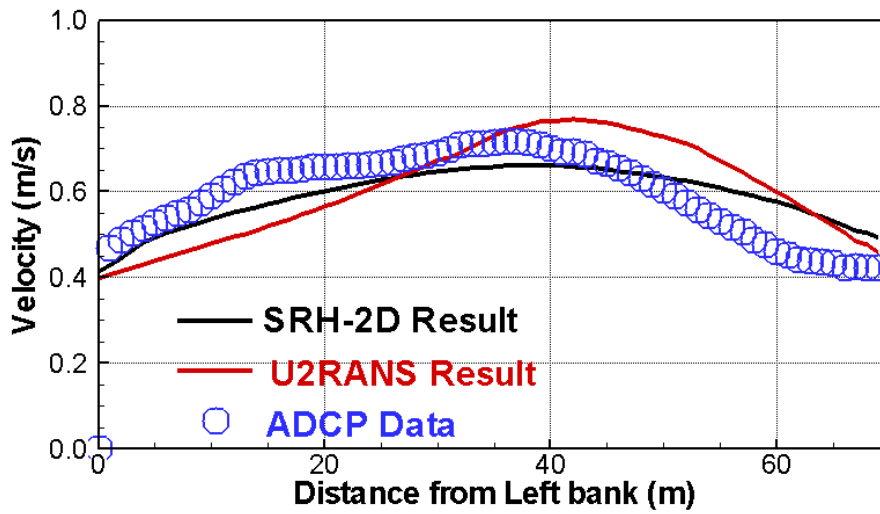
Quantitative Modeling Tools for Large Wood



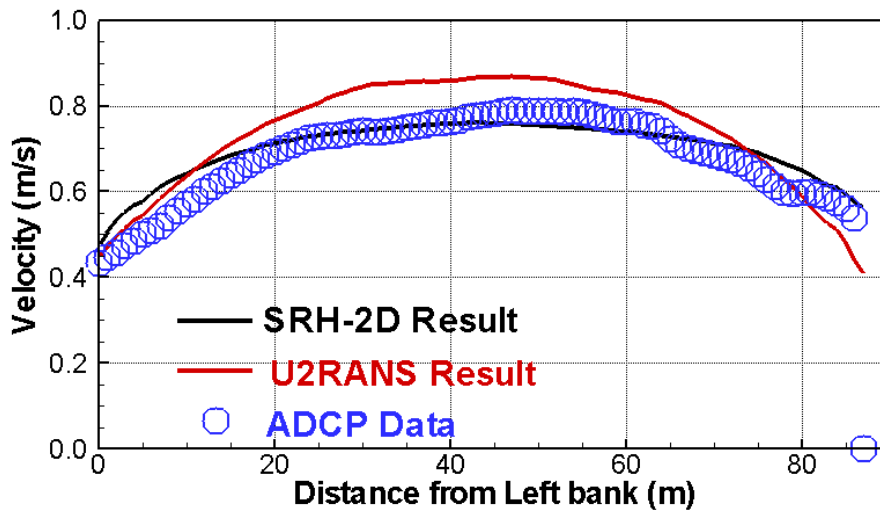
(g) Transect 7



(h) Transect 8



(i) Transect 9



(j) Transect 10

Figure 80. Comparison of depth-averaged velocity along 10 transects between 3D, 2D and ADCP results for the Low-Q run on January 26, 2015

## Quantitative Modeling Tools for Large Wood

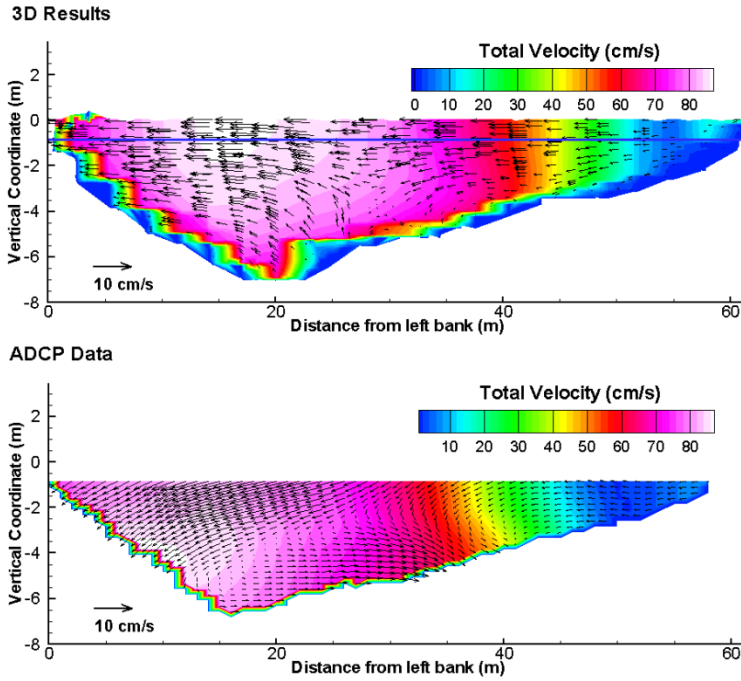
One of the advantages in using a 3D model is that secondary flow patterns may be predicted in a curved section of a channel even without in-stream structures. In the following, the 3D model predicted secondary flow patterns are compared with the ADCP data.

Secondary flows can be classified into two kinds: Prandtl's first kind (or pressure-driven) and Prandtl's second kind (or turbulence-driven). Pressure-driven secondary flows are induced by local pressure imbalances created by, e.g., flow curvature; while turbulence-driven secondary flows are due to anisotropy of turbulence normal stresses. Turbulence anisotropy may occur near sharp corners such as the corner of a square channel or across channels with transverse roughness changes. In general, pressure-driven secondary flows can reach 10% of the total flow velocity and is relatively easier to detect. The 3D RANS model such as U2RANS can predict the pressure-driven secondary flows reasonably. However, turbulence-driven secondary flows are typically small (about 1-2% of the main flow) and much harder to measure even in the laboratory environment. RANS models with two-equation turbulence models are also incapable of predicting turbulence-driven secondary flows. Therefore, the comparison of the present 3D model results with the ADCP data can only be done in a qualitatively sense for the pressure-driven secondary flows. The ADCP measurement equipment in the field is not capable of measuring the turbulence-driven secondary flows accurately and the uncertainty in measuring the pressure-driven secondary flow is also high.

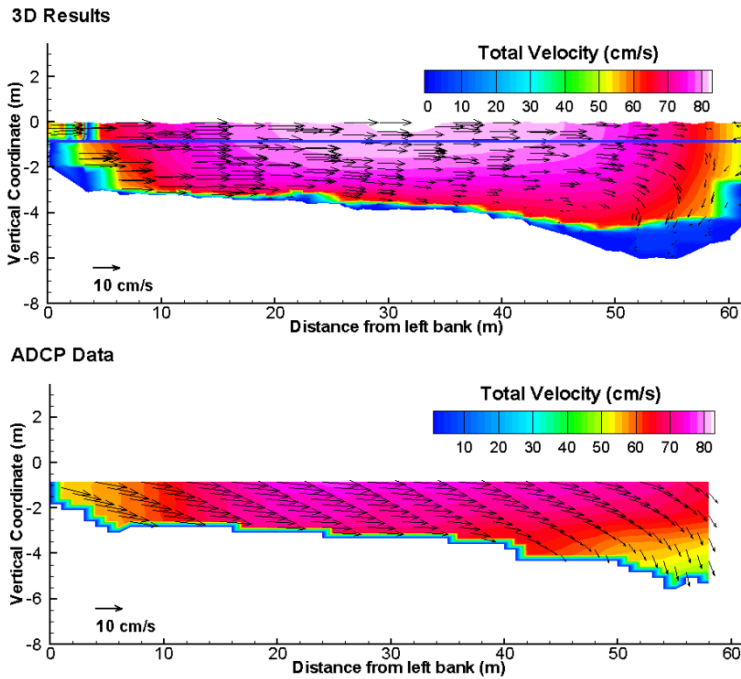
Predicted and ADCP measured secondary flow patterns are compared in Figure 81 at ten transects. The total velocity magnitude is also compared as color contours in the same figure. Some transects show circulating secondary flows such as transects 1, 3 and 4; while recirculating secondary flows at other transects are not visible. It is not that there are no recirculating secondary flows on these transects; but rather, they are probably "overwhelmed" by the longitudinal (streamwise) flow. Secondary flows are much smaller in magnitude than the longitudinal velocity. The display of secondary flow patterns is not easy as a transect has to be properly oriented so that it is as normal to the stream flow as possible. However, defining the "normal" of transect is difficult in a natural river. Other ways of rearranging the transect orientation may display the secondary flow pattern better.

Overall, the 3D results agree with the ADCP data in regards to the qualitative secondary flow patterns at most transects except for transect 8. This is consistent with the comparison of the depth-averaged velocity. The mismatch in results at transect 8 (see Figure 81h) may be caused by the local river bathymetry. The cross section bed elevation comparison shows that the river cross section used by the model is different from ADCP data. The ADCP cross section has a deeper thalweg and a higher right bar than the numerical model. Transect 8 is located near the exit of the big bend. It was reported by the survey crew that flow in this area was very unsteady and bed morphology may change significantly over time.

This may explain why the bathymetry used by the model, surveyed at a different time, is different from the ADCP data bed profile.

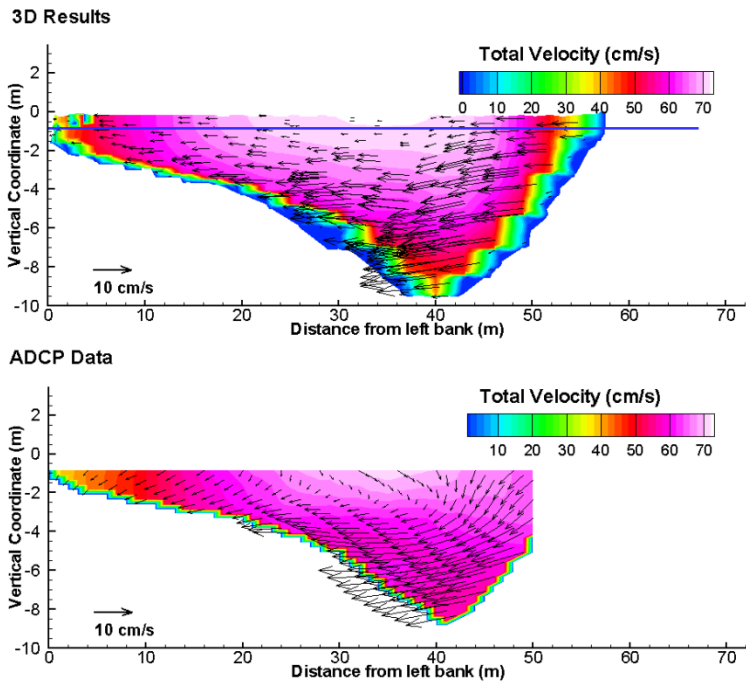


(a) Transect 1

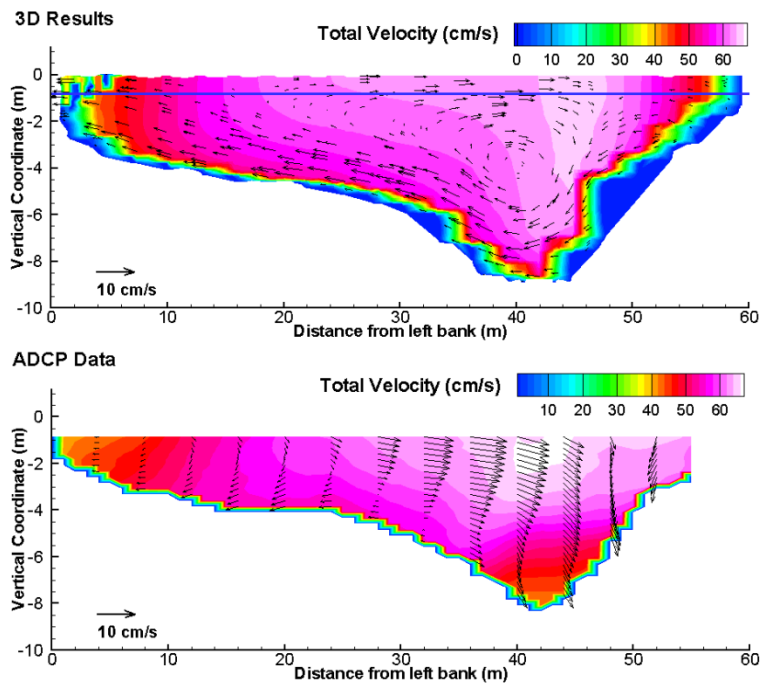


(b) Transect 2

## Quantitative Modeling Tools for Large Wood



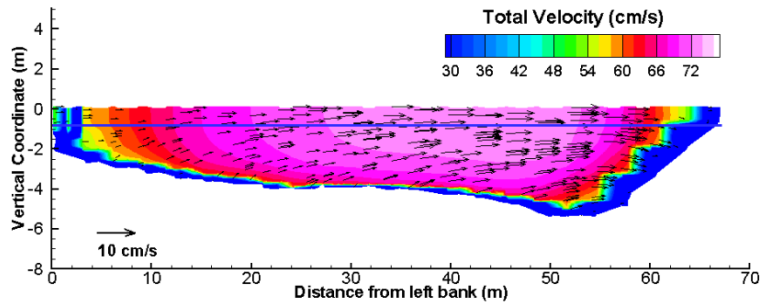
(c) Transect 3



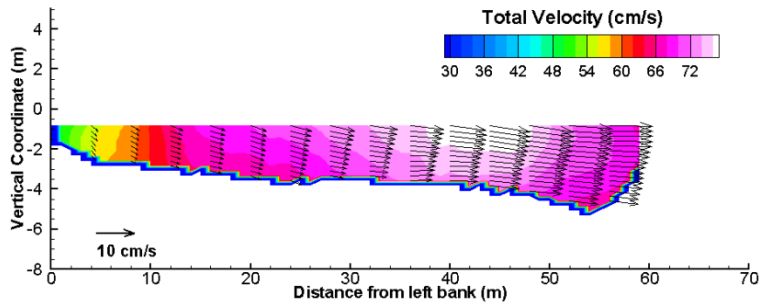
(d) Transect 4

## 8. Flow Module Results

### 3D Results

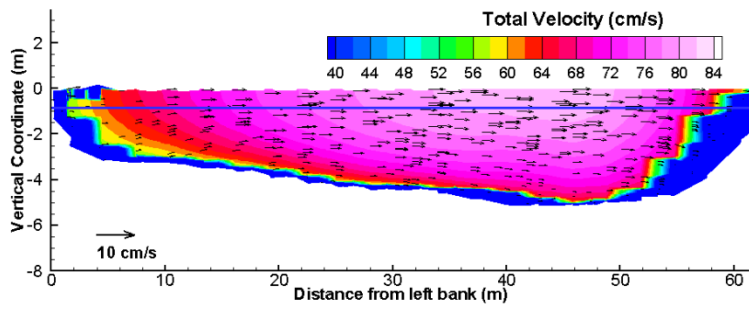


### ADCP Data

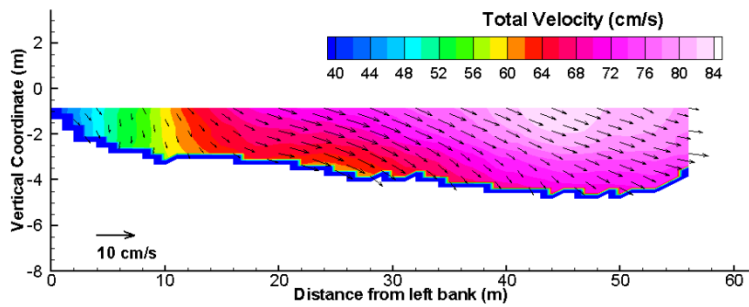


(e) Transect 5

### 3D Results

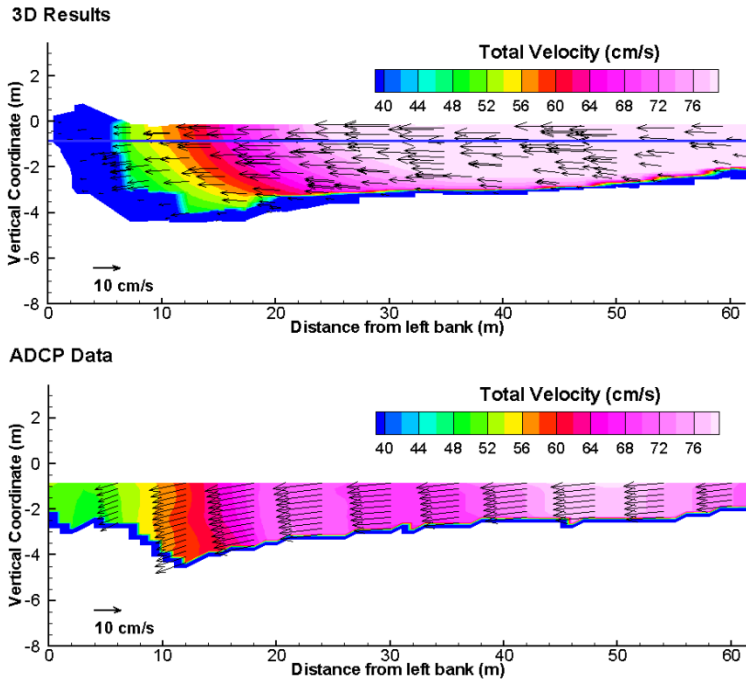


### ADCP Data

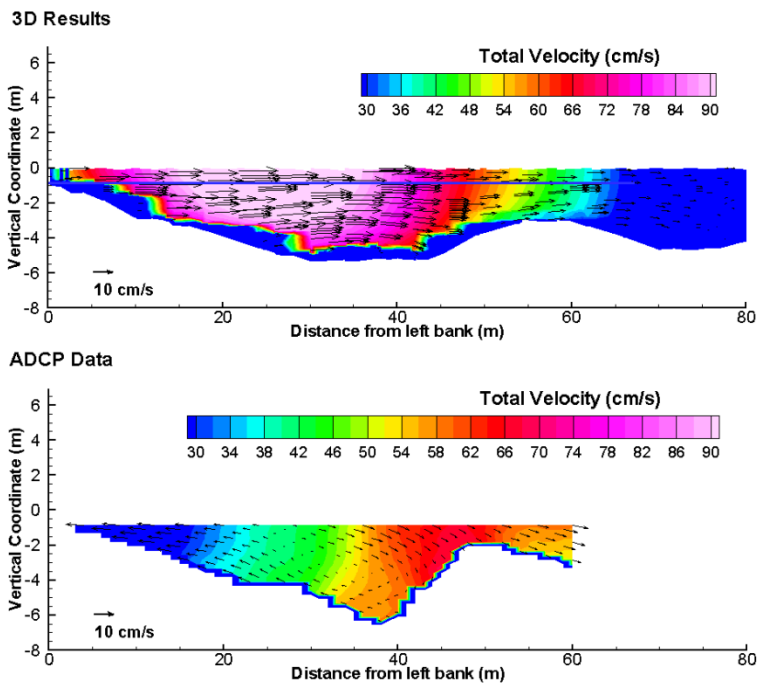


(f) Transect 6

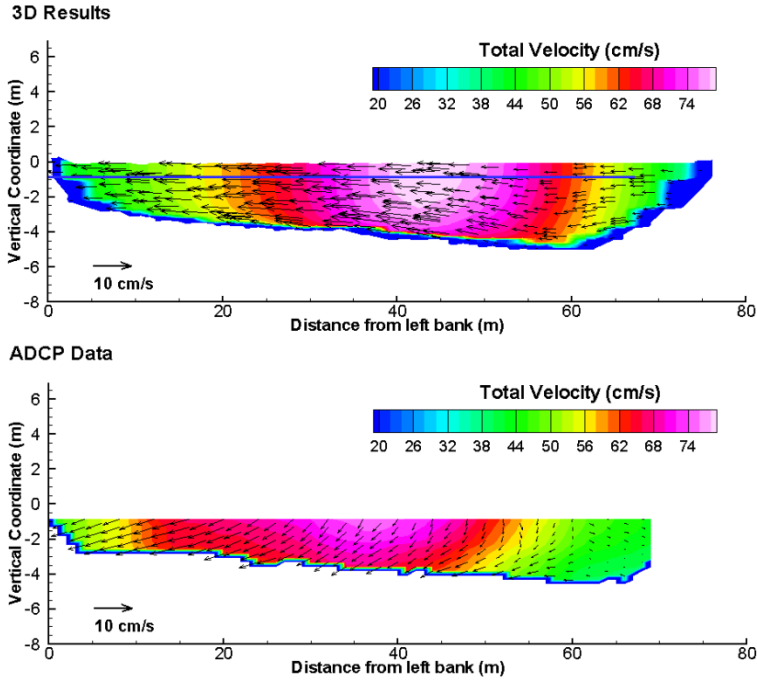
## Quantitative Modeling Tools for Large Wood



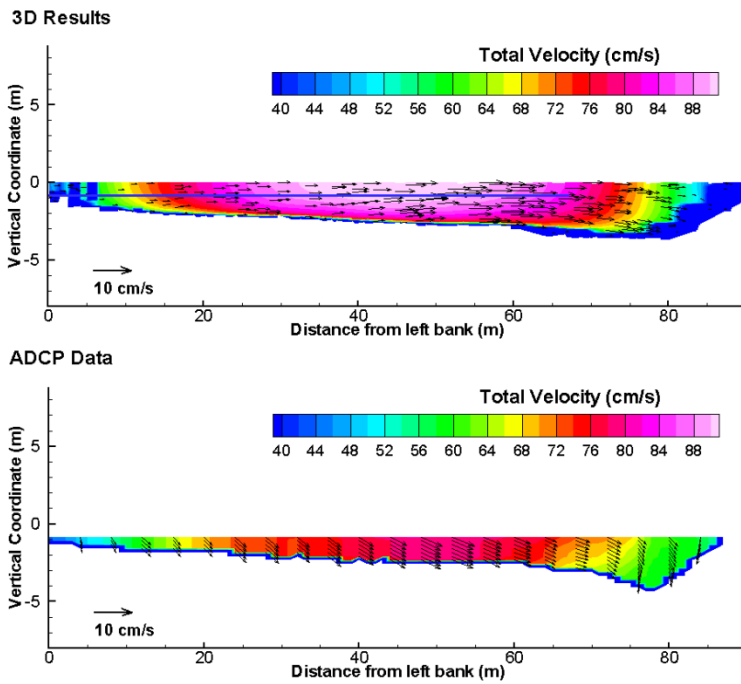
(g) Transect 7



(h) Transect 8



(i) Transect 9

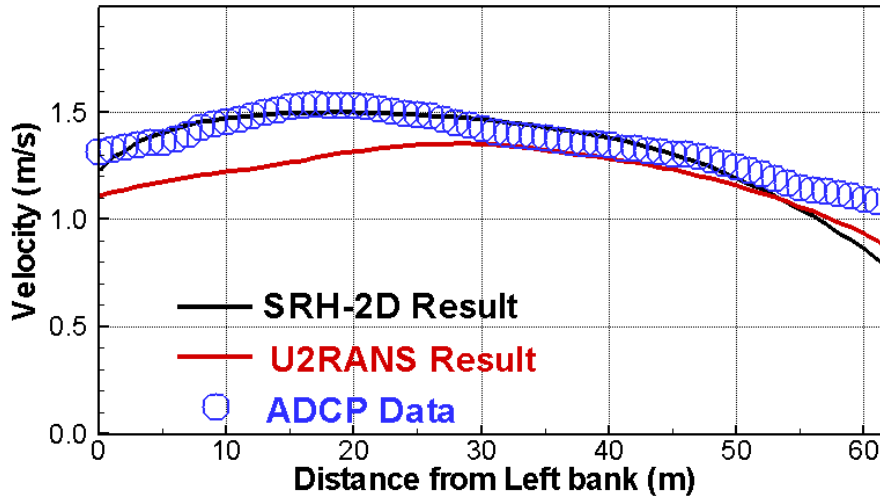


(j) Transect 10

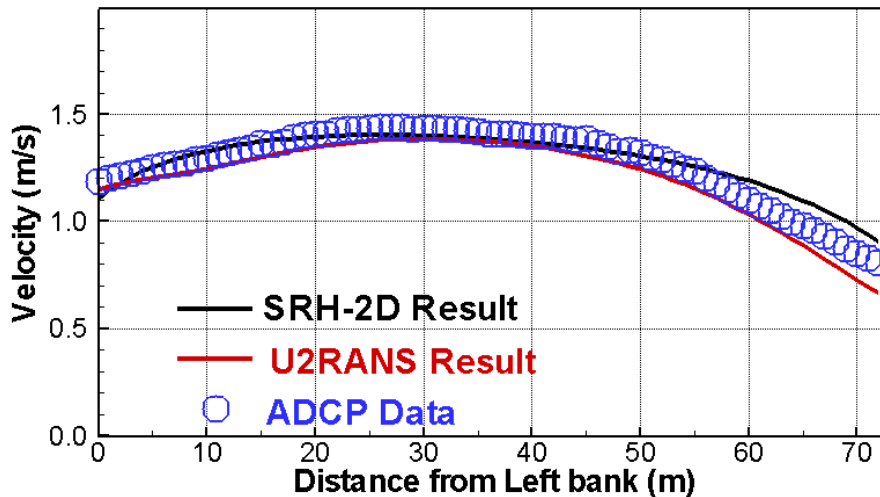
Figure 81. High-Res-3D predicted (top) and ADCP measured (bottom) secondary flow patterns at 10 transects for the Low-Q run

### 8.4.5 High Discharge Results and Comparison with ADCP Data

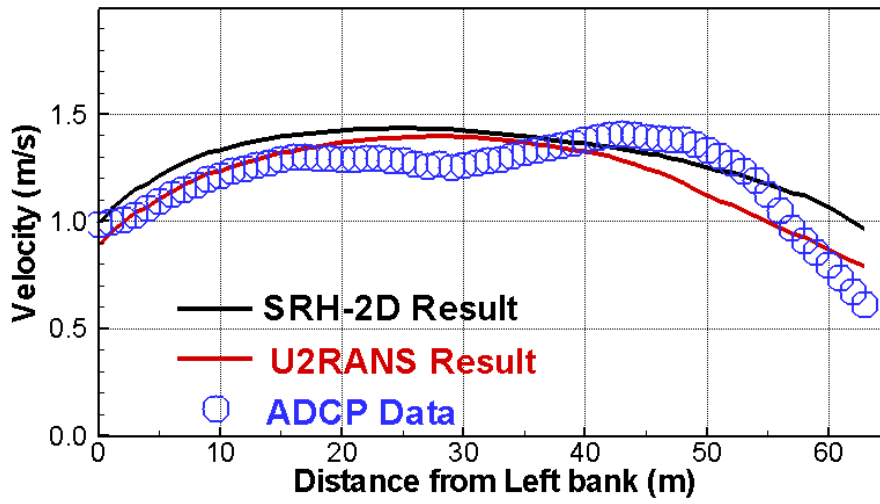
The High-Q run corresponds to February 11, 2015 flow conditions. The 3D and 2D model results (High-Res-3D and High-Res-2D2) are compared with the ADCP data for the depth-averaged velocity at ten transects in Figure 82. Overall, the conclusions reached with the Low-Q run still hold. That is, 3D and 2D model results agree well with the ADCP velocity data; and 3D and 2D model results also agree with each other well. Model comparison at transect 8 is much better than the Low-Q run. The local river bathymetry mismatch usually has a lesser impact on velocity than the Low-Q run.



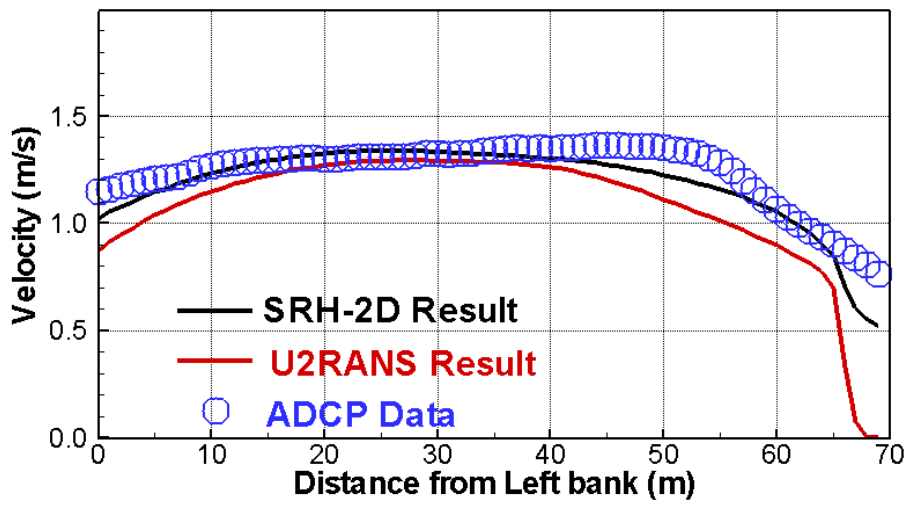
(a) Transect 1



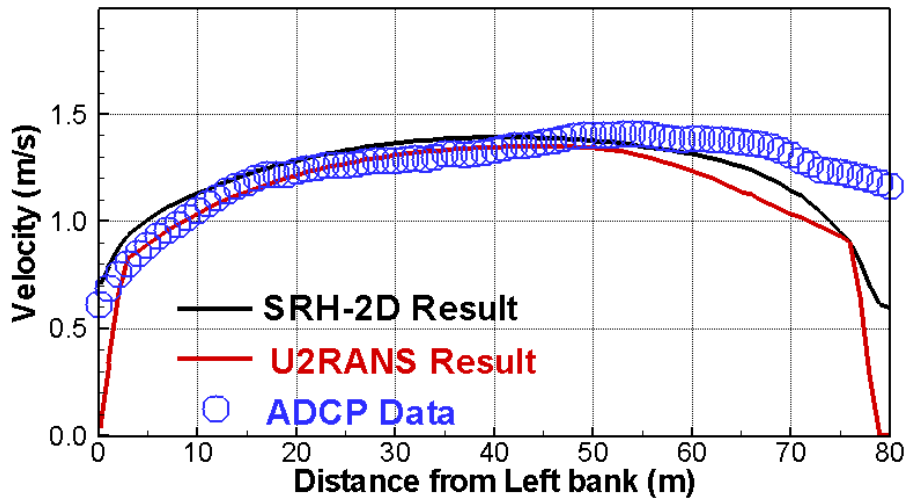
(b) Transect 2



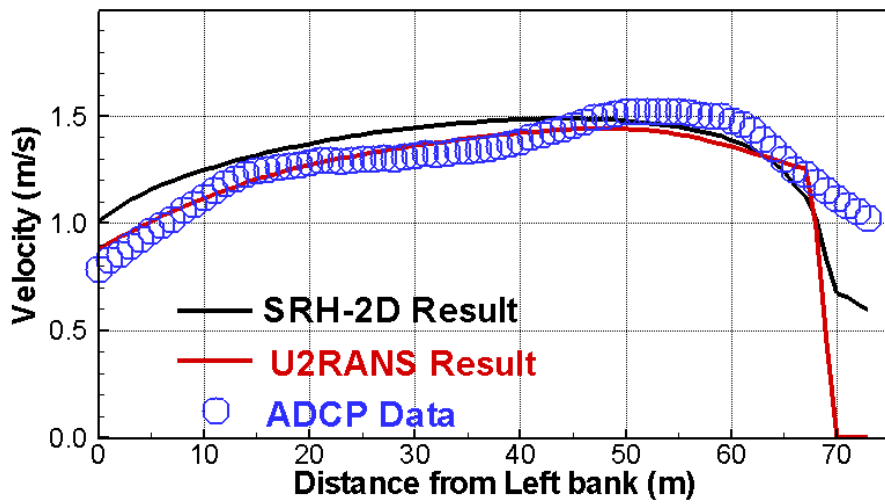
(c) Transect 3



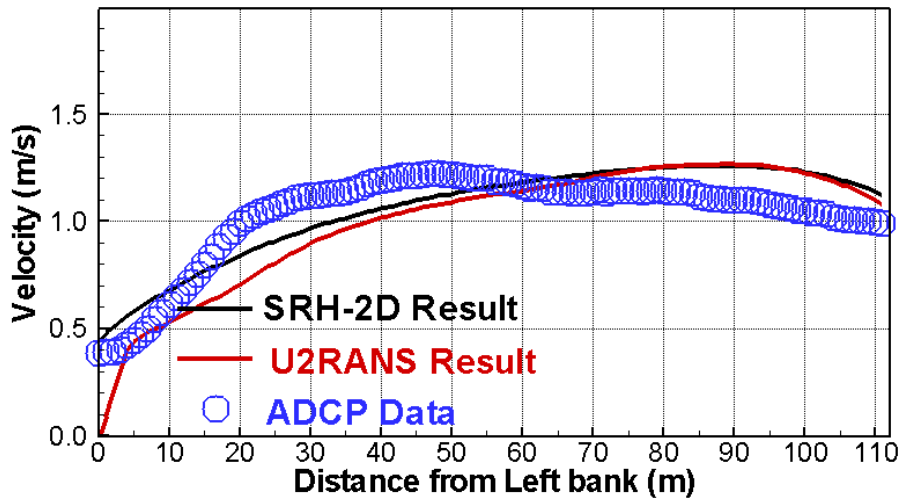
(d) Transect 4



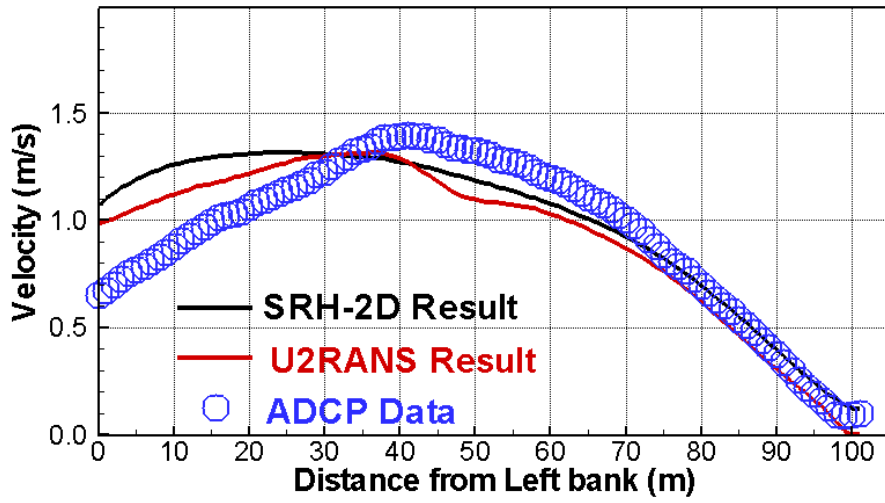
(e) Transect 5



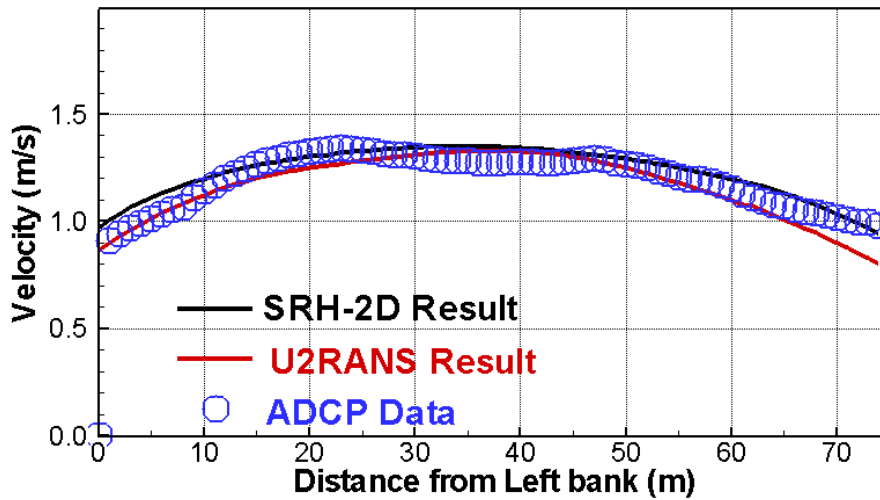
(f) Transect 6



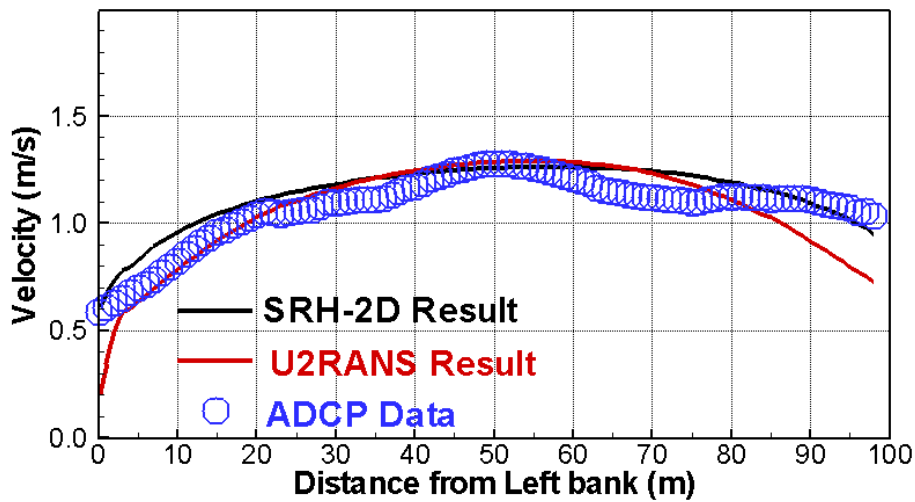
(g) Transect 7



(h) Transect 8



(i) Transect 9

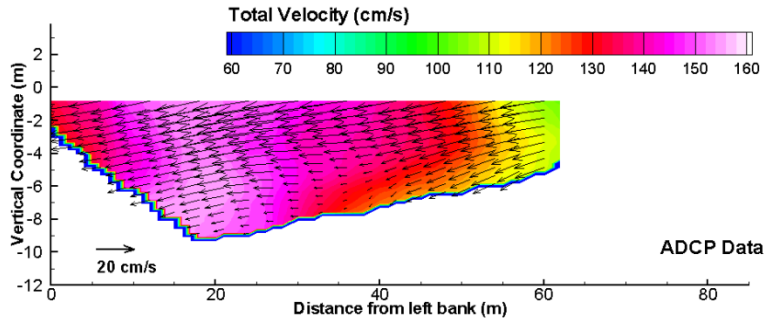
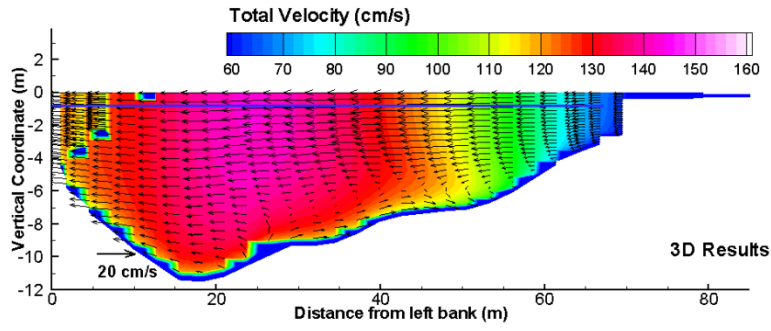


(j) Transect 10

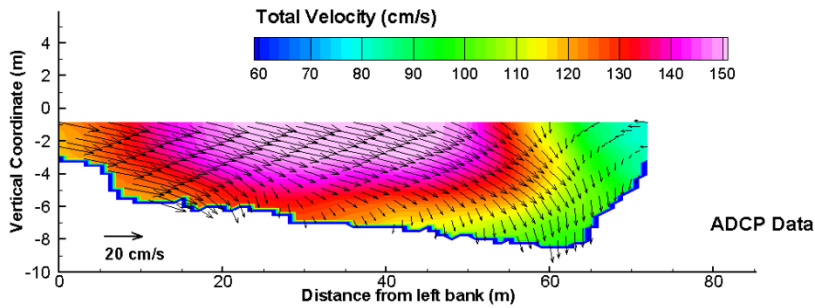
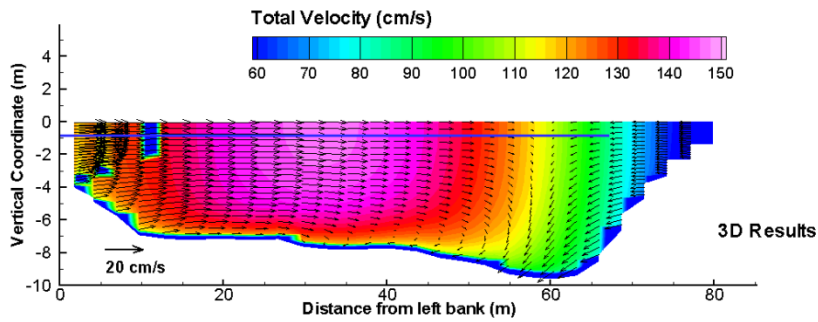
Figure 82. Comparison of depth-averaged velocity along 10 transects between 3D, 2D and ADCP results for the High-Q run on February 11, 2015

Similarly, 3D model predicted secondary flows are compared with the ADCP data qualitatively in Figure 83 at ten transects. The total velocity magnitude is also compared in the same figure as color contours. Overall, the 3D model predicted secondary flow patterns agree reasonably with the ADCP data at all transects.

## 8. Flow Module Results

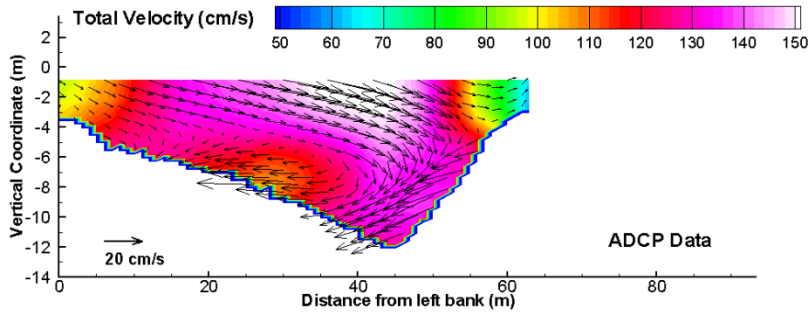
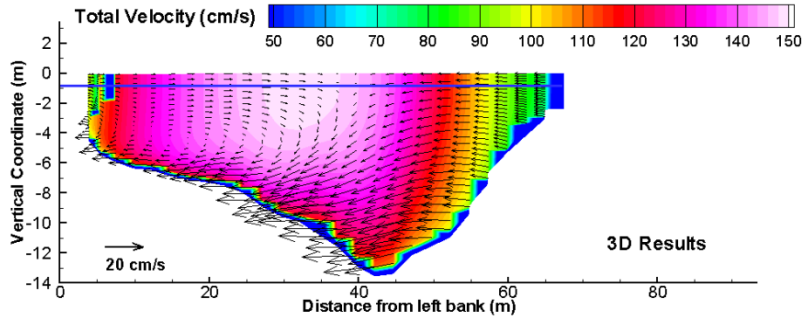


(a) Transect 1

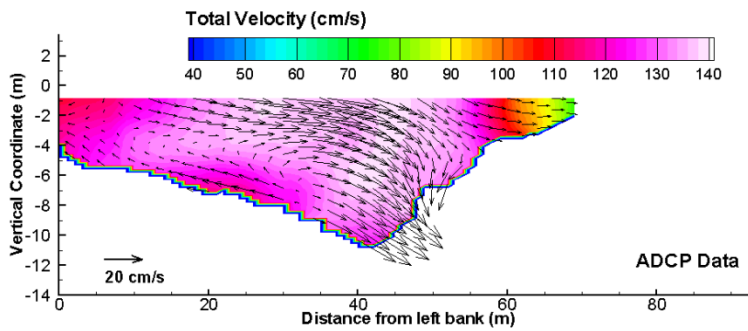
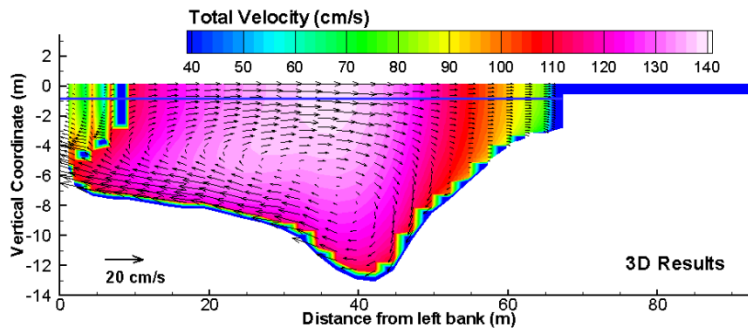


(b) Transect 2

## Quantitative Modeling Tools for Large Wood

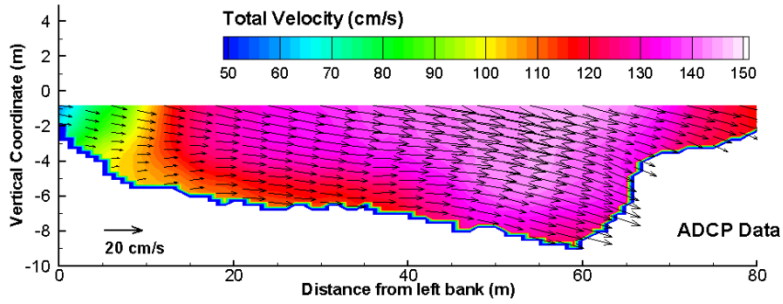
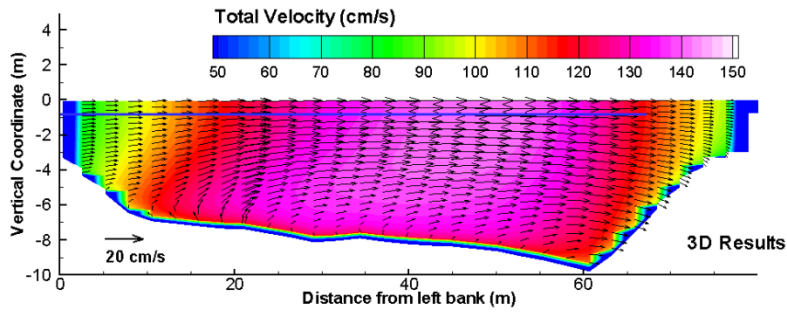


(c) Transect 3

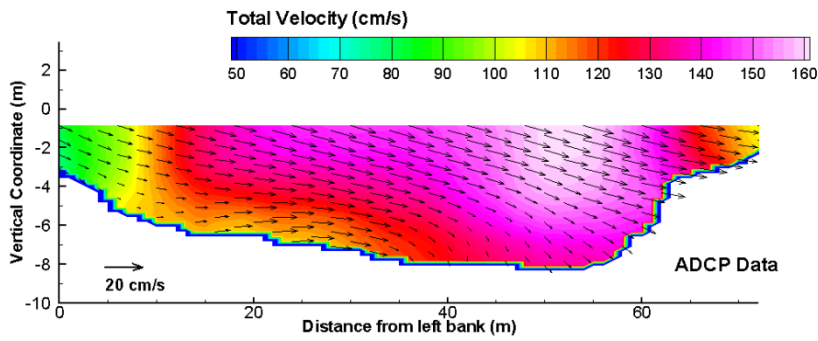
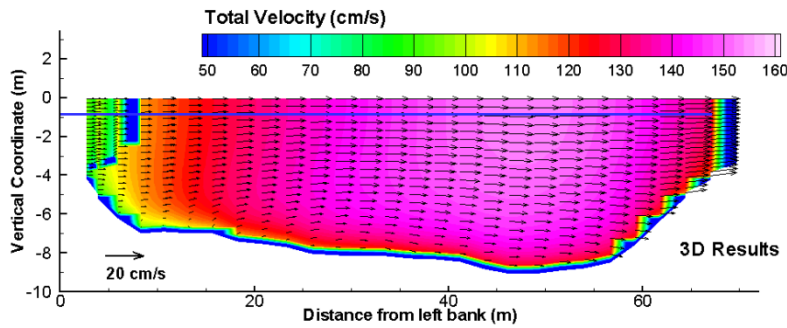


(d) Transect 4

## 8. Flow Module Results

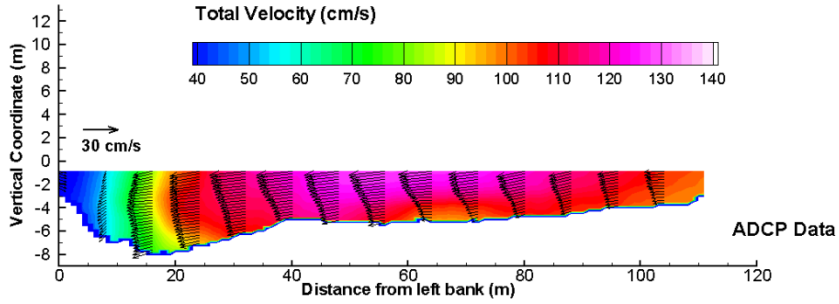
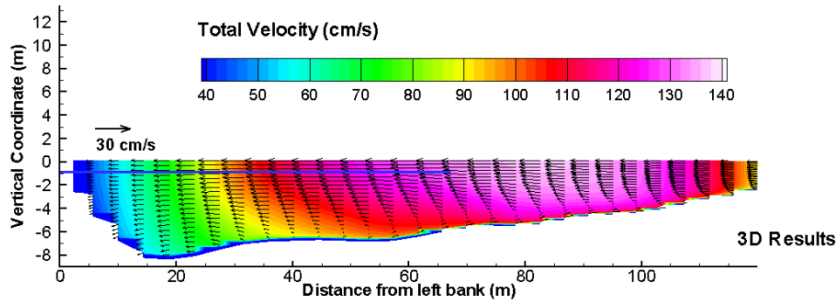


(e) Transect 5

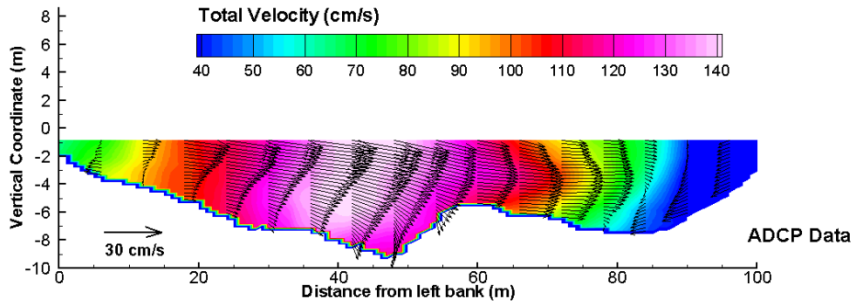
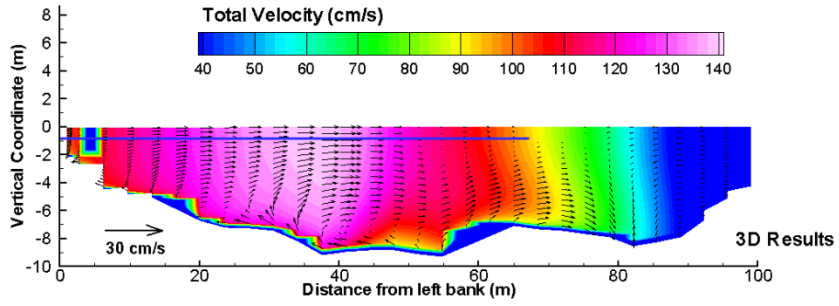


(f) Transect 6

# Quantitative Modeling Tools for Large Wood

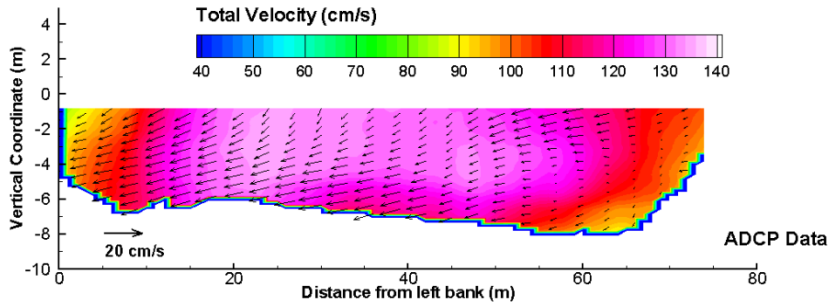
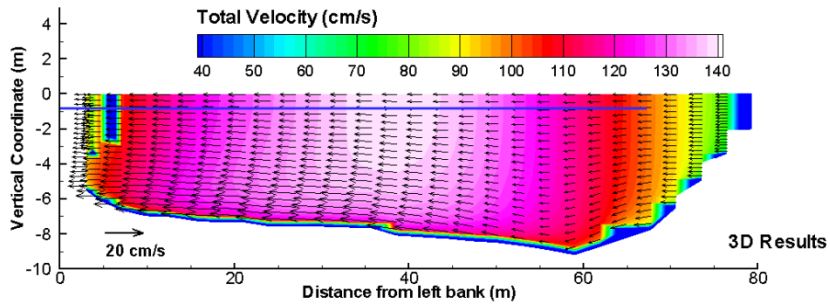


(g) Transect 7

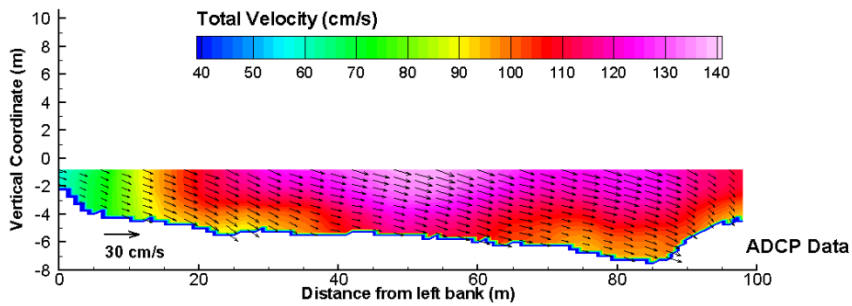
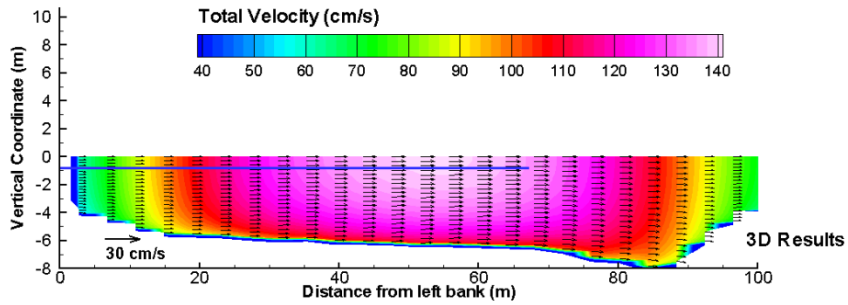


(h) Transect 8

## 8. Flow Module Results



(i) Transect 9



(j) Transect 10

Figure 83. High-Res-3D predicted (top) and ADCP measured (bottom) secondary flow patterns at 10 transects for the High-Q run

## 9. References

- Abbe, T. B., and D. R. Montgomery. (2003). Patterns and processes of wood accumulation in the Queets River basin, Washington. *Geomorphology* 51:81–107.
- Apsley, D. D., and Stansby, P. K. (2008). “Bed-load sediment transport on large slopes: Model formulation and implementation within a rans solver.” *J. Hydraul. Eng.*, 10.1061/(ASCE)0733-9429(2008)134:10(1440), 1440–1451.
- Armanini, A. (1992). “Variation of bed and sediment load mean diameters due to erosion and deposition processes.” *Dynamics of gravel-bed rivers*, P. Billi, R. D. Hey, C. R. Thorne, and P. Tacconi, eds., Wiley, 352–359.
- Armfield, S., and Street, R. (2002). “An analysis and comparison of the time accuracy of fractional step methods for the Navier-Stokes equations on staggered grids.” *International Journal for Numerical Methods in Fluids*, 38(3):255–282.
- ASCE Sedimentation Manual (2007). *Sedimentation Engineering: Processes, Measurements, Modeling and Practice*. ASCE Manual and Reports on Engineering Practice No.110. Reston, VA. Marcelo Garcia (ed).
- Behr, M., and Tezduyar, T. E. (1994). “Finite-element solution strategies for large-scale simulations.” *Comput. Methods Appl. Mech. Eng.*, 112, 3–24.
- Berger, R. C., and Stockstill, R. L. (1999). “A finite-element system for flows.” *Proc., 1999 American Society of Civil Engineers (ASCE) Water Resources Engineering Conf., Water Resources into the New Millennium, Past Accomplishments and New Challenges*, Seattle.
- Blumberg, A. F. and Mellor, G.L. (1987). “A description of a three-dimensional coastal ocean circulation model.” In: *Three-Dimensional Coastal Ocean Models, Coastal and Estuarine Science*, Vol. 4. (Heaps, N. S., ed.) American Geophysical Union, pp. 1-19.
- Bowen, M. D., Hiebert, S., Hueth, C. and Maisonneuve, V. (2009). 2009 Effectiveness of a Non-Physical Fish Barrier at the Divergence of the Old and San Joaquin Rivers (CA). Technical Memorandum 86-68290-09-05, Bureau of Reclamation.
- Bowen, M. D. and Bark, R. (2010). 2010 Effectiveness of a Non-Physical Fish Barrier at the Divergence of the Old and San Joaquin Rivers (CA). Technical Memorandum 86-68290-10-07, Bureau of Reclamation.
- Casulli, V. (1997). “Numerical simulation of three-dimensional free surface flow in isopycnal coordinates.” *Int. J. Numer. Methods Fluids*, 25, 645–658.
- Casulli, V. and Stelling, G.S. (1998). “Numerical simulation of 3D quasi-hydrostatic, free-surface flows.” *Journal of Hydraulic Engineering*, 124(7):678–686.

- Casulli, V. (1999). "A semi-implicit finite difference method for non-hydrostatic, free-surface flows." *International Journal for Numerical Methods in Fluids*, 30:425–440.
- Cokljat, D., and Younis, B. A. (1995). "Second-order closure study of open-channel flows." *J. Hydraul. Eng.*, 121~2!, 94–107.
- Demuren, A. O. (1993). "A numerical model for flow in meandering channels with natural bed topography." *Water Resour. Res.*, 19(4),1269–1277.
- Eaton, B. C., M. A. Hassan, and S. L. Davidson (2012). Modeling wood dynamics, jam formation, and sediment storage in a gravel-bed stream, *J. Geophys. Res.*, 117, F00A05, doi:10.1029/2012JF002385.
- Francalanci, S., and Solari, L. (2007). "Gravitational effects on bed load transport at low Shields stress: Experimental observations." *Water Resour. Res.*, 43, W03424.
- Fringer, O.B., Gerritsen, M., and Street, R.L. (2006). "An unstructured-grid, finite-volume, nonhydrostatic, parallel coastal ocean simulator." *Ocean Modeling*, 14(3-4):139–173.
- Gaeuman, D., Sklar, L., and Lai, Y. (2014). "Flume experiments to constrain bedload adaptation length." *J. Hydraul. Eng.*, 06014007-1:6
- Ge, L., and Sotiropoulos, F. (2007). "A numerical method for solving the 3D unsteady incompressible navierstokes equations in curvilinear domains with complex immersed boundaries." *J. Comput. Phys.*, 225(2), 1782–1809.
- Gessler, D., Hall, B., Spasojevic, M., Holly, F.M., Pourtaheri, H., Raphelt, N. X., 1999. Application of 3D mobile bed hydrodynamics model. *J. Hydraul. Eng.*, 125(7), 737–749.
- Greimann, B., Lai, Y., and Huang, J. (2008). "Two-dimensional total sediment load model equations." *J. Hydraul. Eng.*, 10.1061/(ASCE)0733-9429(2008)134:8(1142), 1142–1146.
- Hamrick, J. M., (1992). A Three-Dimensional Environmental Fluid Dynamics Computer Code: Theoretical and Computational Aspects. The College of William and Mary, Virginia Institute of Marine Science. Special Report 317, 63 pp.
- Huang, J. C., and Weber, L. J. (1998). "Numerical simulation of the forebay of Lower Granite lock and dam." *Hydro Vision 98*, Reno, Nev., July.
- Huang, J. C. (2000). "Development and validation of a three-dimensional numerical model for application to river flows." PhD thesis, Civil and Environmental Engineering, The University of Iowa, Iowa.
- Issa, R.I. (1986). "Solution of the implicitly discretized fluid flow equations by operator-splitting." *J. Comp. Physics*, 62(1), 40-65.

## Quantitative Modeling Tools for Large Wood

- Kang, S., Lightbody, A., Hill, C., and Sotiropoulos, F. (2011). "High resolution numerical simulation of turbulence in natural waterways." *Adv. Water Resour.*, 34(1), 98–113.
- Khosronejad, A., Rennie, C., Salehi, A., and Townsend, R. (2007). "3D numerical modeling of flow and sediment transport in laboratory channel bends." *J. Hydraul. Eng.*, 10.1061/(ASCE)0733-9429(2007)133:10(1123), 1123–1134.
- Khosronejad, A., Kozarek, J.L., and Sotiropoulos, F. (2014). "Simulation-Based Approach for Stream Restoration Structure Design: Model Development and Validation." *J. Hydraul. Eng.*, 140, (ASCE)0733-9429/04014042.
- Lai, Y. G., So, R. M. C., and Przekwas, A. J. (1995). "Turbulent transonic flow simulation using a pressure-based method." *Int. J. Eng. Sci.*, 33(4), 469–483.
- Lai, Y.G. and Przekwas, A.J. (1994). "A Finite-Volume Method for Simulations of Fluid Flows with Moving Boundaries," *Int. J. Comp. Fluid Dynamics*, Vol.2, pp.19-40.
- Lai, Y.G. (2000). "Unstructured Grid Arbitrarily Shaped Element Method for Fluid Flow Simulation," *AIAA Journal*, Vol.38, No.12, pp.2246-2252.
- Lai, Y. G., Weber, L. J., and Patel, V. C. (2003). "Nonhydrostatic three dimensional method for hydraulic flow simulation. I: Formulation and verification." *J. Hydraul. Eng.*, 129(3), 196–205.
- Landsberg, A., Chtchelkanova, A., Lind, C., Boris, J., and Young, T. (1998). *Fast3D user and programmer reference manual*.
- Lauder, B. E., and Spalding, D. B. (1974). "The numerical computation of turbulent flows." *Comput. Methods Appl. Mech. Eng.*, 3, 269–289.
- Li, S., Lai, Y.G., Weber, L.J., Silva, J.M., Patel, V.C., (2004). "Validation of a Three-Dimensional Numerical Model for Water-Pump Intakes", *J. Hydraulic Research*, IAHS, vol.42(3).
- Liu, X., and Garca, M. (2008). "Three-dimensional numerical model with free water surface and mesh deformation for local sediment scour." *J. Waterway, Port, Coastal, Ocean Eng.*, 10.1061/(ASCE)0733-950X(2008)134:4(203), 203–217.
- Mahadevan, A., Oliger, J., and Street, R. (1996a). "A nonhydrostatic mesoscale ocean model. part i: Well-posedness and scaling." *Journal of Physical Oceanography*, 26(9):1868–1880.
- Mahadevan, A., Oliger, J., and Street, R. (1996b). "A nonhydrostatic mesoscale ocean model. part ii: Numerical implementation." *Journal of Physical Oceanography*, 26(9):1881–1900.
- Malcherek, A. (2007). *Sediment transport und Morphodynamik*, Scriptum Institut fur Wasserwesen, Universitat Munchen.

- Merkel, U.H. and Kopmann, R. (2012). "A continuous vertical grain sorting model for Telemac and Sisyphé." *River Flow 2012 – Murillo* (Ed.). Taylor & Francis Group, London, ISBN 978-0-415-62129-8. Pp.457-463.
- Meselhe, E. A., and Weber, L. J. (1997). "Validation of a three dimensional model using field measurements in a large scale river reach." *Proc., 27th Congress of the IAHR, Theme B, Vol. 2*, pp. 827–832.
- Mittal, R. and Iaccarino, G. (2005). "Immersed Boundary Methods." *Annu. Rev. Fluid Mech.* 37:239–61. doi: 10.1146/annurev.fluid.37.061903.175743
- Nestler, J. M., Pompeu, P. S., Goodwin, R. A., Smith, D. L., Silva, L. G. M., Baigun, C. R. M. and Oldani, N. O. (2011). "The river machine: a template for fish movement and habitat, fluvial geomorphology, fluid dynamics and biogeochemical cycling." *River Res. Applic.* Published online in Wiley Online Library (wileyonlinelibrary.com) DOI: 10.1002/rra.1567.
- Olsen, N., and Melaaen, C. (1993). "Three-dimensional calculation of scour around cylinders." *J. Hydraul. Eng.*, 10.1061/(ASCE)0733-9429(1993)119:9(1048), 1048–1054.
- Olsen, N. R. (1994). "SSIIM: A three-dimensional numerical model for simulation of water and sediment flow." *HYDROSOFT 94*, Porto Carras, Greece.
- Papanicolaou, A., Diplas, P., Balakrishnan, M., and Dancey, C. L. (2001). "The role of near-bed turbulence structure in the inception of sediment motion." *J. Eng. Mech.*, 1273, 211–219.
- Papanicolaou, A.N.T., Elhakeem, M., Krallis, G., Prakash, S., Edinger, J. (2008). "Sediment Transport Modeling Review - Current and Future Developments." *J. Hydraulic Engineering, ASCE*, 134(1), 1-14.
- Parker, G., Seminara, G., and Solari, L. (2003). "Bedload at low Shields stress on arbitrarily sloping beds, alternative entrainment formulation." *Water Resour. Res.*, 397, 1183–1191.
- Parsons, D.R., P.R. Jackson, J.A. Czuba, F.L. Engel, B.L. Rhoads, K.A. Oberg, J.L. Best, D. S. Mueller, K.K. Johnson, and J.D. Riley (2013). "Velocity Mapping Toolbox (VMT): a processing and visualization suite for moving-vessel ADCP measurements." *Earth Surf. Process. Landforms* 38, 1244-1260.
- Partheniades, E., (1965). "Erosion and Deposition of Cohesive Soils." *Journal of the Hydraulics Division, ASCE* 91 (HY 1): 105–139.
- Patankar, S. V. (1980). *Numerical heat transfer and fluid flow*, McGraw-Hill, New York.
- Peric, M., Kessler, R., and Scheuerer, G. (1988). "Comparison of finite volume numerical methods with staggered and collocated grids." *Comput. Fluids*, 16(4), 389–403.
- Pess, G. R., Liermann, M. C., McHenry, M. L., Peters, R. J. and Bennett, T. R. (2012), "Juvenile Salmon Response to the Placement of Engineered Log Jams

## Quantitative Modeling Tools for Large Wood

- (ELJs) In The Elwha River, Washington State, USA”. *River Res. Applic.*, 28: 872–881. doi: 10.1002/rra.1481
- Phillips, B. C., and Sutherland, A. J. (1989). “Spatial lag effects in bed load sediment transport.” *J. Hydraul. Res.*, 27(1), 115–133.
- Rahuel, J.L., Holly, F.M., Chollet, J.P., Belleudy, P.J., and Yang, G. (1989). “Modeling of riverbed evolution for bedload sediment mixtures,” *J. Hydraulic Engineering, ASCE*, 115(11), 1521-1542.
- Rhie, C. M., and Chow, W. L. (1983). “Numerical study of the turbulent flow past an airfoil with trailing edge separation.” *AIAA J.*, 21(11),1526–1532.
- Richardson, J. F. and Zaki, W.N. (1954). “Edimentation and fluidization: Part I.” *I. Trans. Institution of Chemical Engineers* 32: 35–53. 80, 331.
- Roulund, A., Sumer, B. M., Fredsoe, J., and Michelsen, J. (2005). “Numerical and experimental investigation of flow and scour around a circular pile.” *J. Fluid Mech.*, 534, 351–401.
- Salaheldin, T. M., Imran, J., and Chaudhry, M. H. (2004). “Numerical modeling of three-dimensional flow field around circular piers.” *J. Hydraul. Eng.*, 10.1061/(ASCE)0733-9429(2004)130:2(91), 91–100.
- Sinha, S. K. (1996). “Three-dimensional numerical model for turbulent flows through natural river reaches.” PhD thesis, Civil and Environmental Engineering, The University of Iowa, Iowa.
- Smith, D. L., Brannon, E. L., Shafii, B., and Odeh, M. (2006). “Use of the average and fluctuating velocity components for estimation of volitional rainbow trout density.” *Transactions of the American Fisheries Society*, 135(2), 431-441.
- Smith, D. L., Jeffrey B. Allen, Owen Eslinger, Miguel Valenciano, John Nestler, and R. Andrew Goodwin (2010); “Hydraulic Modelling of Large Roughness Elements with Computational Fluid Dynamics for Improved Realism in Stream Restoration Planning”; *Stream Restoration in Dynamic Fluvial Systems*, press 2013
- Sotiropoulos, F., and Patel, V. C. (1992). “Flow in curved ducts of varying cross section.” *IIHR Report No. 358*, Iowa Institute of Hydraulic Research, The University of Iowa, Iowa City, Iowa.
- Stelling, G.S., and Zijlema, M. (2003). “An accurate and efficient finite-difference algorithm for nonhydrostatic free-surface flow with application to wave propagation.” *International Journal for Numerical Methods in Fluids*, 43(1):1–23, 2003.
- Stumpp, S. (2001). *Investigations on Modeling of Large River-Bed Roughness*, M.S. Thesis, University of Stuttgart and IIHR.
- Thompson J. F., Warsi, Z. U. A., and Mastin, C. W. (1985). *Numerical grid generation: Foundations and applications*, North–Holland, New York.

- Thuc, T., (1991). “Two-dimensional morphological computations near hydraulic structures,” Dissertation, Asian Inst. Of Technology, Bangkok, Thailand.
- Udaykumar HS, Shyy W, Rao MM. (1996). Elafint: A mixed Eulerian-Lagrangian method for fluid flows with complex and moving boundaries. *Int. J. Numer. Methods Fluids* 22:691–705.
- Ullmann, S. (2008). “Three-dimensional computation of non-hydrostatic free-surface flows.” MS Thesis, Delft University of Technology.
- van Rijn, L. C. (1987). “Mathematical modeling of morphological processes in the case of suspended sediment transport.” Delft Hydr. Communication No. 382.
- van Rijn, L. C. (1993). *Principles of sediment transport in rivers, estuaries, and coastal seas*, Aqua Publications, Amsterdam, The Netherlands.
- Weber, L.J., Huang, H., Lai, Y.G., and McCoy, A., (2004). “Modeling Total Dissolved Gas Production and Transport Downstream of Spillways – Three-Dimensional Model Development and Applications,” *Int. J. River Basin Management*, vol.2(3), 157-167.
- Wu, W., Rodi, W., and Wenka, T. (2000). “3D Numerical Modeling of Flow and Sediment Transport Open Channels.” *J. Hydraul. Eng.*, 126(1), 4-15.
- Wu, W., (2004). “Depth-averaged two-dimensional numerical modeling of unsteady flow and nonuniform sediment transport in open channels,” *J. Hydraulic Engineering*, 130(10), 1013-1024.
- Ye, J., and McCorquodale, J. A. (1998). “Simulation of curved open channel flows by 3D hydrodynamic model.” *J. Hydraul. Eng.*, 124(7), 687–698.
- Yost, S. (1995). “Three-dimensional nonhydrostatic modeling of free surface flows and transport of cohesive sediment.” PhD thesis, Civil Engineering, University of Michigan, Ann Arbor, Mich.
- Zeng, J., Constantinescu, G., and Weber, L. (2005). “A fully 3D nonhydrostatic model for prediction of flow, sediment transport and bed morphology in open channels.” 31st Int. Association Hydraulic Research Congress, Seoul, Korea.
- Zielinski, D.P., Voller, V.R., Svendsen J.C., Hondzo, M. Mensinger, A.F., and Sorensen P. (2014). “Laboratory experiments demonstrate that bubble curtains can effectively inhibit movement of common carp.” *Ecological Engineering* 67: 95-103
- Zijlema, M., and Stelling, G.S. (2005). “Further experiences with computing non-hydrostatic free-surface flows involving water waves.” *International Journal for Numerical Methods in Fluids*, 48(2):169–197.
- Zijlema, M., and Stelling, G.S. (2008). “Efficient computation of surf zone waves using the nonlinear shallow water equations with non-hydrostatic pressure.” *Coastal Engineering*.



## **Attachment A. Full Conference #1**

Lai, Y.G., and Bandrowski, D.J. (2014). "Large Wood Flow Hydraulics: a 3D Modelling Approach." Proc. 7th International Congress on Environmental Modelling and Software, International Environmental Modelling and Software Society, San Diego, California, USA, D.P. Ames, N. Quinn (Eds.).

## **Attachment B. Full Conference #2**

Lai, Y.G., Goodwin, R.A., Smith, D.L., Reeves, R.L. (2016). "Complex transient flow patterns at a river junction and their relation with fish movement behavior." River Flow 2016, 8th International Conference on Fluvial Hydraulics, St. Louis, Mo. July 12-15, 2016.

## **Attachment C. Full Conference #3**

Lai, Y.G., Smith, D.L., Israel, J. (2016). "2D and 3D Flow Modeling of the Sacramento River Fremont Weir Section." ASCE World Environmental and Water Resources Congress, West Palm Beach, Florida, May 22-26, 2016.

## **Attachment D. Final Report of Prof. Liu**

Xu, Y., Chen, Y, and Liu, X. (2016). Quantitative Modeling Tools for Large Wood Flow Simulation. Project Final Report to Bureau of Reclamation. Department of Civil and Environmental Engineering, Pennsylvania State University

Web Link to the Report:

[http://water.engr.psu.edu/liu/publications/LWD\\_USBR\\_final\\_report\\_5\\_30\\_2016.pdf](http://water.engr.psu.edu/liu/publications/LWD_USBR_final_report_5_30_2016.pdf)